Lappeenranta University of Technology
Faculty of Energy Technology
Master Degree Program in Electricity Markets and Power Systems

Master's Thesis

Miguel Juamperez Goñi

TESTING PLATFORM DEVELOPMENT FOR LARGE SCALE SOLAR INTEGRATION

Examiners: Professor Jarmo Partanen
Professor Olli Pyrhönen

Supervisors: Professor Jarmo Partanen
Researcher Guang Ya Yang (DTU)

ABSTRACT

Lappeenranta University of Technology
Faculty of Energy Technology
Master Degree Program in Electricity Markets and Power Systems

Miguel Juamperez Goñi

Testing platform development for large scale solar integration

Master's Thesis

2013

108 pages, 97 figures, 7 table, and 4 appendices.

Examiners: Professor Jarmo Partanen
Professor Olli Pyrhönen

Keywords: distributed generation, solar power, integration, reactive power, voltage control, optimization, ethernet communication, embedded.

Currently, a high penetration level of Distributed Generations (DGs) has been observed in the Danish distribution systems, and even more DGs are foreseen to be present in the upcoming years. How to utilize them for maintaining the security of the power supply under the emergency situations, has been of great interest for study. This master project is intended to develop a control architecture for studying purposes of distribution systems with large scale integration of solar power.

As part of the EcoGrid EU Smart Grid project, it focuses on the system modelling and simulation of a Danish representative LV network located in Bornholm island. Regarding the control architecture, two types of reactive control techniques are implemented and compare. In addition, a network voltage control based on a tap changer transformer is tested. The optimized results after applying a genetic algorithm to five typical Danish domestic loads are lower power losses and voltage deviation using Q(U) control, specially with large consumptions.

Finally, a communication and information exchange system is developed with the objective of regulating the reactive power and thereby, the network voltage remotely and real-time. Validation test of the simulated parameters are performed as well.

ACKNOWLEDGEMENTS

Firstly, I would like to thank my supervisor Professor Jarmo Partanen for his understanding and invaluable support. His advices and guideline have been of enormous significance to me.

I wish to thank Guang Ya Yang (Researcher at DTU) for the given opportunity to work on this interesting and challenging topic. It would have been impossible to make this thesis without him.

Financial support and exchange possibilities of Lappeenranta University of Technology allowed me to study and obtain my master's degree in one of the best educational systems. Also, thanks to Danmarks Tekniske Universitet (DTU) for giving me the possibility to develop a challenging and exciting master thesis.

I also thank my project room mates of the Electrical Department in DTU for their support and wonderful conversations.

Finally, I express my special gratitude to my girlfriend and parents for their entire and selfless support and understanding. I will always be thankful for you.

Lappeenranta, April 1st, 2013

Miguel Juamperez Goñi

CONTENTS

APPENDICES

List of Figures

List of Tables

ABBREVIATIONS AND SYMBOLS

Roman Letters

$apsel$	PV power production in % of the nominal
B	Susceptance
F,f	Fitness function
G	Conductance
I	Current, RMS
N	number, quantity
P	Active power
Q	Reactive power
R	Resistance
S	Aparent power or power flow
U,V	Voltage, RMS
X	Reactance
w	weighted average voltage parameters
Z	Impedance

Greek Letters

cosφ	Power factor
φ	MOGA penalty factor
θ	voltage angle

Subscripts

cdm	command value
cu	copper
D	consumed
dev	deviation
dmax	maximum dead-band value
dmin	minimum dead-band value
elec	electric generated value
fe	iron
gen	generation value
G	Generator
h	magnetic or iron

i	row number, bus under study
inv	solar inverter
j	column number, rest of buses
L	load
l	line or feeder
loss	losses
max,mx	maximum value
min,mn	minimum value
nom,n	nominal value
ord	order or command value
r	rated
ref	reference value
sc	short-circuit
T	transformer
term	PCC value

Abbreviations

AC	Alternating Current
ADN	Active Distribution Network
AL	Aluminium
ANM	Active Network Management
CET	Centre for Electric Power and Energy
cRIO	CompactRIO
DG	Distributed Generation
DMS	Distribution Management System
DNO	Distribution Network Operator
DSP	Digital Signal Processing
DTU	Danmarks Tekniske Universitet
FIFO	First In First Out
FPGA	Field Programmable Gate Array
GA	Genetic Algorithm
GTO	Gate Turn-Off
HV	High Voltage
IP	Internet Protocol
LabVIEW	Laboratory Virtual Instrumentation Engineering Workbench
LV	Low Voltage
MOGA	Multi-Objective Genetic Algorithm

MV	Medium Voltage
NI	National Instruments
OLTC	On-Load Tap-Changer
ORDP	Optimal Reactive Power Dispatch
PCC	Point of Common Coupling
PEX	Cross-linked PolyEthylene
PF	Power Factor
RES	Renewable Energy Source
STATCOM	Static Synchronous Compensator
SVC	Static VAR Compensator
TCP	Transmission Control Protocol
UDP	User Datagram Protocol
VAR	Volt-Amperes Reactive
VI	Virtual Instrument

1 INTRODUCTION

1.1 Background

Electric power system's structure has been mainly based on large generating centralized units since its first implementation (Viawan, 2008), from where the electricity is transmitted over long distances at HV levels. Voltage is then stepped down and distributed through radial MV networks and finally transform to LV at loads level.

During the last years, DG penetration in the grid is becoming deeper worldwide as a result of several factors. Firstly, the opening of the energy markets to the self-supply allows the installation of new and small-scale generators in the medium and low-voltage networks. Secondly, the rapid development of efficient and renewable energy technologies, along with the increase of fossil-fuelled energy prices and the rising rejection to nuclear technologies, maximize their promotion. Last but not least, the global warming awareness and environmental friendly supply concerns restrain the expansion of large centralized generation plants as well as the construction of new transmission lines (Caldon et al., 2005).

The layouts of a traditional electric power system and a power system with distributed generation are represented in Figure 1.

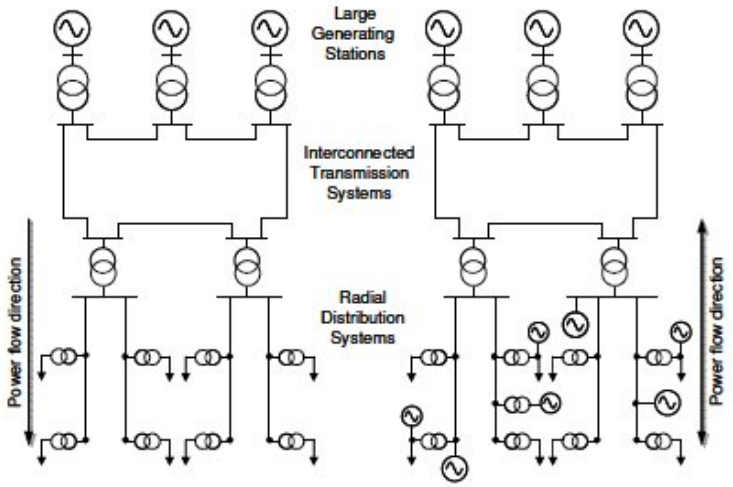

Figure 1. Centralized (left) and distributed generation (right) power systems (Viawan, 2008).

The incentives given by the governments to promote the small-scale generation have made the number of self-suppliers grow quickly, changing the traditional unidirectional way of energy distribution to bidirectional (Caldon et al., 2005). As the majority of electricity networks in Europe were designed and built around 50 to 60 years ago according to the demand scheme of that time, which largely differs from nowadays, a strong reinforcement or new solutions should be implemented. Besides, new emerging energy markets, such as electrical vehicles, also contribute to a significant increment of the current energy demand. As a consequence, a large number of research projects, using smart grid technologies, are on going in the present. Although still an immature technology, smart grids solutions are gradually adopted as the most appropriate way to control the flux between suppliers and consumers at the medium and low-voltage levels because of the theoretical benefits achieved in power coordination and control. A glance of the future developments and research is described in (McDonald, 2008).

Distributed generation technologies involve renewable and non-renewable energy resources, such as, internal combustion engines, wind turbines, solar photovoltaic, fuel cells, biomass or small gas turbines. The aggregation of different technologies in the grid can affect the system voltage level and power flow causing undesirable disturbances to the customers, especially with a significant share of DG (Viawan, 2008). As the technology evolves, the manufacturing costs fall resulting in a massive RES power installation without paying enough attention to the possible drawbacks. The lack of regulation provokes, in some places, a vast investment that the economic recession restrained recently. The past events lead the researchers to investigate deeply the real impact of RES into the grid in terms of operational issues concerning voltage and power control (Barker and Mello, 2000). The level of coordination required in the new electric scenario, where both large generators, small generators and consumers interact actively, is much higher. Therefore, both control and communication systems must be updated in order to achieve the main objective of secure and reliable energy supply to all consumers.

Distribution networks are facing the challenge of moving from a long period of stability and passivity to a dynamic and potentially updating time. An ADN is set as a new low and medium voltage network system based on small and intermittent generators, easily managed by the network operators due to the total integration of control and communication technologies (D'Adamo et al., 2009). Consumers gain autonomy by means of self-supply and freedom to select the energy source, not just the distribution company. Electricity markets liberalization creates a new energy scenario in which everyone: generators, consumers, distribution companies, retailers, network operators, etc, can participate actively. The dynamism of grids brings both advantages and weaknesses (D'Adamo et al., 2009).

Worth mentioning strengths are the high level of automation and control of networks which facilitates the integration of small generators at the same time as improving the reliability of supply without having to reinforce the whole distribution system. On the other hand, some handicaps are the absence of historical data and experience, or operation and planning concerns (Hashim et al., 2012).

Solar Energy

The acceptance of PV, as a energy source, is constantly growing due to its flexibility and accessibility. The quality of life strongly depends on the access to electricity which is an issue in isolated placed. Manufacturing costs have been significantly reduced as the technology has evolved. For instance, the rapid development of semiconductors' technology results in costs reduction and consequently make solar energy more competitive despite the low efficiency of panels (Timbus, 2007). The main reasons for the PV energy promotion are the low maintenance costs, long life-time and absence of pollution. On the contrary, the low efficiency (15-20%) and the high costs hinder its growth (Man, 2012), (*Power Electronics Handbook: Devices, Circuits and Applications*, 2011).

Solar energy, as a high potential energy source, contributes to the achievement of the successful integration of distributed generators within the new sustainable energy system. However, diverse operational issues related to power quality regulation due to PVs discontinuous energy generation, must be faced (Yang et al., 2011). In fact, one of the main obstacles to the expansion of RES in the distribution networks is the voltage control problem, under study in this work involved in PVNET.dk project continuation of EcoGrid EU project, the Danish Cell Project, and Photovoltaic (PV) Island Bornholm project. The high penetration of RES in the island turns it into a real-time laboratory where measurement and tests are taken place. The installation of approximately 5MWp of PV covers around 9% of the total energy demand of the island, close to the EPIA goal of 12% in 2020 (Yang et al., 2011). Moreover, Bornholm Island is considered a perfect example of Denmark energy scheme because it corresponds to 1% of the total supply and demand of the country. According to this fact, the island is the ideal platform to study the effects of large amount of RES integration in the network and extrapolate the results afterwards.

1.2 Problem statement and motivation

Photovoltaic technology was first thought to provide electricity in isolated places where no connection to the grid is possible. Global warming issues leaded to the establishment

of pollution constrains and the promotion of renewable resources usage. The majority of European countries promoted the installation of PV panels with subsidies. Lots of small investors became energy producers due to the business opportunities. According to (IEA, 2010) global solar PV market experienced a 60% expansion between 2004 and 2009, mainly grid connected panels.

Germany, as an example of photovoltaic energy promotion, strongly invested in small-scale PV installations connected directly to the LV network. Voltage variations due to the injection of large amount of active power and reverse power flow, may affect the normal operation of electric devices and loads in the grid. Rural areas are more affected than urban areas as a consequence of the large distances and low loads. To overcome this problems without having to reinforce the network, PV inverters are required to participate actively in the grid stability under the command of the system operator (Man, 2012). The main contribution is done by co-ordinate voltage regulation techniques between the inverters and the transformer. A visual representation of the over voltage problem facing in this project is presented in Fig.2.

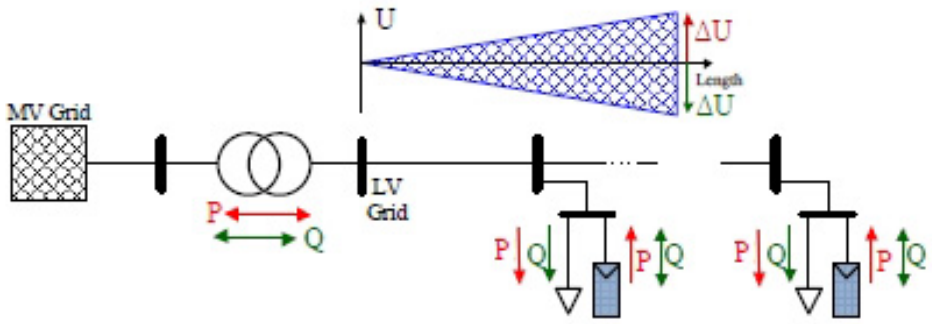

Figure 2. Bidirectional power flow and voltage fluctuations in LV networks with PV integrated (Timbus, 2007).

Increase the penetration level of DG in the LV grid may cause several technical issues:

1. System overvoltage
2. Transformer overloading
3. Cable overloading
4. Reverse power flow
5. Protection system failure

This study will focus on the two first issues as they are the more critical from the DNO point of view. Depending on the characteristics of the network the probability of occurrence differs. Thus, it is important to categorize the grid under study which in this case belongs to the **Sub-urban** type as the majority of Bornholm system.

An analysis of the over voltage phenomena in the LV voltage network at high levels of PV penetration is performed. Several voltage control methods will be described and the strategy selected will be applied and tested.

1.3 Objectives and Restrictions

The growing presence of small-scale generators in the grid makes the conventional networks to reach a critical level of collapse unless countermeasures are performed. Fundamentally, impacts of DG are on voltage control and stability (McDonald et al., 2012), (Hemdan and Kurrat, 2012), (Omole, 2010). The conventional operation of voltage control based on voltage drop along the feeder is no longer applicable in bidirectional power systems. The unpredictable and intermittent power generation of DG can cause the voltage stability to deteriorate (Viawan, 2008).

Regarding these drawbacks, the fundamental objective of the proposed thesis is to develop a testing platform to monitor and control the voltage in a LV network with high PV penetration, **with the minimum reinforcement**. Reinforce of feeders, transformers or inverters can be avoided or reduced by software developments. These thesis concerns hardware, theory and software implementation. The work is divided into diverse tasks:

- Research the voltage regulation methods developed for LV networks with RES integration and select the most appropriate for this case.
- Study and model the voltage regulation strategy requirements according to LV grid connected PV codes such as (ENTSOE, 2012), (Troester, 2009) and (Markiewicz and Klajn, 1999).
- Create a model of the LV network and the voltage control method selected in Simulink in order to monitor and control the voltage variations within the limits.
- Optimize the voltage regulation by implementing an algorithm capable of finding the maximum PV power to be installed while minimizing the reactive power consumption.

- Implement and test the optimized control on a laboratory platform. NI hardware (cRIO) will be used as the communication system between the inverters and the system operator software.

- Evaluate and validate the control platform by comparison between the simulation results and the real measurements.

Simplifications and limitations are enumerate below : .

- Phasor simulation is performed in order to reduce complexity and computation time as just voltage variations are wanted to be analysed.

- PV inverters will be modelled as current sources, not considering the switching or filtering phases.

- Frequency control will be not implemented in the active power model.

- As the objective is to minimize the reinforcement of the grid, no energy storage is considered.

- One PV plant will be installed at every bus of the network containing load.

- An OLTC LV transformer is used in simulations as it is required for the co-ordinated control strategy. The real one could be updated as explained in (Monroy et al., 2007), (Bauer and De Haan, 1999) or (Demirci et al., 1998).

- Laboratory tests will be performed in just one three-phase inverter (top-roof plant).

- Limitations of cRIO.

1.4 Structure of the Thesis

The first chapter of the report collects the background of the research project, the objective and motivation of the work and the structure of the document. The next five chapters are structured in two main parts: modelling&simulations, and validation. The first one is covered in Chapters 2 & 3 while the second which involves practical implementation is described in Chapters 4 & 5.

Chapter 2 presents an overview of the current state of Bornholm Island power system, defining the different DG technologies installed and the technical issues for the integration in the system. Secondly, an extensive explanation of the existing voltage and power control strategies and architectures is stated. Then, the initial electrical data of the LV network and its layout is shown. Finally, the design of the network model including the Voltage/VAR control loop, control parameters calculation and tuning process, is explained in detailed. The grid voltage model is developed in Matlab/Simulink software as block schemes.

Chapter 3 focuses on the optimization process of the model according to power losses and voltage variations. Simulations and results obtained implementing a multi-objective genetic algorithm are presented. Several cases are launched under different load conditions in order to obtain the maximum PV power to be hosted in the grid without violating any constraint. Ideal reactive power control parameters resulted from the simulations which should be tested in reality afterwards.

Chapter 4 comprises the communication and data transfer systems. A Danfoss inverter located in the laboratory and connected to solar panels in the roof works as the testing station. On the first stage a LabVIEW code is used to read and set parameters directly from the computer and then, take advantage of the cRIO in real-time operation.

Chapter 5 resumes the validation test, comparing the measurements with the simulation results to approve the designed model or platform. Measurements from two data acquisition or power analyser devices are compared.

Chapter 6 collects a short summary, a list of achievements and some suggestions for tasks or improvements in future projects related to this thesis.

2 LV GRID CONTROLLER MODEL DESIGN

2.1 Bornholm power system

Bornholm Island, located in the south of Sweden, belongs to Denmark. The power system of the island is reminiscent of the Danish distribution system as well as part of the Nordic interconnected power system and market. Despite the fact that Bornholm network is directly connected to the Swedish grid by a 132kV cable, the system can be operated in island mode manipulating the HV/MV transformer located in Sweden (Østergaard and Nielsen, 2012). In addition, the electrical and geographical characteristics of the island corresponds to about 1% of Denmark, making it an ideal and singular experimental facility for researching purposes mainly related to Smart Grids technologies. Danish universities and private energy companies invest and promote PowerLabDK platform for the development of the future smart power system. The Bornholm island network is shown in Fig.3.

Power experiments and real-time measurements are enable thanks to the total interconnection of all facilities and the Intelligent Control Laboratory, located at the electrical department of the DTU. Vast amount of data is collected periodically in order to assess the impact of physical and real-scale solutions implemented in the network (Østergaard and Nielsen, 2012). By this method, new smart grid solutions can be safely performed and validated before being installed in large scale permanently. An illustrative example of the activities performed in Bornholm Island can be found described in the following pages where the impact of large-scale integration of photovoltaic power systems in the LV networks, as a smart grid solution, is assessed.

Sweden and Bornholm are interconnected by a 60kV undersea cable. Power exchange is available when needed, such as, peak hours, generator's blackouts or maintenance. The German company E-ON controls the supply and distribution of electricity in the south of Sweden while ØSTKRAFT is the distribution system operator at Bornholm, in charge of supplying more than 28000 customers. The voltage levels used are 60/10/0.4kV including several primary substations with 60/10kV OLTC transformers capable of modifying the voltage level at the secondary side according to the load changes while keeping it within the limits ($\pm 5\%$). LV level is maintained using 10/0.4kV transformers. The 60kV network, operated remotely from the control room, consists of 184km of overhead lines and 730km of cables, while the 400V grid consists of 478km of overhead lines, 1409km of cables and 1006 transformers of 268MVA power (Østergaard and Nielsen, 2012).

Bornholm power system had a total peak load of 56MW and 262GWh of energy consumption in 2007. Power demand can be covered by the 60MW capacity cable to Sweden, 30MW of wind turbine capacity (35 turbines), 34MW of diesel generator capacity (14 generators), 62MW of steam turbine capacity (2 turbines), 2MW of gas turbine capacity (2 turbines) and 5MW of PV capacity in the near future. Voltage and frequency are controlled by the diesel generators and steam turbines due to their flexibility of power generation. On the other hand, wind turbines and solar panels can handle both, active and reactive power, as part of smart grid solutions. Data metering, essential in smart grid technologies, is performed every 15 minutes in users with annual consumption higher than 100000kWh but only once a year in the rest. All facilities and devices are interconnected by optical fibre communication (Østergaard and Nielsen, 2012).

The future target of Bornholm as a power system is to reach the total energy independence by owning 100% of the generation from renewable resources. The island will continue functioning as a experimental facility involved in new projects such as electric vehicle market, energy storage systems, new communication solutions or modern control strategies.

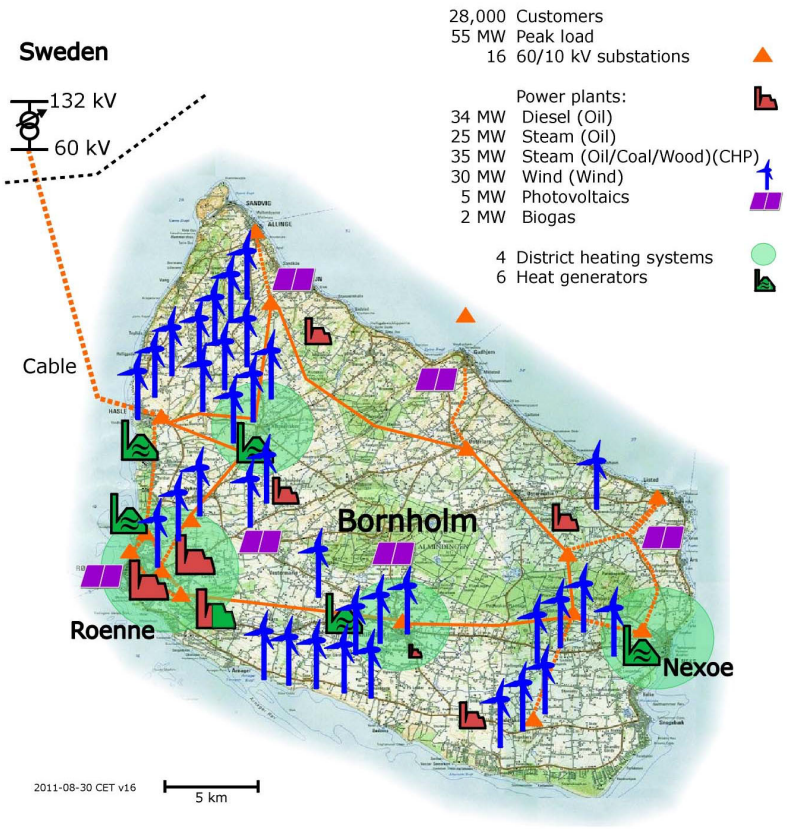

Figure 3. Bornholm system overview (Østergaard and Nielsen, 2012).

2.2 Photovoltaic integration studies in Bornholm

The PV systems are to be installed as rooftop systems on private buildings, on facilities of the municipality of Bornholm and a single or few larger PV power plants. Solar photovoltaic integration analysis is the fundamental task of this project. So far, the study of energy capacity value has been focused specially on wind turbines, having the PV energy still long way to go. As a drawback, solar capacity analysis requires large amount of historical radiation data for the term planning while for the short term only real-time meteorological measurements are needed. For this project, a PV testing laboratory, recently settled in DTU, will be served as our testing platform of PV integration studies. A low-voltage network, similar to the Bornholm systems ones, is selected for the simulations. Real measurement data from the solar panels and inverted installed in the roof of the electrical department in DTU will be used.

2.3 EcoGrid EU Smart Grids concept

EcoGrid EU project aims to demonstrate the efficient way to operate a distribution network with large penetration of renewable energy resources in the current market system by the use of innovative communication and market solutions. Bornholm island, with more than 50% of its electricity consumption coming from RES, is the most appropriate platform to develop this demonstration.

The real-time market designed for the Bornholm system will be compatible with the existing power exchange markets, more specifically with the Nordic power market where it will participate. The installation of smart grid solutions (smart meters) will provide daily real-time measurements and prices for approximately 2000 residential customers with flexible demand response. Consumers will benefit from the complete automation and the possibility to set beforehand the specific demand-respond to be implemented.

The 21 million euros of EcoGrid EU budget is funded equally by the EU and private industries as Danfoss Solar Inverters, CET, Energimidt and Østkraft. During four years of project, started in 2011, researchers will try to accelerate the process towards the deployment of new smart grid solutions in distribution networks, as a part of the european road map (Jorgensen et al., 2011).

2.4 Summary of voltage control methods for Distribution Networks

Introduction

This chapter briefly discuss a variety of voltage and reactive power control methods available for active MV and LV distribution networks, interconnected and isolated of the grid. A deeper explanation of the control strategy to be tested in the LV active distribution network with PV generation integrated is developed. After that, the grid connected code for PV plants is mentioned. The second half of the chapter focuses on the technical description of the specific LV grid under study including the global electrical data, the system's layout and the controller model's design.

Power systems regulation is structured in standards, one of which is the European Standard EN 50160 that defines the proper operating conditions as the control of the distribution voltage level within the range of $\pm 10\%$ of the nominal value (Markiewicz and Klajn, 1999). A wide range of voltage and reactive power control methods have been already developed and successfully tested for voltage regulation in distribution networks. Despite the global validity of the standards, their practical implementation differs from one country to another as well as the voltage control methods used in HV, MV and LV systems. However, all of them aim ideal operating conditions in order to avoid disturbances and therefore, prolong the life-time of the electrical equipment installed along the electric lines.

In transmission lines, voltage level is fixed with the reactive power flow generated by stand-alone centralized power plants. Additionally, elements such as shunt capacitors, STATCOMs and SVCs, may generate or consume reactive power to keep a balance. On the other hand, due to the substantial resistive value of distribution lines, the voltage level is regulated by OLTC transformers. Nevertheless, as the voltage level at the end PCC rises with distributed generation, more sophisticated Voltage/VAR control methods are required (Lund, 2007).

Active Management Methods

The rising integration of renewable energies characterizes the new ADN regarding issues such as bidirectional power flow, fault current or voltage levels. Traditional control methods based on voltage drop along the feeders are no longer applicable. Therefore, new coordination schemes known as ANM have been designed to provide better grid control in cases of large distributed generation (Hashim et al., 2012).

Control strategies are categorized in centralized and decentralized. The first one relies on a central coordination remote control system based on a wide communication network. On the contrary, as the decentralized system are based on local information, it reduces the communication requirements by controlling the voltage at each bus independently (Santos et al., 2010). Some examples of both control schemes are described below.

Distribution Management System Control - Centralized

A DMS is an utility IT system used to support the control room in order to monitor the entire distribution system. The versatility of this control system allows the operators to enhance the efficiency of the networks, prevent faults and optimize the load flow, without disturbing the customers. Normally, DMS is implemented with the objective of finding the optimal combination of operations which leads to a minimization of the operational costs (Hashim et al., 2012).

Coordination of Distribution Systems Components - Centralized

It is probably the most studied method of voltage control based on estimated maximum and minimum voltage level for the distribution networks (Hashim et al., 2012). The voltage level can be regulated automatically by a relay in charge of the tap changer at the substation transformer or by the injection of reactive power using SVC. Additionally, sensors installed along the feeders provide data (variables) to the centralized control, as shown in Figure 4

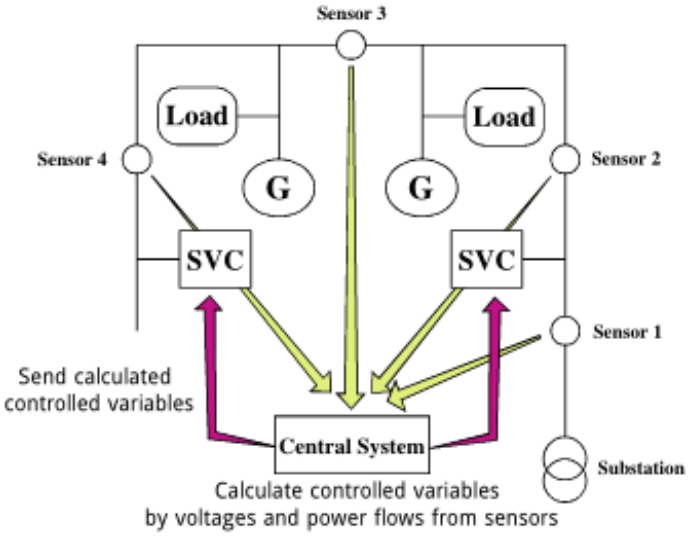

Figure 4. Centralized control scheme (Hiroyuki and Kobayashi, 2007).

Reactive Power Compensation - Decentralized

The overvoltage caused by the injection of active power can be fixed by allowing the distributed generators to absorb reactive power. The implementation of devices such as STATCOM, SVC or shut capacitor, has proved promising results in terms of supply efficiency and reliability (Hashim et al., 2012). However, the high price of these devices and the limitation of power balance between the transmission and the distribution systems, restrict this strategy (Lund, 2007).

On the other hand, the high versatility of solar inverters to provide voltage control techniques, makes this method very easy to be implemented locally. Four possible techniques are available: fixed power factor (PF), fixed reactive power (Q), local Q(U) and local PF(P) (Demirok et al., 2011). The two last strategies are further explained in 2.5.

Active Power Curtailment - Decentralized

Active power derating is normally performed by DNOs when required less amount of power generation. PV plant owners are negatively affected, economically talking, by active power reduction as they usually earn money for each kW injected into the grid. Therefore, it seems that reactive power regulation strategy should be activated first and then active power, only if reactive compensation is not sufficient to keep voltage level within limits (Constantin et al., 2012).

OLTCs scheme - Decentralized

It can be stated that OLTC transformers along with capacitor banks are the main technologies currently used to regulate the voltage level in distribution networks. It is at primary substations where transformer's tap manoeuvres modify the reactive power flow in order to balance the change of voltage downstream. Voltage sensors and relays work together in order to provide the transformer with the command to alter the tap position when needed. However, the total reliability of radial low voltage networks on the primary substation OLTC transformers for the voltage regulation, is insufficient for bidirectional power flow grids (Hidalgo et al., 2010).

On the other hand, conventional MV/LV transformers are equipped with a single tap manually operated for maintenance or scheduled interruptions. Economic and reliability of on-load manoeuvres are the principal reasons (Demirci et al., 1998). As additional features are clearly necessary, a new generation of electronic switches are under investigation and test. With the premise of significant enhancement of consumer's voltage profile, es-

pecially in large and overloaded lines, a new generation of electronics valves, also called solid-state valves, has arisen (Monroy et al., 2007). The quick evolution of technology allows the replacement of mechanical actuators by thyristor-based bidirectional switches (Bauer and Schoevaars, 2003) with enough turn-off capabilities. (Bauer and De Haan, 1999).

The increasing use of power electronics can affect the quality of the power supply as a result of harmonics' injection into the grid. The negative consequences are shut-downs as a result of large current unbalances capable of blowing fusses or tripping breakers, or even costumer's devices failure (Chung et al., 2003). OLTC transformers based of solid-state switches aims to mitigate these problems with the main difficulty of making them economically competitive. Furthermore, costs can be reduced choosing the topology with the optimal number of switches for a given number of taps or voltage steps. Several configurations are described in (Monroy et al., 2007), (Expósito and Berjillos, 2007).

Several disadvantages of electronic valves that affect the expansion of solid-state valves should be taken into account. For instance, conducting losses, forward voltage drop, switching losses growth, limited blocking capabilities and over-costs (Monroy et al., 2007). Moreover, the forward voltage applied to the thyristor when turning off during a tap changing, due to the phase shift between current and voltage in bidirectional power flow, could damage it severely. This drawback can be solved by using new GTO thyristors able to support forward voltage while disconnecting (Shuttleworth et al., 1996).

Performed simulations assure that electronic switches are 50 times faster than the mechanical ones, 100ms vs. 5s. With the purpose of saving money, a hybrid OLTC is presented in (Brewin et al., 2011) combining both technologies. This last option could be interesting in terms of retrofit.

2.5 Grid connection regulation requirements

The grid connection requirements for DG in MV and LV networks are collected in standards, some of which are mention below:

- DIN V VDE V 0126-1-1:2006-02, Automatic disconnection device between a generator and the public low-voltage grid.
- IEEE 1547-2003, IEEE Standard for Interconnecting Distributed Resources with Electric Power Systems.

- IEEE 1547.1-2005, IEEE Standard Conformance Test Procedures for Equipment Interconnecting Distributed Resources with Electric Power Systems.
- UL 1741-2005, Converters, Controllers and Interconnection System Equipment for Use with Distributed Energy Resources.
- Standard EN 50160, Voltage Characteristics in Public Distribution Systems.
- ENTSO-E 2012, Network Code for Requirements for Grid Connection. Applicable to all Generators. (Kaestle and Vrana, 2011)

Despite the large extension of the regulation standards, we will focus on the aspects important for this system.

1. *Voltage*

   Due to the large resistive value of the impedance in low voltage lines, the voltage rise at the PCC is a clear issue which must be constrained (Braun et al., 2009).

   According to (Markiewicz and Klajn, 1999) the maximum voltage level variations allowed in MV and LV networks are (-10%,+10%). Deeper deviations are considered as under voltages and over voltages. The first ones, also known as dips, are characterized by small drops (<10% respect the nominal value) and long duration (>10ms)(*Grid Converters for Photovoltaic and Wind Power Systems*, 2011). Over voltages, on the contrary, caused by ground faults, lightings, disconnection of large loads, rises the voltage level up to 1.8pu. After 200ms of fault duration, the generator must be disconnected (Man, 2012). FRT requirements are not applied to LV networks.

   Under normal operations, the maximum voltage rise allowed at the PCC is set to 3% over the level without distributed generators connected. The disturbances caused by the voltage rise during the switching operation of generators will not exceed the limits whether they happen sporadically, maximum once per 10 minutes (Kumm, 2011).

$$\Delta u \leq 3\% \tag{1}$$

2. *Frequency*

   The priority issue in electric systems is to maintain a balance power flow, between production and consumption. The increasing number of generators can destabilize

the balance and hence, affect the consumers. Therefore, all power plants are required to adjust their power production in order to keep the frequency within limits (Kumm, 2011).

According to VDE-AR-N 4105 standard, every generator with a capacity over 100kW must be capable of power output reduction steps of at most 10% of the rated active power (Troester, 2009). DSO regulates the frequency control ratio of small power plants. Any operating point, typically 100%, 60%, 30% and 0%, set by the DSO must be reachable in every case (Man, 2012).

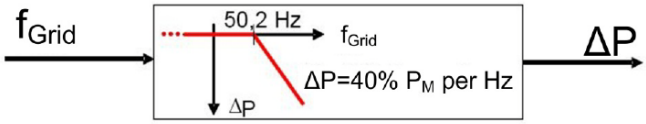

Figure 5. Frequency control - Active power drop function (Troester, 2009).

$$\Delta P = 20\, P_M \frac{50.2\, Hz - f_{grid}}{50\, Hz} \qquad at\ 50.2\, Hz \leq fgrid \leq 51.5\, Hz \tag{2a}$$

Where:

- P_M: Output Power
- ΔP: Power Reduction
- f_{grid}: System Frequency

According to figure 5, power plants are forced to reduce their output power with a 40% gradient when the system frequency exceeds 50.2Hz. Above 51.5Hz and below 47Hz the plant must be disconnected. From 47Hz to 50.2Hz no limitation exits (Troester, 2009).

3. *Reactive Power Control*

Generators are required to supply static grid support, in terms of voltage stability, on demand of the DSO. PV inverters are supposed to provide reactive power at any operating points, which can be done by several methods:

- A fixed power factor, cosφ.
- A variable power factor depending on the active power, cosφ(P).
- A fixed reactive power, Q.
- A variable reactive power depending on the voltage at the PCC, Q(U).

The two first methods are widely implemented in LV networks, but the type of method and reactive power adjustment depend exclusively on the DSO. The first method is suitable for generators capable of producing a constant power output. However, as PV production is mainly fluctuating, a variable displacement factor depending on the active power output is more appropriate. Further description of theses strategies can be found in Section 2.7. A summary of the new requirements for the connection of generators to the grid at MV/LV levels is in Appendix 1.

2.6 Representative LV network and PV generation

A LV network configuration of Bornholm electric system, as well as of the Danish system, has been selected and depicted in Figure 6. The grid supplies electricity to 71 consumers of a residential area on the island. The voltage is stepped down from 10kV to 400V with an off-load tap changer MV/LV transformer of 0.1MVA of power. The fundamental target of the transformer is to keep a constant voltage of 400V at the busbar. The power is then supplied to customers through two main feeders, 52 & 19 respectively. Loads are grouped and connected at variable distances (30-576 m) from the point of supply. The transformer parameters as well as line interconnections are detailed in Appendix 1.

Distribution networks present typically two possible dispositions, radial and interconnected. While rural areas are mainly radial, the majority of urban areas are interconnected in order to assure an uninterrupted supply, without exception. In case of fault, enough backup capacity is necessary to maintain the reliability and quality of supply, otherwise electrical devices may fail and consumers will complain. This network has a radial structure with an intermediate interconnection (536 - 10154) allowing the energy supply when fault occurs upstream. Any fault can be isolated manoeuvring the circuit breakers. Furthermore, the backup path can facilitate the integration of distributed generators by means of load flow and continuous supply.

In accordance to (Man, 2012), a profitable solar investment in a residential level is reached at S_r = 5 kVA per consumer. Therefore, 100% PV penetration is equivalent to install the rated power at each residence, 355 kW in this network. The great advantage is the uniform PV power distribution along the feeder. The total installed PV power $S_{PVfeeder}$ is determined by Equation 3 based on the percentage of PV penetration level L_{PV}, the total number of consumers n_{loads} and the rated power of each resident S_r.

$$S_{PVfeeder} = \frac{L_{PV}}{100} \cdot n_{loads} \cdot S_r \qquad [kVA]. \tag{3}$$

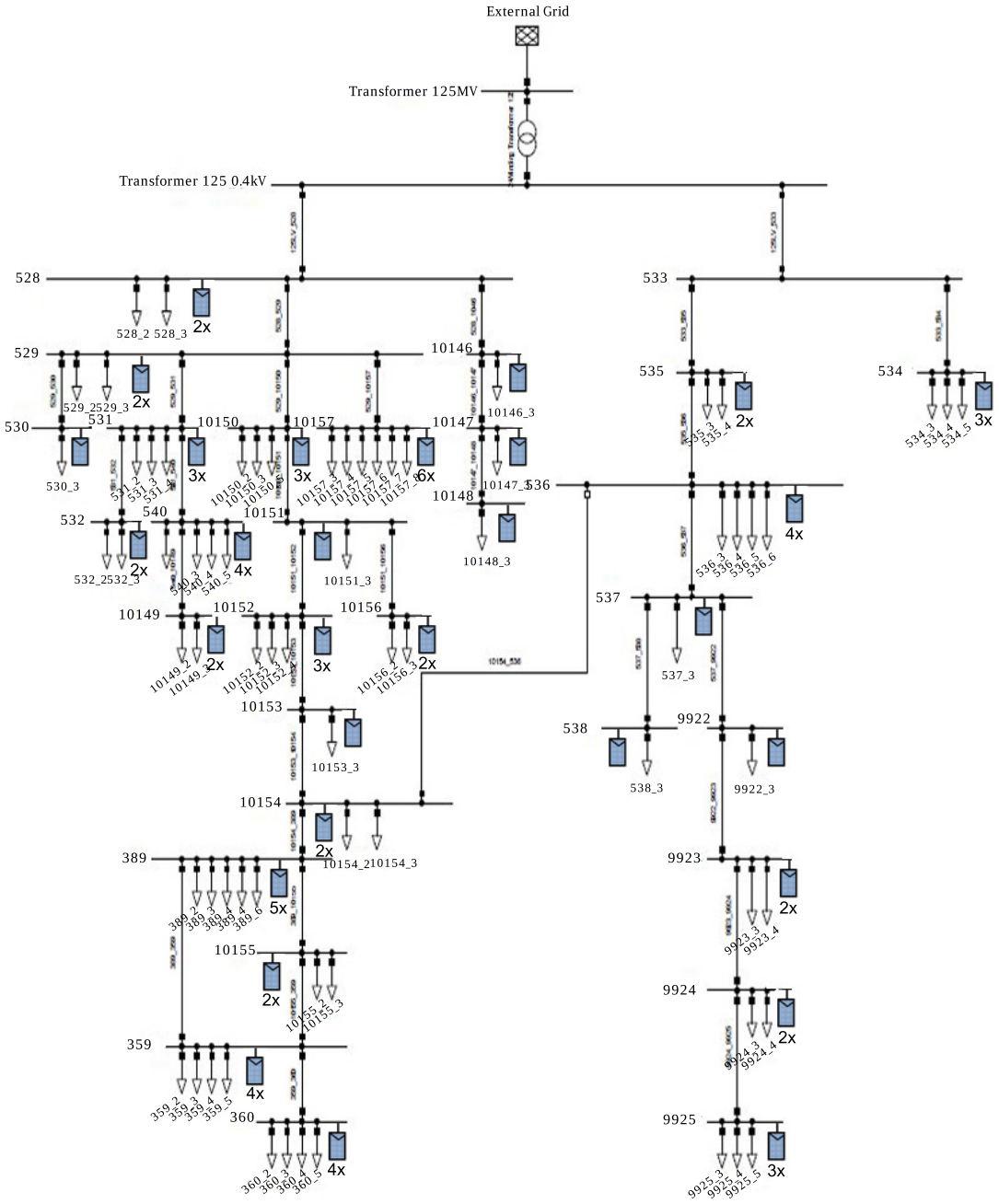

Figure 6. Bornholm low-voltage network layout under study.

Power generation data measured in a 5kVA inverter located inside the electrical department laboratory of DTU is used as a power profile of PV inverters in this study. Power values every second during 7 days in August were measured. As the simulation time chosen is 96 seconds, the data is reduced to one measure each 15 minutes. Seven different power profiles, one for each day, can be observed in Figures 7-9.

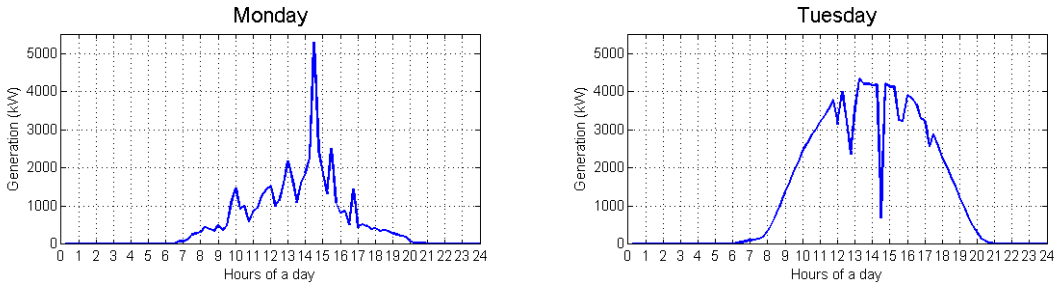

Figure 7. PV generation measured at the inverter's AC side on the 10-11/08/2012.

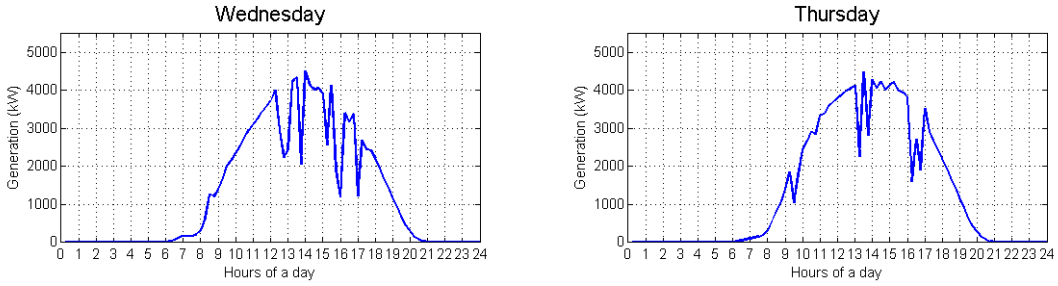

Figure 8. PV generation measured at the inverter's AC side on the 12-13/08/2012.

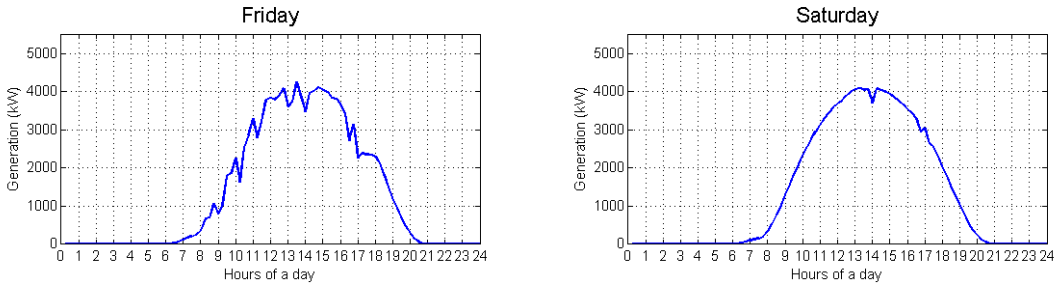

Figure 9. PV generation measured at the inverter's AC side on the 14-15/08/2012.

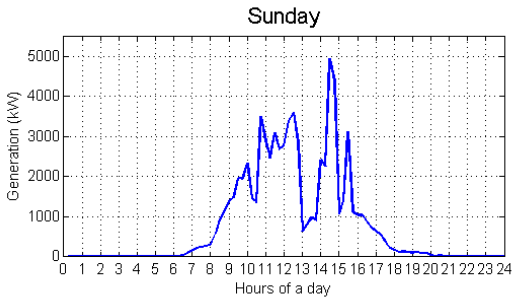

Figure 10. PV generation measured at the inverter's AC side on the 16/08/2012.

For simplicity, the impedances of the cables connecting the PVs to the grid are assumed negligible. Consumers are modelled as dynamic loads. Four load profiles of two summer days and two winter days were provided for the simulations. The days where selected for being representative in each season. The data shown in Figures 11,12,13 was measured from 10 representative Danish domestic consumers. The measurements have a resolution of 15 minutes, recording data during 24 hours.

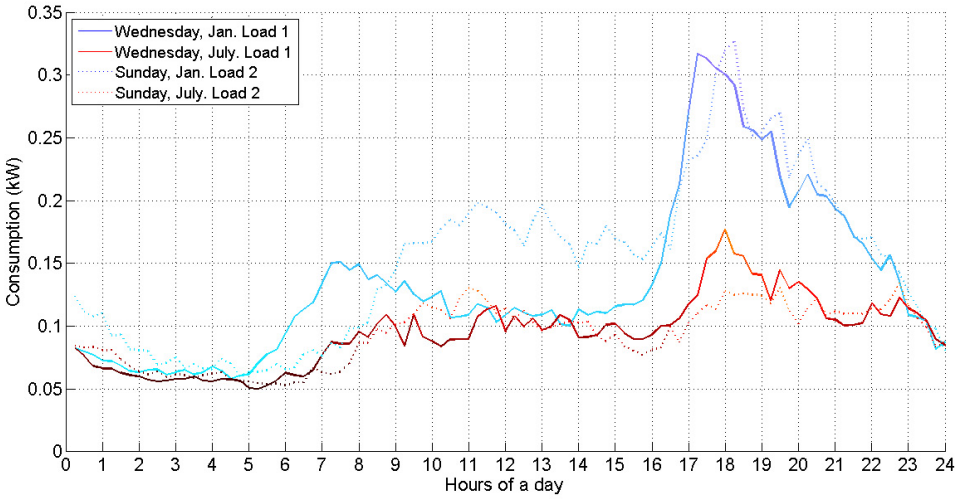

Figure 11. Load profile of 4 representative summer and winter days of 2 typical Danish consumer with higher resolution.

The variety of load profiles, power demand peaks at different times, allow a deeper study and optimization of reactive power control for voltage stability in LV networks. A detailed view of the model is presented in Figure 14. Regarding the construction, some specific elements such as OLTC transformer, Voltage/VAR controller or PV inverter were own design or model's modification, while the rest were taken from the library browser.

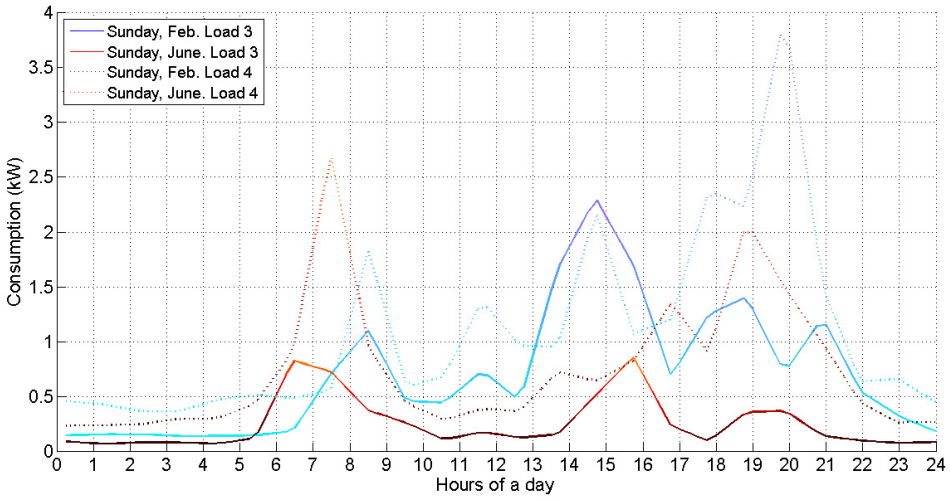

Figure 12. Load profile of 4 representative summer and winter days of 2 typical Danish consumer in 2011.

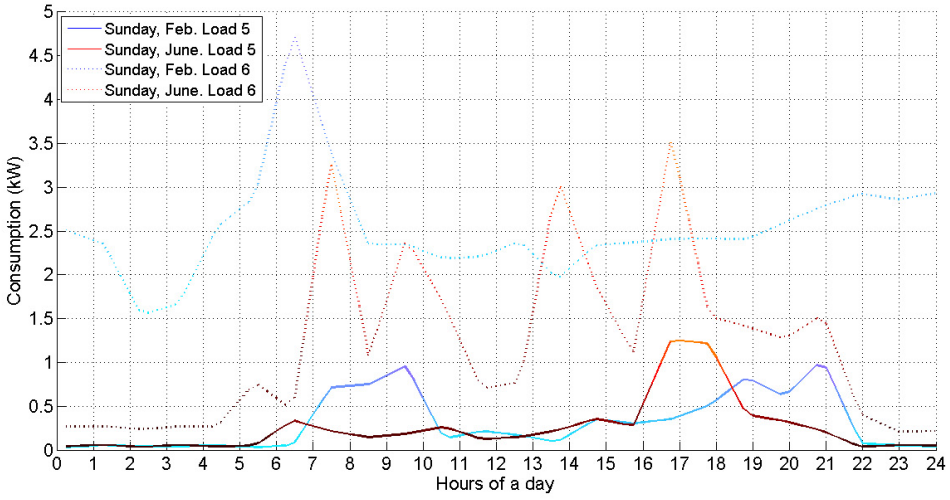

Figure 13. Load profile of 4 representative summer and winter days of 2 typical Danish consumers with electric heating in 2011.

The LV system of Bornholm under study consisted of cable feeders. Cables, characterized by low X/R ratios, requires the solar inverter to consume large proportion of reactive power to significantly mitigate the voltage rise at the PCC which depends on the X/R ratio of the whole network. Additional losses appears as a consequence of increasing the current flow in the distribution network, leading to a reduction of the generator efficiency. Voltage raise may be also mitigated by a reduction of the bandwidth voltage values at the distribution transformer. However, this action would increase the tap change operation frequency, and would also cause customers to experience very low voltage levels.

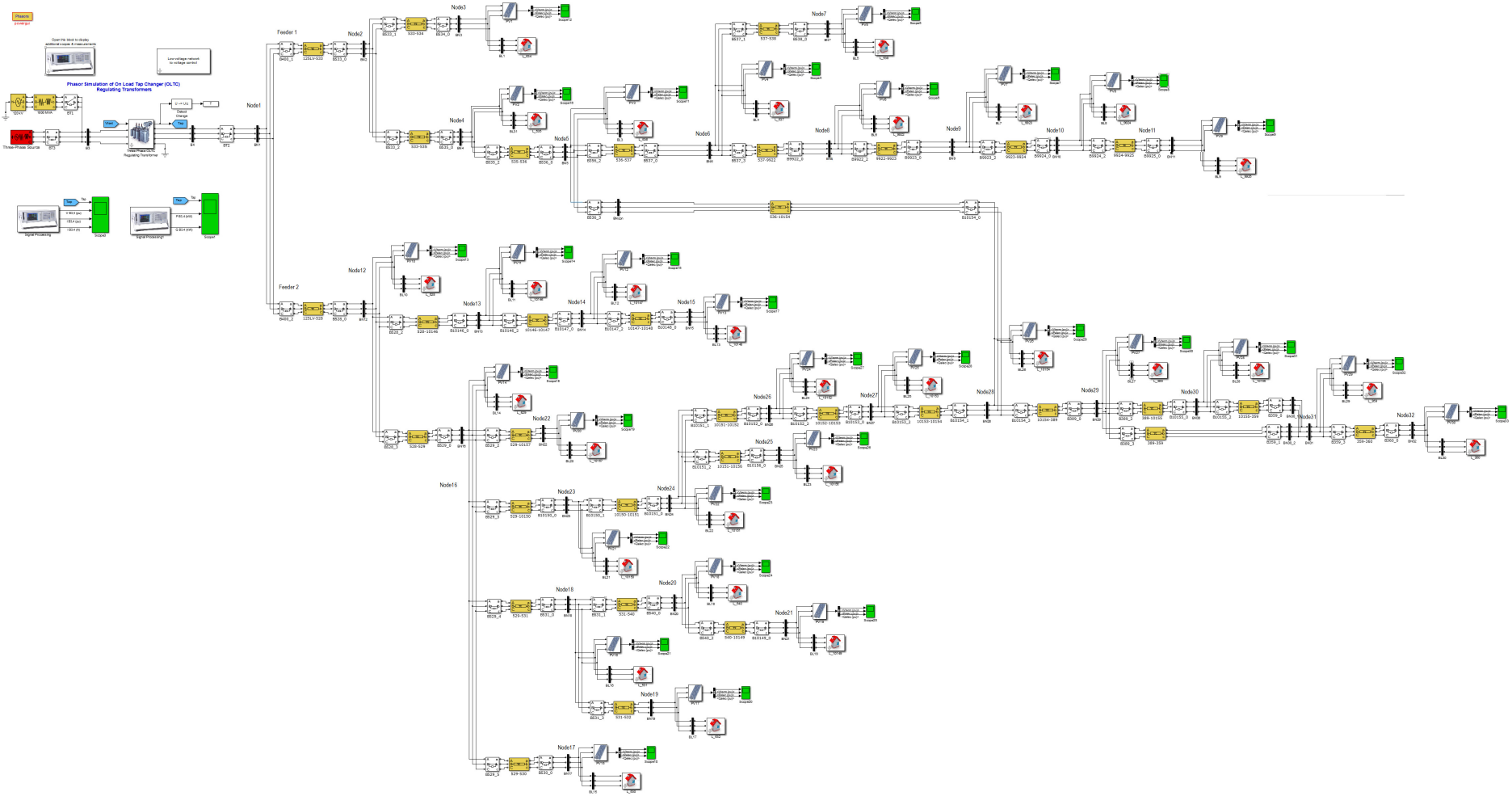

Figure 14. Three-Phase Low-Voltage grid under study Simulink model

2.7 Co-ordinated 'Voltage/VAR' control model

Traditional voltage regulation, based on unidirectional power flow, can be affected by the uncontrolled active and reactive power injection of generators integrated in the grid, particularly nearby the PCC. Although, theoretically reactive power is regulated, in practice, the uncertainty of the generation characteristics make the voltage control difficult to be implemented (Caldon et al., 2004).

The voltage compensation with reactive devices strongly depends on the R/X ratio of the network. The lower the resistance of the lines (lower R/X ratio) the higher efficiency, as the reactive power has a larger impact on voltage. According to this statement, overhead lines and transformers of transmission systems with R/X ratios around 0.1 are preferred to underground cables with R/X ratios of 0.5-1 used in distribution lines, in order to control de voltage (Trebolle et al., 2012).

The network under study is interconnected by underground cables with high resistive impedances resulting in ratios R/X over the unit. As a consequence, the active power injection can easily rises the voltage at the point of PV connection over the limit.

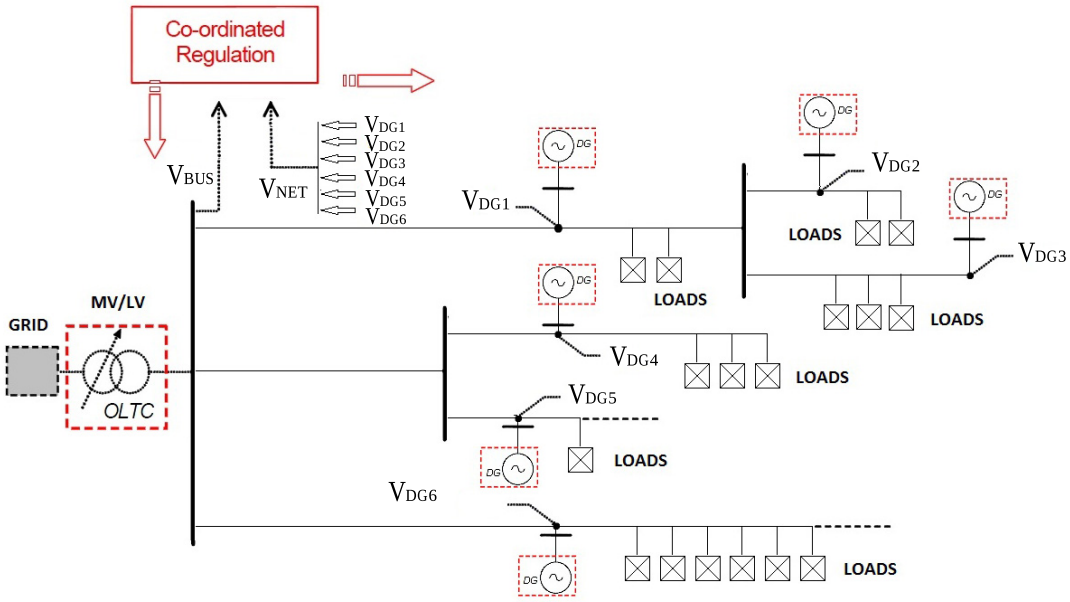

Figure 15. Voltage and reactive power regulation method based on distributed generators and OLTC transformer coordination in LV networks, (Caldon et al., 2005) modified.

DG may affect considerably the voltage at the PCC by injecting active power in LV and MV networks. Reactive power absorption is required to avoid damages in the grid. However, the high amount of reactive power needed to compensate the voltage variation in distribution networks, makes this method inefficient.

The number of published research papers focused on the study of new or revised voltage control methods for networks with increasing diffusion of RES, are exponentially growing. Therefore, after researching and filtering the available strategies (section 2.4), the most appropriate method for low-voltage networks with increasing diffusion of PV panels is a coordinated control strategy. A coordinated regulation between a centralized control, performed by an OLTC MV/LV transformer, and a reactive power balance carried out by the solar inverter. This method was design and tested in primary substation transformers (Caldon et al., 2004). A graphical representation can be observed in fig15.

The determination of the maximum PV capacity to be installed in a residential network and its influence in the voltage stability is performed using Matlab and Simulink software.The Voltage/VAR controller developed for this platform is based on two models ((Caldon et al., 2005),(Clark et al., 2010)) already tested for MV networks. Several modifications have been made to adapt the controllers to the specific network and purposes. More in detail, the model is composed of two controllers. An active and reactive power control at each PV inverter and a voltage average control of the network using an OLTC transformer. As stated in Section 2.5, PV inverters support diverse operating modes. In this case, only a local PF(P) and Q(U) modes are implemented and described below.

Power factor variation with active power - cosφ(P)

The selection of the regulation method and the reactive power adjustment values is basically based on the network conditions and can therefore vary within generating units, under the control of the DSO. The adjusting time to the curve determined by the DSO is set to 10 seconds (Man, 2012).

From the wide variety of cosφ(P)-characteristic curves, two are presented in Figure 16. The power factor sign convection chosen for this report is shown in Figure 17, IEEE convention. Lagging power factor and reactive power absorption (Q inductive) are treated as synonyms.

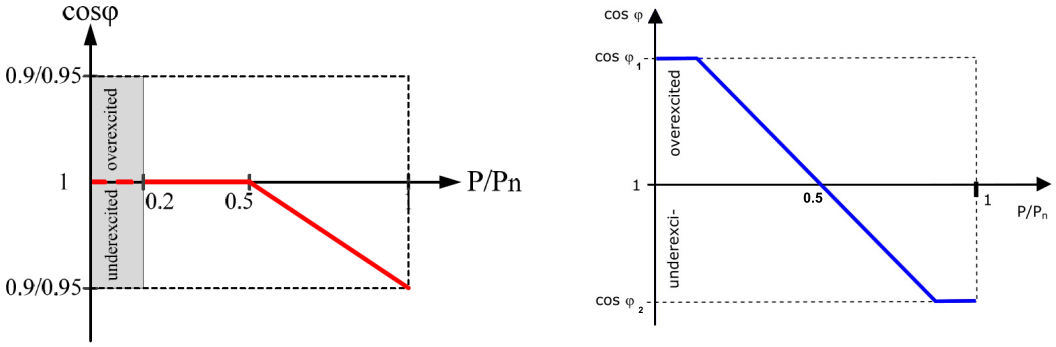

Figure 16. cosφ(P) VDE-AR-N 4105 and BDEW curve

According to Figure 16, at low production levels PV inverters may be required to inject reactive power (capacitive) into the grid by the DSO. When half of the rated power is reached, the power factor decreases towards 0.9/0.95 (function of nominal power) absorbing reactive power (inductive) in order to reduce the voltage level at the PCC. As the over voltage is the relevant issue under study in our case, the first curve is preferable.

The main disadvantage observed is the consumption of reactive power, even at voltage levels within limits. Moreover, as this procedure does not take into account the impedance of the lines, every PV generator will absorb or inject the same amount of reactive power which leads to higher losses (Man, 2012).

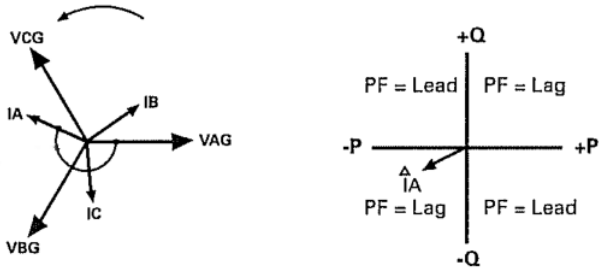

Figure 17. Power factor sign convention (IEEE).

Reactive power variation with voltage - Q(U)

In contrast to cosφ(P) method, the Q(U) strategy calculates the reactive power reference according to the voltage level measured at the PCC of each PV system. The main advantage is the proportional reactive power generation to the voltage level, as a result of the local measurements (Man, 2012). Indeed, this method is aware of the tap changer position of the MV/LV transformer managing a coordinated regulation.

The risk of the local regulation is the misuse of the available power capacity as the inverters located at the end of the line, will work at full capacity while the ones nearby the transformer will be almost stopped. Hence, reliability issues may appear. No electricity producer would like to be forced to reduce the power injection and hence, the revenue. The reactive power and voltage dependency implemented in this study is presented as a red curve in Figure 18.

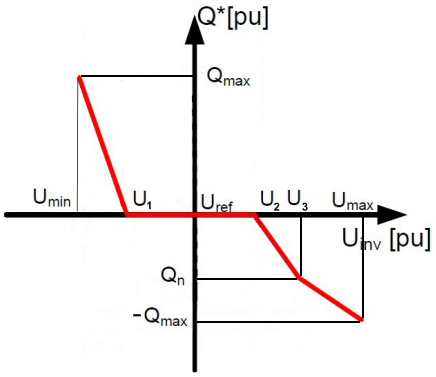

Figure 18. Generic Q(U) curve, (Constantin et al., 2012).

The parameters defined in Figure 18 are:

- A: capacitive operation of the PV inverter.
- B: Dead-band, not injecting or consuming reactive power.
- C: inductive operation of the PV inverter.
- U_{min}: Minimum voltage for the controller to apply maximum capacitive reactive power.
- U_{dmin}: Minimum voltage of dead-band.
- U_{ref}: Reference voltage chosen according to the output voltage of the LV/MV transformer and the voltage tap-setting.
- U_{dmax}: Maximum voltage of dead-band.
- U_{max}: Maximum voltage for the controller to apply maximum inductive reactive power.
- Q_{min}: Maximum under excited reactive power capability.
- Q_{max}: Maximum overexcited reactive power capability.

EN50160 standard (Markiewicz and Klajn, 1999) establishes a voltage magnitude variation criterion of $\pm 10\%$. Hence, as the maximum voltage value allowed at normal operation conditions at the PCC is 3% , the voltage range value employed is:

$$[U_{min}, U_{max}] = [0.9, 1.1] \tag{4}$$

The dead-band region should restrict the injection of unnecessary reactive power while small variations in voltage are present.

Solar plants collect the output power of the different PV converters in a local LV grid and then, the injection is realized in a single point of connection to the MV distribution network. The approach to approximate a group of residences with identical PV converters to a large converter is used.

The PV power system model (unifilar) depicted in Figure 19, consists of an active and a reactive power control models followed by an electrical control model and a converter model. Parameter values and Simulink models are collected in Appendix 1.

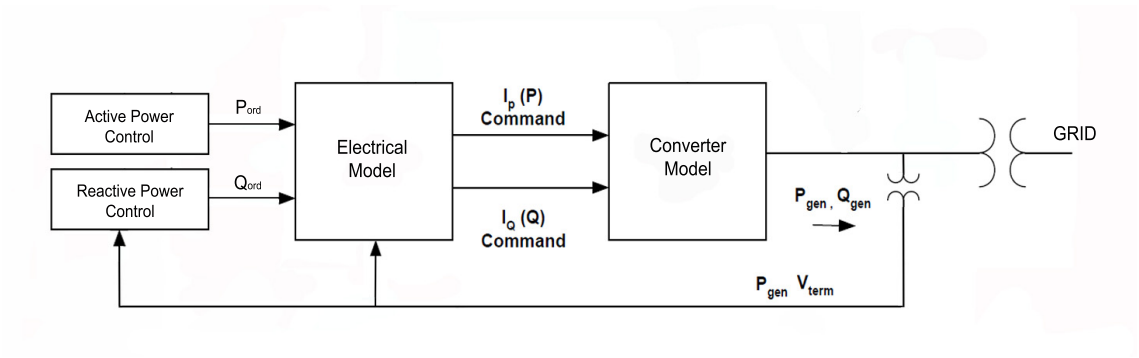

Figure 19. PV solar dynamic model, (Clark et al., 2010).

- **Active Power Control**

  Solar power profiles are uploaded by the user as inputs. The model incorporates the feature of frequency control based on a standard curve, shown in Figure 20. Nevertheless, as frequency control is not relevant for this case, it is not used during the simulations. It is enable by setting *apfflg* to 1.

  According to current solar codes, active power curtailment may be performed by the DNO to keep the energy balance in the network. Therefore, reductions of variable percentage of power production are available by setting *apsel* parameter. This model dictates the active power (P_{ord})to be delivered to the electrical control model.

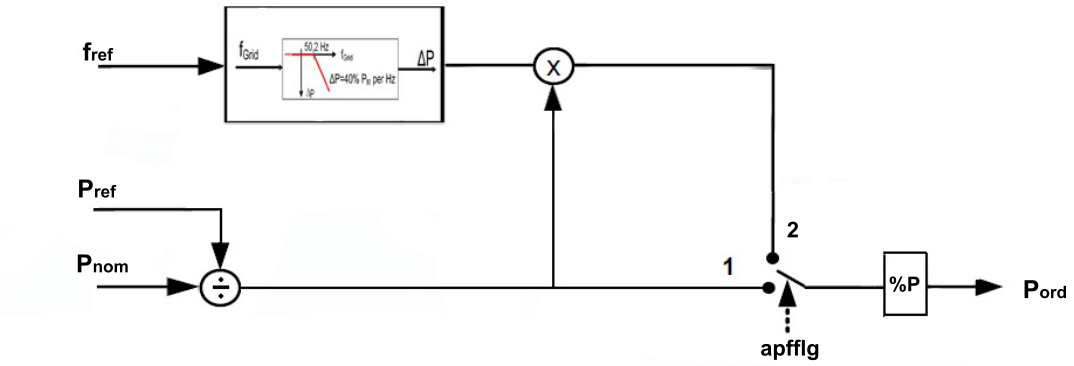

Figure 20. Active Power control model

- **Reactive Power Control**

  A detailed representation of the reactive control model is presented in Figure 21. GE model (Clark et al., 2010) proposes a closed loop based on a PI controller to provide the supervisory VAR output (Q_{ord}), but in solar plants open loops are widely implemented and tested.

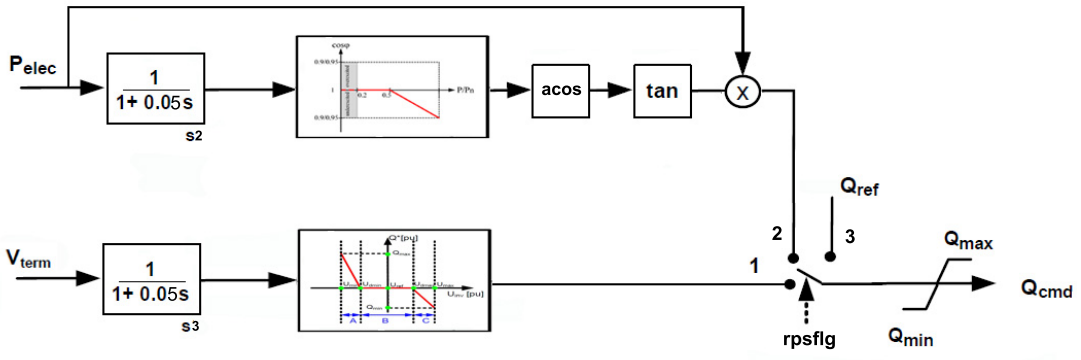

Figure 21. Reactive Power control model, (Clark et al., 2010).

The two reactive power control methods selected are the power factor control and the reactive power variation with voltage. The first one provides the reactive power command (Q_{cmd}) based on the variation of the power factor with the active power production. On the other hand, the calculation of the reactive power of the second depends on the voltage measured at the PCC.

Both curves are implemented in Simulink as Matlab functions (Q_P & Q_volt), defined in intervals and parameters to be optimized afterwards.

- **Electrical control**

  The reactive power command from the reactive power control is compared to the generated by the converter, and the error is then integrated with a gain K_{Vi} to generate the reactive current command (I_{Qcmd}). Additionally, the real current command (I_{Pcmd}) is developed from the power order (P_{ord}) and the terminal voltage (V_{term}). It is shown in Figure 22.

  The converter capability is applied in terms of converter current limits. The priority to active or reactive power is specified by the user with pqflag.

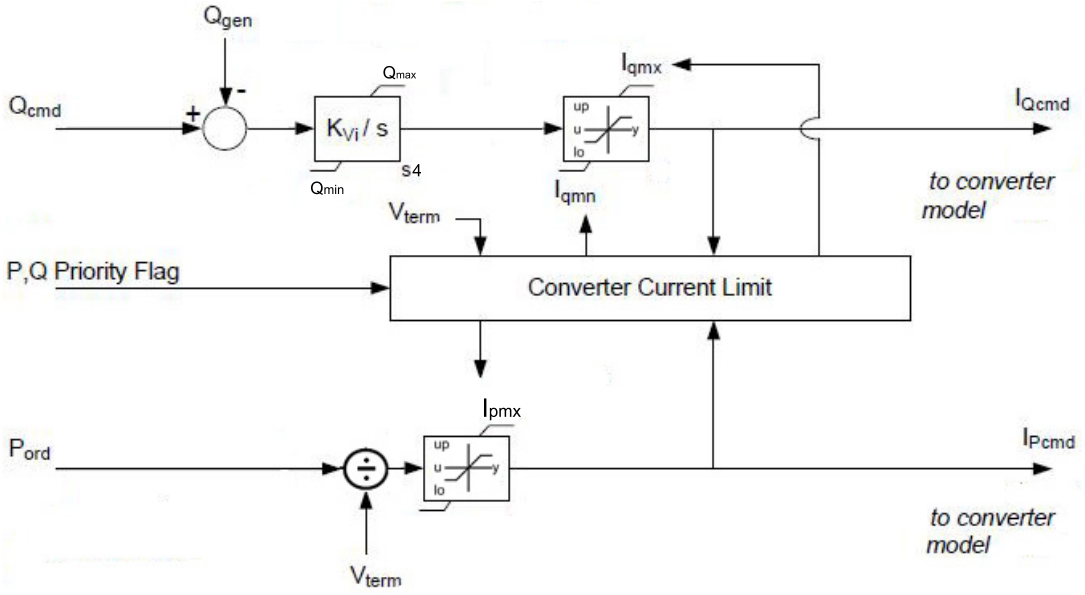

Figure 22. Electrical control model, (Clark et al., 2010).

- **Converter**

  The converter provides the link between the PV panels and the grid. The electrical control model provides the active and reactive current commands to the converter which using three controlled-current sources inject the required current to the grid. The model is presented in Figure 23.

  The small lag (0.05s) provides a reasonable approximation to the fast electronic control system. Both commands are converted to real values by using a base current gain. Single-phase switches allow stopping or restarting the power injection to the grid.

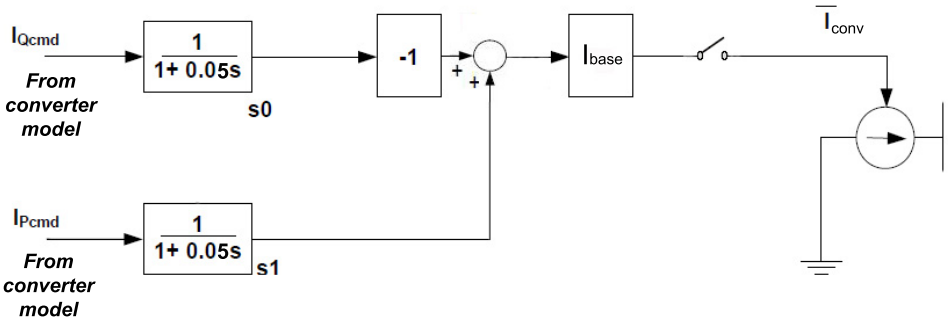

Figure 23. Converter model, (Clark et al., 2010).

VOLTAGE CONTROL

As a secondary control strategy, the OLTC is capable of stepping up and down the voltage in the network, and therefore at the point of injection of the solar inverters if necessary. This technique relies on the development of the distribution transformers technology as the majority of equipment currently installed is manually operated. In addition, a tap change may provoke the costumers at the end of the line to suffer undesirable under voltages. Figure 24 presents a simplified voltage control model developed in Simulink Figure A1.1. The first idea was based on a power factor controlled by a bandwidth average voltage (Caldon et al., 2005). However, the complexity to coordinate it with a local reactive power regulation while keeping it stabled made the final decision to be a bit simpler. A weighted average voltage based on every point of connection was deployed finally.

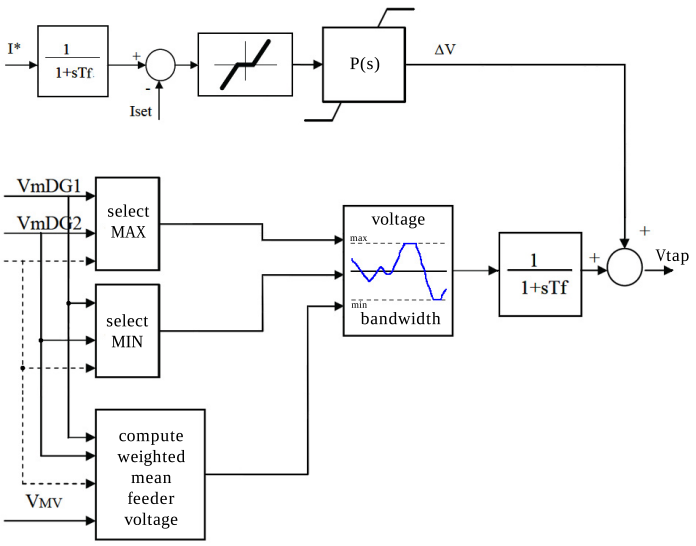

Figure 24. Voltage control model.

3 OPTIMIZATION

In the present electricity network scheme, usage of DG has benefits in power loss reduction. The impact depends especially on the generators location, size and type as well as on the network topology (Teng et al., 2002). A wide number of algorithms have been developed to solve problems of different nature and complexity. For instance, "suitable algorithms designed for linear problems to converge to the optimal solution, do not work properly in non-linear problems" (*Introduction to operations research*, 2006). The presence of multiple local maxima or minima in the objective function forced the development of higher level algorithms which under any conditions converge to the global optimum.

The target of finding the optimal PV penetration in a LV network can be formulated as a non-linear multi-objective optimization problem. The objective functions to be optimized are ORPD and voltage stability. In short, the reactive power sources are allocated so that the active power losses of the grid are to be minimized and the voltage stability margin is to be maximized. The control parameters include the reactive power capacity; the converter voltages and the transformer tap setting. Typically, conventional methods such as gradient-based optimization algorithm (Lee et al., 1985) or interior point method (Momoh et al., 1994), are implemented. However, the main drawback of the low reliability to converge to the global solution, have leaded to the development of evolutionary algorithms as the GA.

Diverse GA has been recently proposed for efficiently solving the ORPD problems. Real implementations (Aruna Jeyanthy and Devaraj, 2010*a*) provide evidence of the useful approach of this technique in optimization problems. The highlighted feature of convergence towards the global solution due to the evaluation of large populations, makes it suitable for many real-world applications (Aruna Jeyanthy and Devaraj, 2010*b*).

A genetic algorithm is defined as a non-deterministic global search technique inspired by the natural selection mechanism. The basic principle is the selection of individuals (solutions) according to their aptitudes to evolve from generation to generation (Anisa Shereen, 2012). The searching procedure of GA algorithms compromises three operators:

1. *Selection* The selection of individuals with highest fitness values from a random initial population is performed to create enhance generations. Non selected individuals are eliminated from the solution (Anisa Shereen, 2012), (Aruna Jeyanthy and Devaraj, 2010*b*).

2. *Crossover* The crossover operator performs the recombination of individuals previously selected with the purpose of increasing the diversity of the population. The swap the genes between two different individuals (parents) forms an new enhance chromosome (Popov, 2005).

3. *Mutation* Mutation operator is used to explore new possibilities of changing some random genes of the population. Most of these changes are caused by mistakes during the crossover process. The low efficiency minimizes its use (Anisa Shereen, 2012), (Popov, 2005).

In this paper, genetic algorithm is used to solve the voltage constrained reactive power dispatch problem. The proposed algorithm identifies the optimal values of generation bus voltage magnitudes, transformer tap setting and the output of the reactive power sources so as to minimize the transmission loss and to improve the voltage stability.

The optimized PV power generation depends on diverse factors such as the type of load, the aggregation level of PV panels, feeders' characteristics or the definition of photovoltaic penetration. Therefore, each specific case needs to be tested in order to get the ideal parameters. As a result, the model designed in this project provides the appropriate dynamic platform to set the network conditions for each case.

3.1 Problem Formulation

A MOGA to minimize the total power losses and the voltage deviation of the LV network is performed. Additionally, the reactive power optimization problem is subjected to a series of constraints that must be fulfilled. The active power losses of the distribution transformer and the LV cable system losses are the target to be minimized. The reactive power losses must be also taken into account, finding the optimal balance between capability and voltage stability.

The optimization problem includes two types of variables: **control variables** and **state variables**. While control parameters are intrinsically restricted by the own algorithm, in terms of lower and upper bounds, he state variables required to add penalty terms in the fitness function to being satisfied.

The Objective function is defined as:

$$\mathbf{f} = \mathbf{min(f1)} + \mathbf{min(f2)} + \boldsymbol{\varphi_1} \cdot \sum_{\mathbf{N_T}} \mathbf{\Delta V_L^2} + \boldsymbol{\varphi_2} \cdot \sum_{\mathbf{N_I}} \mathbf{\Delta Q_G^2} + \boldsymbol{\varphi_3} \cdot \sum_{\mathbf{N_L}} (\mathbf{S_i} - \mathbf{S_i^{max}})^{\mathbf{2}} \tag{5}$$

Where φ_1, φ_2 and φ_3 are penalty factors for those buses where the variables excess the limits.

Control Variables

- MV/LV transformer tap setting parameters [w_1,w_2,w_3,w_4].

  OLTC transformer steps up and down the secondary voltage according to a reference calculated based on an voltage average of all the buses of the grid. The farther to the transformer the larger voltage deviation for the same power injection. Therefore, I decided to implement a weighted average dividing the buses in 4 areas, applying one parameter to each area (w_i). The sum of all must be 1 and also increasing in value from the transformer location. The model can be found in Appendix 1.

- Reactive power capability curve parameters [cosφ_1,cosφ_2,U_1,U_2,U_3,Q_n].

  The first two parameters refers to Figure 16 and the rest to Figure 18. The reason of adding one extra point to over-voltage conditions is the minimization of reactive power consumption of the solar inverters.

- Active power generation level of each solar inverter [apsel]

  The optimal active power production of the solar inverter is a parameter which changes with the network characteristics, especially with the load.

State Variables

- Load bus voltages [$V_{L_{max}}$,$V_{L_{lmim}}$].
- Line flow limit [$S_{i_{max}}$].
- Reactive power limit [$Q_{G_{max}}$,$Q_{G_{min}}$].

Power Losses

Minimization of the power losses will cause a reduction of the costs and hence, a higher efficiency of the system. Power losses can be calculated as described below and the result will be part of the multi-objective fitness function (f).

1. Transformer Losses

   The losses of a distribution transformer are classified as:

   - *Iron Losses (P_h)*

     The power losses at the magnetic iron core of a transformer are constant and can be measured implementing a no-load test. The power consumed by the transformer working at nominal primary voltage and open circuit at the secondary side, corresponds to the iron losses. Hysteresis and Foucault currents are the origin of these losses, which depends on the network voltage, the frequency and the inductance applied over the magnetic circuit (Unicrom, 2012).

   - *Copper Losses (P_{cu})*

     The total energy dissipated when the rated current flows through both windings of a transformer, is known as copper losses. These losses vary proportionally with the square of the currents and the resistance of the windings. Dealing with a three-phase system, it is multiplied by 3.

$$P_{cu} = 3 \cdot (I_1^2 \cdot R_1 + I_2^2 \cdot R_2) \simeq 3 \cdot R_e \cdot I_1^2 \tag{6}$$

     Where:

     I_1, I_2 = primary and secondary currents.

     R_1, R_2 = primary and secondary resistance.

     R_e = Equivalent transformer resistance.

     The resistance values are defined as:

$$R_i = \frac{P_{cu_{nom}}}{I_{in}^2} = \frac{P_{cu_{nom}}}{(\frac{S_n}{U_{in} \cdot \sqrt{3}})^2} \tag{7}$$

     Where:

     I_{1n}, I_{2n} = primary and secondary nominal currents (A).

     U_{1n}, U_{2n} = primary and secondary nominal line voltages (V).

     S_n = transformer nominal power (VA).

All values are collected in Appendix 1. In practice, the copper losses can be measured when the secondary winding is shorted and the primary is supplied with enough voltage to reach both rated currents.

Hence, the total transformer power losses are:

$$P_T = P_h + P_{cu} \tag{8}$$

2. Cable Losses

   Power losses in cables are defined as current-dependent and voltage-dependent. While the first type refers to the heat dissipation in metallic conductors such as copper, the second one focuses on cable insulation losses.

   For our case, only the copper losses are considered in all three phases. Aiming the calculation of the total power losses of the network, all line losses will be added together as following:

$$P_L = \sum 3 \cdot I_i^2 \cdot R_i, \quad i = 1 : m \qquad m : number\ \ of\ \ lines \tag{9}$$

   The total power loss to minimize in the system as well as the first component of the fitness function is:

$$\mathbf{f_1} = \mathbf{P_{loss}} = \mathbf{P_T} + \mathbf{P_L} \tag{10}$$

Voltage Stability

In the reactive power optimization the second objective consist on the maximization of the voltage stability by means of minimizing the voltage deviation from the voltage reference (1pu) at every point of connection of PV panels to the grid.

$$\mathbf{f_2} = \mathbf{V_{dev}} = \sum |\mathbf{V_i} - \mathbf{V_{ref}}| \quad \mathbf{V_{ref}} = \mathbf{1(pu)} \tag{11}$$

Constrains

1. Equality constraints

   Typically, the equality constraints are satisfied by running a power flow. Nevertheless, the model's design precludes its implementation by the use of current sources

to emulate the power injection of the solar inverters. As a consequence, the solution adopted was running a dynamic analysis to satisfy the constraints.

$$P_{Gi} - P_{Di} = V_i \sum V_j (G_{ij} \cdot \cos\theta_{ij} + B_{ij} \cdot \sin\theta_{ij}), \quad i = 1, 2, ..., N_I \tag{12}$$

$$Q_{Gi} - Q_{Di} = V_i \sum V_j (G_{ij} \cdot \sin\theta_{ij} - B_{ij} \cdot \cos\theta_{ij}), \quad i = 1, 2, ..., N_I \tag{13}$$

The power generated and injected by the PV panels minus the power consumed by the loads must be equal to the power running through the lines or feeders.

2. Inequality constraints The system or network operating limitations are:

   Voltage boundaries:

$$\begin{aligned} &V_{Li}^{min} \leq V_{Li} \leq V_{Li}^{max} && i = N_T \\ &\Delta V_L = V_L^{min} - V_L && V_L < V_L^{min} \\ &\Delta V_L = V_L - V_L^{max} && V_L > V_L^{max} \end{aligned}$$

   Reactive power capability limits:

$$\begin{aligned} &Q_{Gi}^{min} \leq Q_{Gi} \leq Q_{Gi}^{max} && i = N_G \\ &\Delta Q_G = Q_G^{min} - V_G && Q_G < Q_G^{min} \\ &\Delta Q_G = Q_G - V_G^{max} && Q_G > Q_G^{max} \end{aligned}$$

   Line flow restrictions:

$$S_i \leq S_{imax} \qquad i = N_L$$

   Where:
   G_{ij}: conductance between bus i and j
   B_{ij}: susceptance between bus i and j
   θ_{ij}: voltage angle difference between bus i and j
   V_{Li}: bus voltage [pu].
   P_{Gi}: inverter active power injected at bus i [kW].
   P_{Di}: load active power consumed at bus i [kW].
   Q_{Gi}: inverter reactive power injected/consumed at bus i [kVAr].
   Q_{Di}: load reactive power consumed at bus i [kVAr].

S_i: line flow [kVA]
N_I = 30: number of PV inverter and load connection buses.
N_T = 32: number of total buses (adding LV and MV buses of the transformer).
N_L = 32: number of lines.
i: bus under study; j: rest of buses connected to i

All boundary values used are collected in Table 1:

Table 1. MOGA variables and parameters boundaries

MOGA variables boundaries		
Variable	Lower limit	Upper limit
V_L	0.95	1.05 [pu]
P_G	0	5 [kW]
P_D	0	4.75 [kW]
Q_G	-2.18	2.18 [kVAr]
Q_D	-2.3	2.3 [kVAr]
S_i	0	100 [kVA]

MOGA parameters boundaries		
Parameter	Lower limit	Upper limit
w_1	0.01	0.04
w_2	0.02	0.05
w_3	0.025	0.06
w_4	0.04	0.08
cosphi	0.9	1
$cosphi_1$	-0.975	-0.9
U_1	0.95	0.98 [pu]
U_2	1.01	1.04 [pu]
U_3	1.04	1.06 [pu]
Q_n	-0.4	-0.15 [pu]
apsel	0	0.6 [pu]

Figure 25 depicted the flow chart of the MOGA implemented to the Simulink model to optimize the system under different conditions of load and PV penetration.

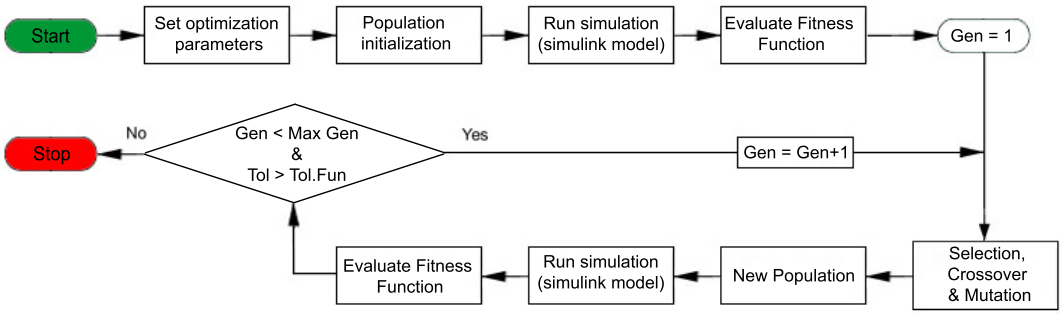

Figure 25. Flow chart of multi-objective genetic algorithm.

3.2 Optimization Simulation Results

MOGA aims to obtain the best fitness function values according to the characteristics of the network and the constraints. Previous studies related to PV penetration in a Bornholm low voltage grid (Constantin et al., 2012), revealed the most suitable amount of PV power to install which minimize the power losses and the voltage deviation. The Matlab code developed to implement the algorithm along with the data acquisition are presented in Appendix 2. Along the following pages, the results obtained when applying MOGA to different network conditions are shown as well as the conclusions after their comparison.

For comparison and validation purposes, all the simulations were run using the same PV power profile, Saturday(August) 10. The reason to choose this profile was its production homogeneity throughout the day. Load profiles from winter and summer days were selected to compare the optimization results. The idea of performing these tests is to compare the results of both Volt/VAR control performance. Once the results are obtained, the model can be used to regulate the voltage and reactive power of all the solar inverters in a LV network, using CompactRIO hardware as data acquisition and EtherLinx as the communication protocol.

Simulation cases:

Despite the fact that four typical Danish domestic residences were chosen, both winter and summer consumptions, only the most relevant are shown below and the rest can be found in Appendix 3. Voltage and VAR controls were enabled and disable to measure the positive or negative effect on the voltage level and the losses.

With the aim to summarizes the optimization result, Table 2 includes the best pareto and parameter values of the fitness function obtain in each simulation case. Red values are the best of the two reactive power techniques compared for each load case.

Table 2. MOGA pareto and parameters values

Case	1	2	3	4	5	6	7	8	9	10
F1	**7.1607**	7.22	**7.692**	8	**6.5635**	6.5905	29.281	**28.381**	**11.146**	11.531
	7.2511	7.253	7.717	6.579	6.644	6.644	31.671	29.955	11.61	10.371
F2	**0.1315**	0.1299	**0.1526**	0.1654	**0.0702**	0.0711	1.492	**0.499**	**0.25107**	0.2591
	0.1259	0.1287	0.1506	0.1519	0.069	0.0699	1.386	0.4639	0.2504	0.2271
apsel(%)	**4.52**	4.4	**9.6**	9.55	**2.9**	2.88	18.55	**18.8**	**14.39**	15.02
	2.77	5.4	10.4	15.59	2.2	4.22	10.46	24.5	17.86	26.9
$cosphi_1$	0.949		0.9519		0.9509		0.961		0.9483	
	0.905		0.9506		0.9532		0.986		0.9837	
$cosphi_2$	-0.906		-0.934		-0.941		-0.941		-0.944	
	-0.901		-0.938		-0.934		-0.941		-0.946	
U_1		0.963		0.957		0.961		0.979		0.979
		0.963		0.9604		0.961		0.979		0.978
U_2		1.024		1.018		1.021		1.020		1.022
		1.023		1.016		1.023		1.020		1.017
U_3		1.048		1.047		1.045		1.045		1.048
		1.048		1.046		1.046		1.045		1.047
Q_n		-0.34		-0.28		-0.275		-0.28		-0.32
		-0.3		-0.3		-0.245		-0.27		-0.32
w_1	0.027	0.019	0.019	0.016	0.017	0.018	0.015	0.019	0.016	0.019
	0.027	0.019	0.023	0.015	0.017	0.018	0.016	0.019	0.016	0.019
w_2	0.029	0.029	0.027	0.028	0.030	0.029	0.028	0.029	0.031	0.029
	0.029	0.029	0.028	0.031	0.029	0.029	0.028	0.029	0.031	0.029
w_3	0.029	0.035	0.034	0.037	0.035	0.035	0.034	0.035	0.036	0.035
	0.029	0.035	0.032	0.037	0.035	0.035	0.034	0.034	0.036	0.035
w_4	0.043	0.046	0.048	0.048	0.048	0.046	0.052	0.047	0.048	0.046
	0.043	0.046	0.043	0.048	0.048	0.046	0.051	0.048	0.048	0.046

Where:

- F_1, F_2: fitness function values(losses and voltage)
- apsel: PV power in % of nominal power
- $cosphi_1$,$cosphi_2$: cosphi(P) curve under/overexcited parameters
- U_1,U_2,U_3,Q_n: Q(U) curve parameters
- w_1,w_2,w_3,w_4: weighted average voltage parameters

Table 3. Simulation cases

Case	Load	Season/day	Reactive power control
1	1	winter/Wednesday	cosφ(P)
2	1	winter/Wednesday	Q(U)
3	3	winter/Sunday	cosφ(P)
4	3	winter/Sunday	Q(U)
5	3	summer/Sunday	cosφ(P)
6	3	summer/Sunday	Q(U)
7	5	winter/Sunday	cosφ(P)
8	5	winter/Sunday	Q(U)
9	5	summer/Sunday	cosφ(P)
10	5	summer/Sunday	Q(U)

In the following pages, results of voltage, active and reactive power, feeder's loading and losses are presented and compared. The rest of results are gathered in Appendix 3.

Voltage

The voltage values at the point of connection of the solar inverters to the grid are measured. These values will vary according to the active power and reactive power injected or consumed by the inverter. According to the regulation (Markiewicz and Klajn, 1999), the voltage limits (-10%,+10%) are represented with blue lines. On the other hand, the voltage unbalance limit is set to 5% for LV networks. Thereby, the network voltage control was designed to change the tap when voltage exceeds 5% of the reference value (F2 is the sum of deviations).

The pictures below compare the simulated voltages for both VAR control techniques with the 2 representative loads winter/summer (see Figures 11, 12, 13), but the same PV power profile during 24 hours. Voltage control effect is compared at the same time.

Load 3 (summer)

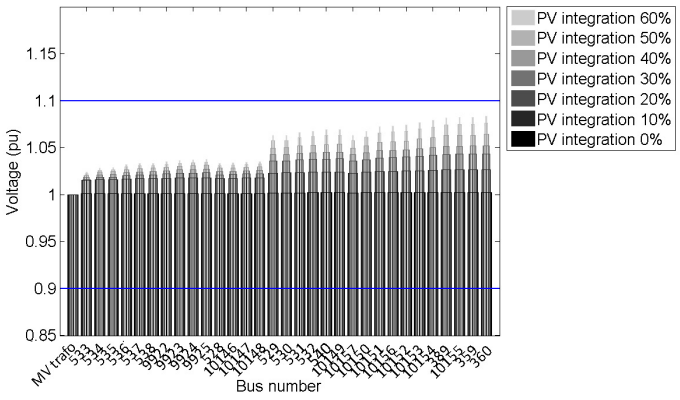

Figure 26. cosφ(P) voltage values at PCC. Network voltage control disable.

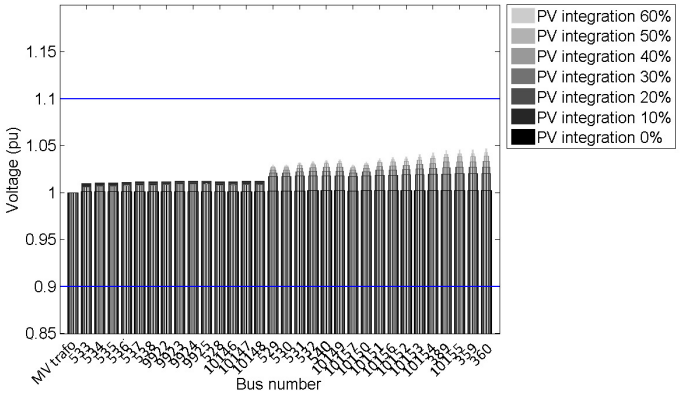

Figure 27. Q(U) voltage values at PCC. Network voltage control disable.

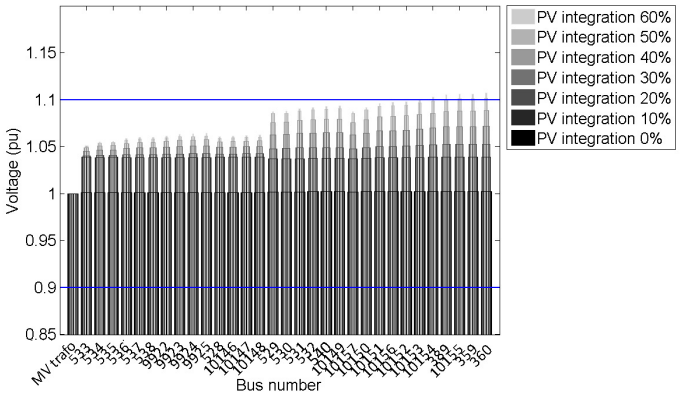

Figure 28. cosφ(P) voltage values at PCC. Network voltage control disable.

The limit of 10% over voltage is reached at 60% PV installation or higher, but only when cosφ(P) curve is implemented in the inverter. This worst case is depicted in Figure 31. Otherwise, voltages at higher penetration levels goes up until 5-6%. Thereby, Q(U) curve manage to keep the voltage level closer to the reference especially when the amount of PV power distributed in the grid increases.

Load 5 (winter)

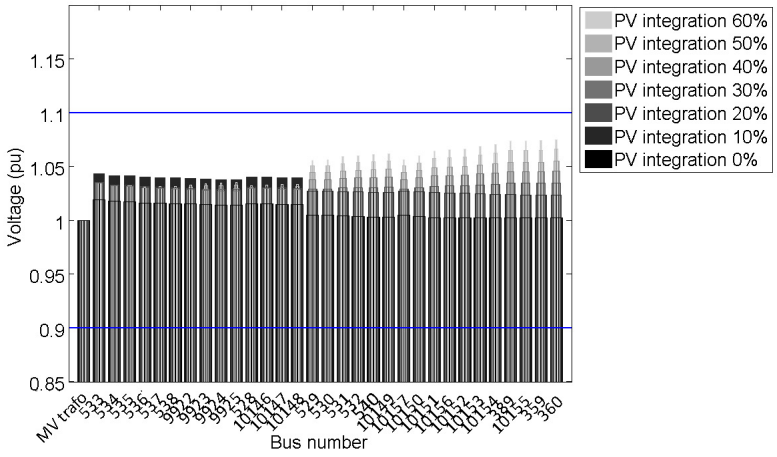

Figure 29. cosφ(P) voltage values at PCC. Network voltage control disable.

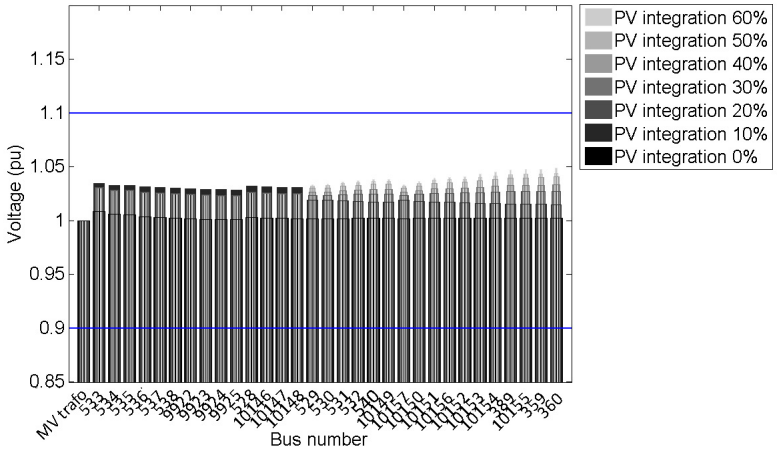

Figure 30. Q(U) voltage values at PCC. Network voltage control disable.

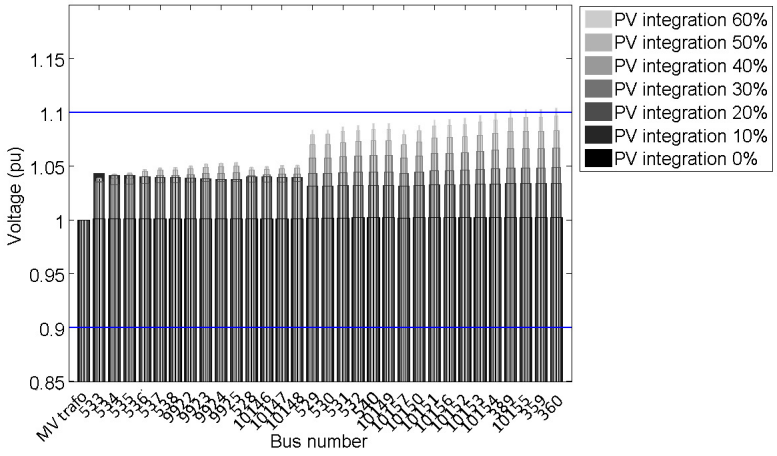

Figure 31. cosφ(P) voltage values at PCC. Network voltage control disable.

In all cases, Q(U) control achieves better results, reducing the voltage deviation at all PV penetration levels. On the contrary, applying cosφ(P) control, 5% deviation occurs even at 20% solar integration. Therefore, we can conclude that Q(U) control strategy improves significantly the voltage stability in case of high PV penetration in low-voltage networks. However, other electrical features must be analysed before concluding which reactive power control is better.

Losses

Total losses of the network are minimized in the optimization process (F1). Losses in the feeders grow faster than the transformer losses. Reactive power and voltage control techniques are compared within each other.

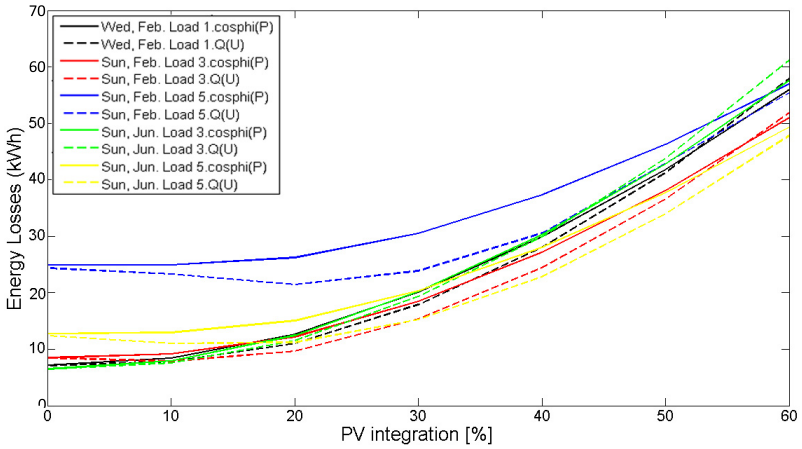

Figure 32. cosφ(P) vs Q(U) losses with network voltage control enabled.

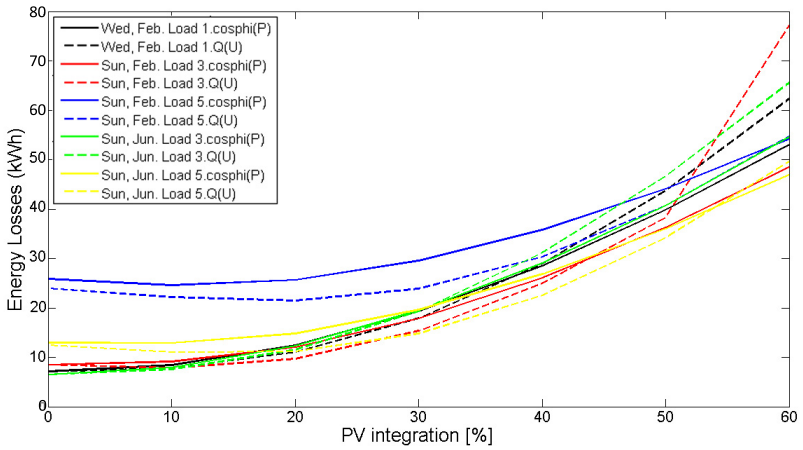

Figure 33. cosφ(P) vs Q(U) losses with network voltage control disabled.

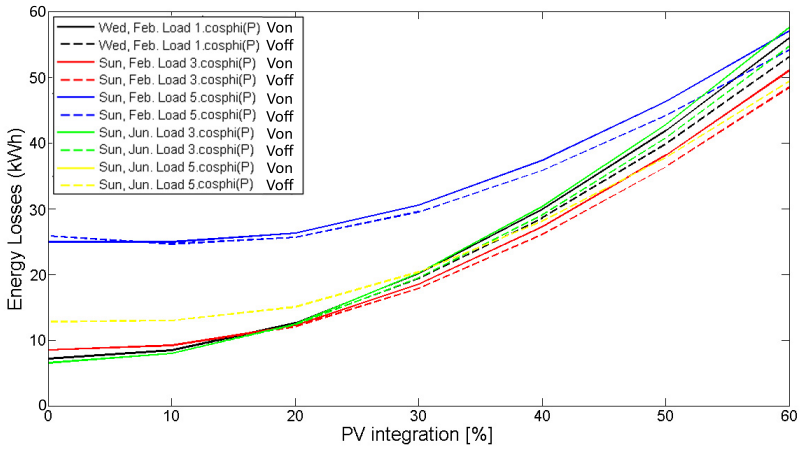

Figure 34. Voltage control enabled vs disabled losses with cosφ(P) control technique.

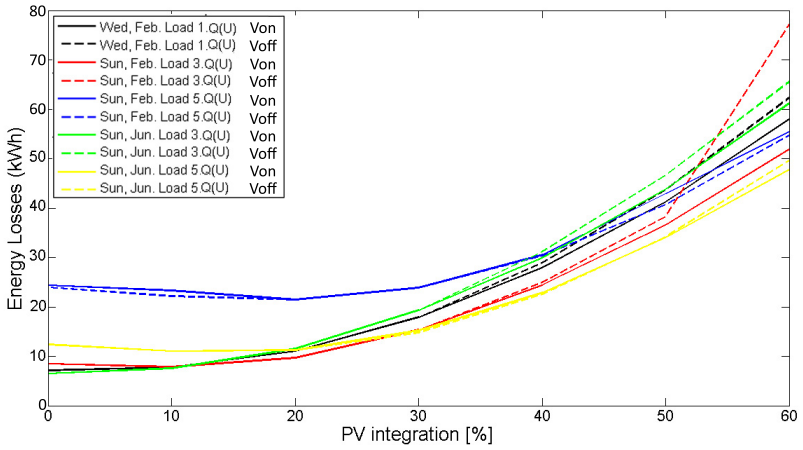

Figure 35. Voltage control enabled vs disabled losses with Q(U) control technique.

According to the graphs, losses are basically equal at low PV penetration levels for both reactive power control curves. However, as the solar power installed increases, the losses differences also increase and Q(U) achieves better results, especially for larger consumers. Losses are reduced at low solar penetration levels, but some loads are such small that it can not be appreciate with the precision of the graphs.

The transformer tap changer helps cosφ(P) to drop losses down as the current injected is lower for the same power produced. On the other hand, the effect is the opposite for Q(U) as the higher the voltage difference the more current injected to the grid. Furthermore, at all solar installation levels the voltage remains closed below the tap changer bounder (2.5% deviation) which leads to high reactive power production and therefore, larger losses.

Feeders loading

Electricity cables are constrained by load flow limits based on the current level. Lines' lifetime strongly depend on the working conditions. Step up and down the network voltage level may affect cables' loading. Thereby, it is required to study this restriction in each of the cases previously compared. The following figures present the lines loading ratio, over nominal loading 100%, in each feeder.

Load 5 (winter)

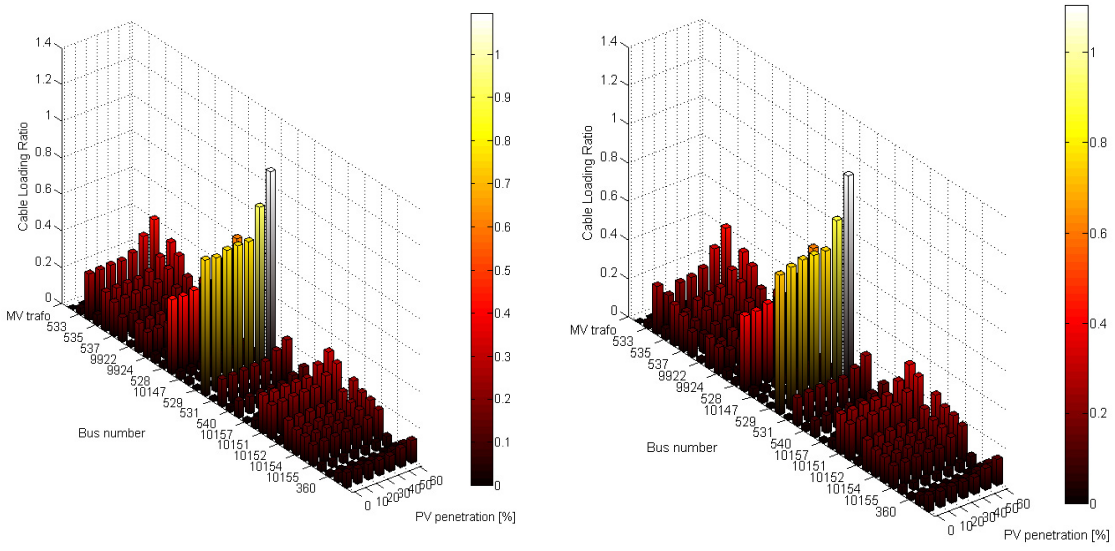

Figure 36. cosφ(P) vs Q(U) load flow ratio with network voltage control enabled.

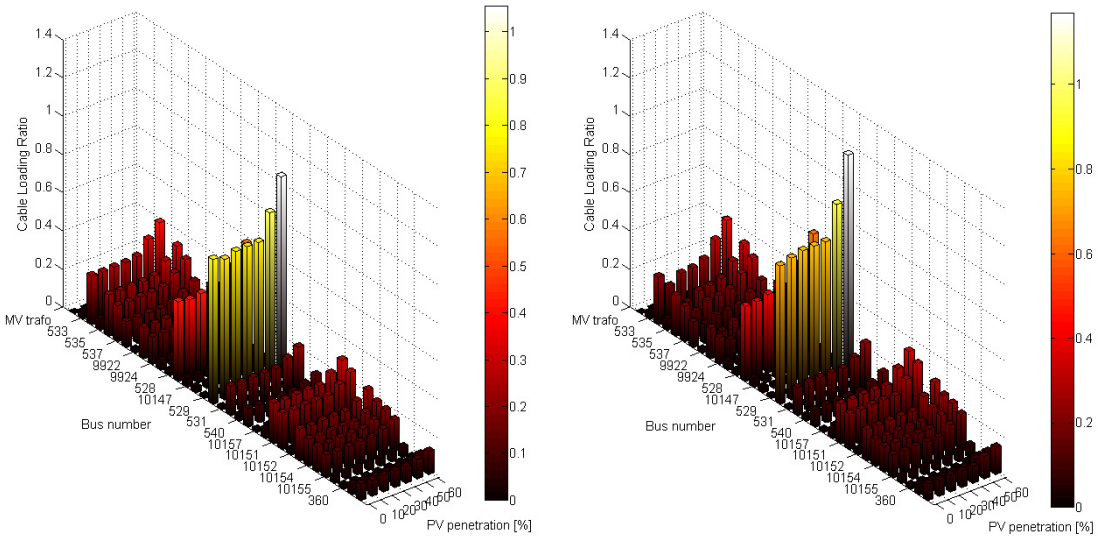

Figure 37. cosφ(P) vs Q(U) load flow ratio with network voltage control disabled.

Load 3 (summer)

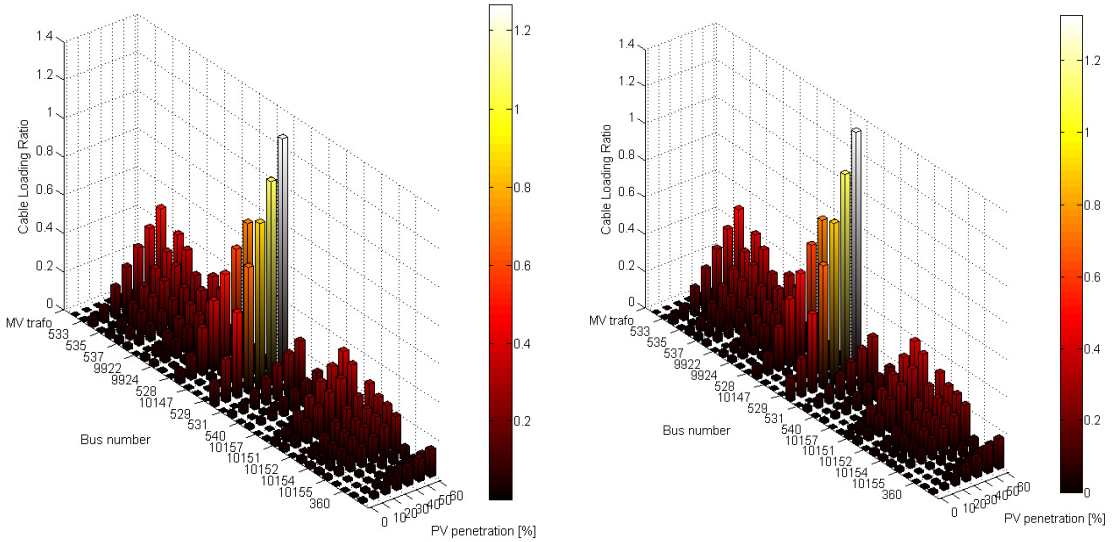

Figure 38. cosφ(P) vs Q(U) load flow ratio with network voltage control enabled.

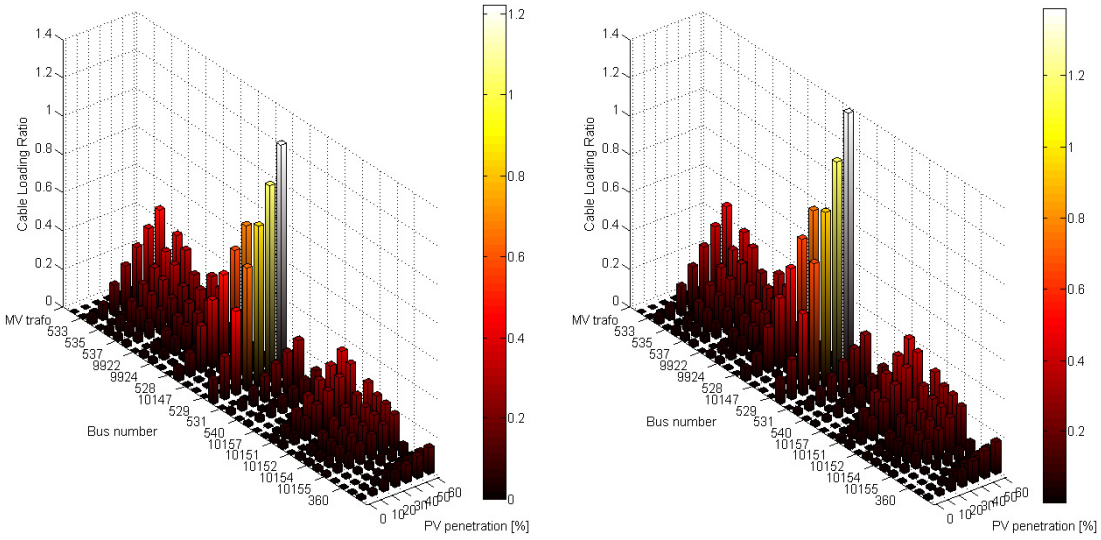

Figure 39. cosφ(P) vs Q(U) load flow ratio with network voltage control disabled.

Over loading conditions occurs at high penetration levels and the situation get worst with Q(U) mode. These results are consistent with the previous ones as the current increase at voltage values near the tap changer limit. Stepping down the voltage contributes to increase weakly the load flow through the feeders.

Cables are well designed to stand up to 50% of PV penetration. Beyond that, the lifetime of cables will decrease considerably. Nevertheless, the optimized values of solar penetration also minimizes the loading levels of feeders.

Transformer's loading

As a consequence of the increasing PV power capacity in the network, the transformer loading situation changes. Active power graphs show over loading conditions in the transformer with more than 30% of solar integration during peak production hours. The worst case studied occurs at 60% penetration when the transformer reaches 1.5 times its nominal capacity. Therefore, considering the transformer rating as a limiting parameter for PV integration, the highest hosting capacity of the Bornholm network is around 40% which corresponds to 140kW.

Peak production and consumption hours mismatch limit the PV installation as a result of the loading and losses conditions. On the other hand, reactive power values differs between control modes. Lower reactive currents, transformer loading and losses are obtained applying Q(U) technique compare to the other strategy.

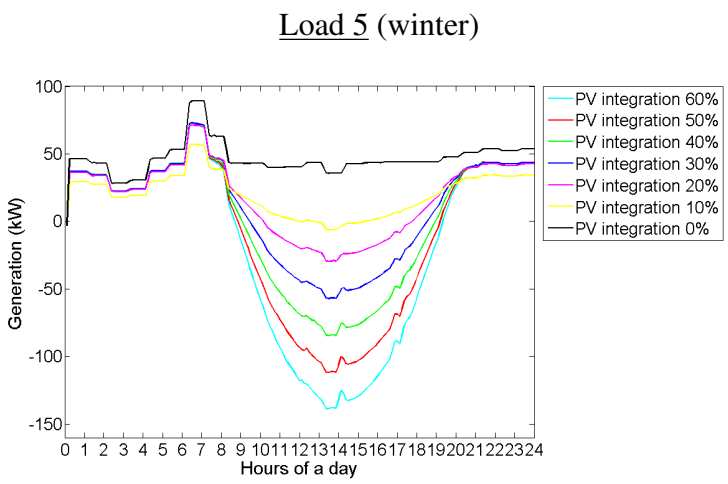

Figure 40. Active power at transformer LV side. Network voltage control enable.

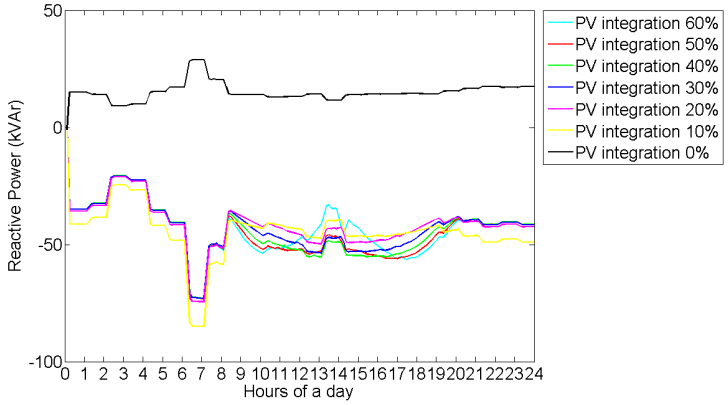

Figure 41. cosφ(P) reactive power at transformer LV side. Network voltage control enabled.

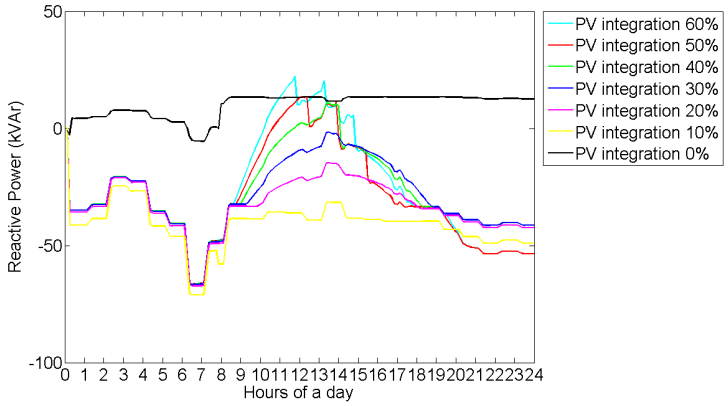

Figure 42. Q(U) reactive power at transformer LV side. Network voltage control enabled.

Load 3 (summer)

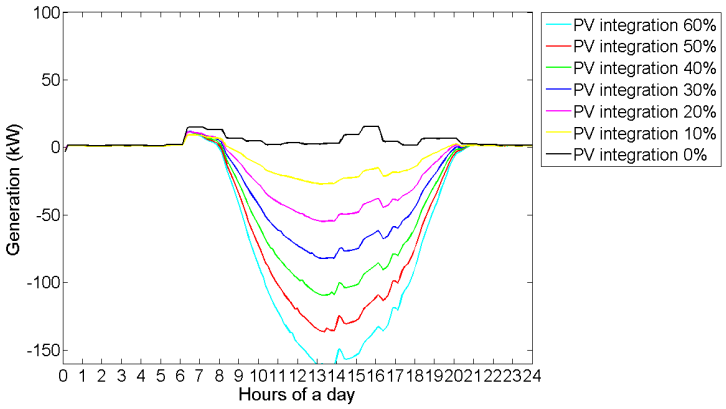

Figure 43. Active power at transformer LV side. Network voltage control enabled.

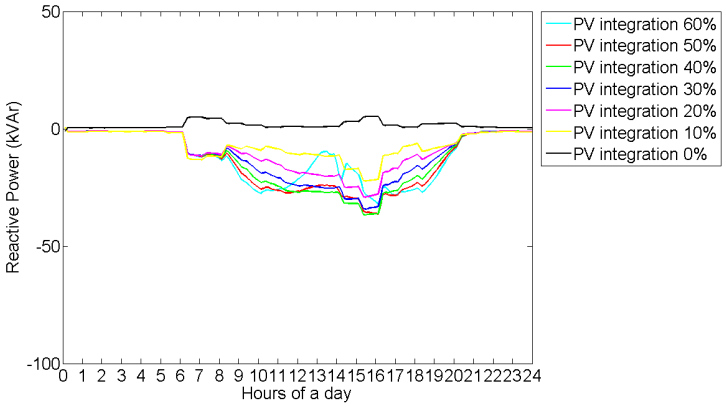

Figure 44. cosφ(P) reactive power at transformer LV side. Network voltage control enabled.

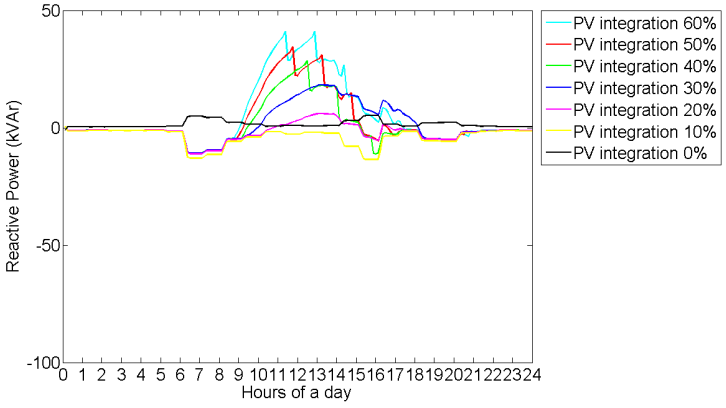

Figure 45. Q(U) reactive power at transformer LV side. Network voltage control enabled.

The graph differences are due to the absorption of reactive power of the inverter with Q(U) applied at over voltages, leading to positive reactive power values through the distribution transformer. On the contrary, low active power injection means reactive power export when implementing cosφ(P) mode.

4 PRACTICAL IMPLEMENTATION

Once modelling and optimization stages are completed and the objective parameter values are obtained, a practical implementation using a real solar inverter is performed. Despite the fact that the model was developed for multi PV inverters installed in a low-voltage grid, the validation process can only be carried out in a single inverter connected to strings of PV modules of a total power of 5kW. In other words, the solar inverter will serve as a testing equipment to compare the simulation results and the real data. A communication platform capable of reading, gathering and sending data at real time between the inverter and the user PC is also developed and tested. NI cRIO hardware was selected for this purpose.

4.1 Hardware: CompactRIO

CompactRIO is a flexible and reconfigurable embedded control and acquisition system. Features such as small and compact size, ruggedness and chassis flexibility make it popular within industrial applications for control purposes. Additionally, it contains all the advantages of NI LabVIEW graphical programming in control and monitoring applications (NI, 2012).

CRIO hardware consists on a solid and reconfigurable FPGA chassis where to place a wide variety of multi-task input/output (I/O) modules, and an embedded controller. I/O modules are easily accessed through LabVIEW FPGA I/O functions. Currently, dozens of modules are available for different measurements. The temperature working ranges goes from -40 °C to 70 °C, covering the majority of industrial and military applications.

The cRIO architecture makes FPGA technology accessible to both high and low level programmers. Reconfigurability allows creating your own control circuitry at low cost and complexity. The lack of operating system usage, increase the reliability of FPGA programming. The main advantages of this device are: small size, low consumption, modularity, wide operating boundaries and graphical representation and design.

4.2 Software: LabVIEW

LabVIEW is a flexible graphical programming environment with powerful configuration-based tools widely used for hardware and software integration purposes. It provides rapid and successful solutions for daily problems and offers the capability to solve future challenges. LabVIEW helps professionals from design to test to obtain the maximum accuracy within the minimum time (NI, 2012). Acquiring data and processing signals, instrument control, embedded monitoring and control systems, are examples of applications.

LabVIEW uses dataflow programming language, based on a graphical block diagram defined by the programmer and executed by order and function. Wires connect blocks and propagate the data. Once all inputs data become available the node can be executed. One main advantage of dataflow language is the possibility of parallel execution.

LabVIEW programs are called VIs. Each one includes a block diagram, a front panel and a connector panel. Controls (inputs) allow the user to supply information and indicators (outputs) display the results. Each VI can be tested before being embedded as a subroutine into a larger program.

4.3 Communication protocol

The inverter chosen to validate the communication protocol developed in LabVIEW code is manufactured by Danfoss. It is a three-phase transformer less inverter(TLX Pro+ series). The inverter's data sheet is shown in Appendix 4.

Regarding the communication system, several protocols are available currently. A communications protocol is defined as a message-based exchange system well-governed by rules used in computing systems and telecommunications. It describes the syntax, semantics and synchronization of communication. Technical standards are developed to help protocols to reach an agreement.

Some examples of industrial protocols for data transfer are:

- CAN bus
- TCP/IP
- UDP

Danfoss offers two types of electrical communication standards with and between the inverters: Ethernet and RS485. As cRIO include en Ethernet connection port, I will focus on that. 'EtherLynx' is the name of the protocol that governs the Ethernet communication with Danfoss inverters. EtherLynx uses *UDP* based on the IP protocol packet sending functionality. The reason to select UDP is the support of messages broadcast which ensures an efficient data transfer and thereby, capable of sending large amount of data among the inverters. UDP port 48004 is used for both packet source and destination.

UDP allows computer applications to send messages to other hosts on an IP network. Suitable applications are those where checking and correction is not performed, minimizing the time of delayed packets. This is not the case of real-time systems.

EtherLynx gives access to a number of inverter parameters, for instance, measurement data from AC and DC sides or status information. In addition, parameters are configurable not just readable.

4.4 Implementation

The first step required to program a LabVIEW code based on EtherLynx protocol (UDP) to communicate with TLX Pro+ inverter connected to solar panels located in the roof of the electrical department in DTU. It is a simple code capable of reading and writing parameters in the inverter. Figures 46, 48 show the block diagram developed. A flexible and easy-working program has been built to read and/or write data from the computer the control board of the inverter.

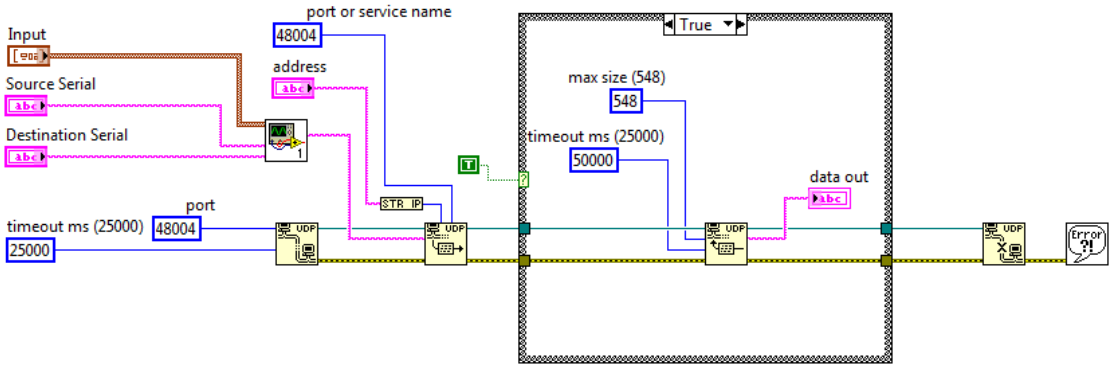

Figure 46. UDP protocol read/write LabVIEW diagram.

The code was firstly tested by means of direct Ethernet communication between the a computer (host) and the solar inverter located in the laboratory. Different reactive power modes and curve parameters were read and set in the control board through EtherLynx protocol. Measurements were performing through a power quality analyser. The electrical power quality analyser, Elspec G4400 Series BlackBox installed in the inverter's cabin, is capable of measuring and recording larger amount of data than its competitors. It is design for continuous measurements, including waveforms, without the need of an external storage or computer. An embedded website provides an interface for the user to set parameter values and configuration at real time. Measurements are deployed in Chapter 5.

After that, cRIO hardware was connected to the inverter as a data acquisition system. Modules NI 9225 and 9227 were selected to measure phase voltages and currents. FPGA programming was required to collect measured data and display it in the computer. Built-in examples were utilized for that purpose. Measurements from both devices were compared in order to validate the platform, see Chapter 5. As an advantage of cRIO, only one device can successfully substitute several BlackBox analysers in a solar plant. Set specific parameters automatically via Ethernet in each inverter based on real time measurements, is the goal to reach implementing cRIO and LabVIEW programming.

An overview of the real system is presented in below:

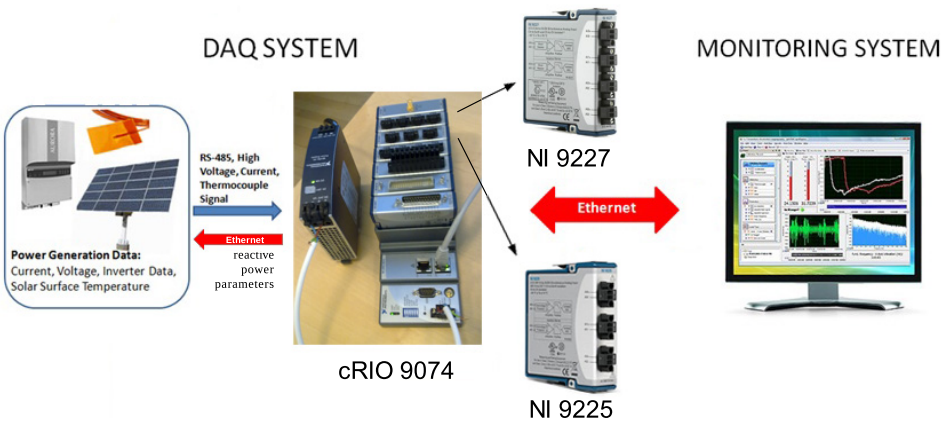

Figure 47. Communication connection scheme.

Typically, in real-time applications cRIO works as stand-alone. However, as the model optimization process takes long time, the final decision to utilize a host computer was taken. Measurements of voltage, current and active power values from the inverter were inputs of simulations, getting reactive power parameters as an output to overwrite.

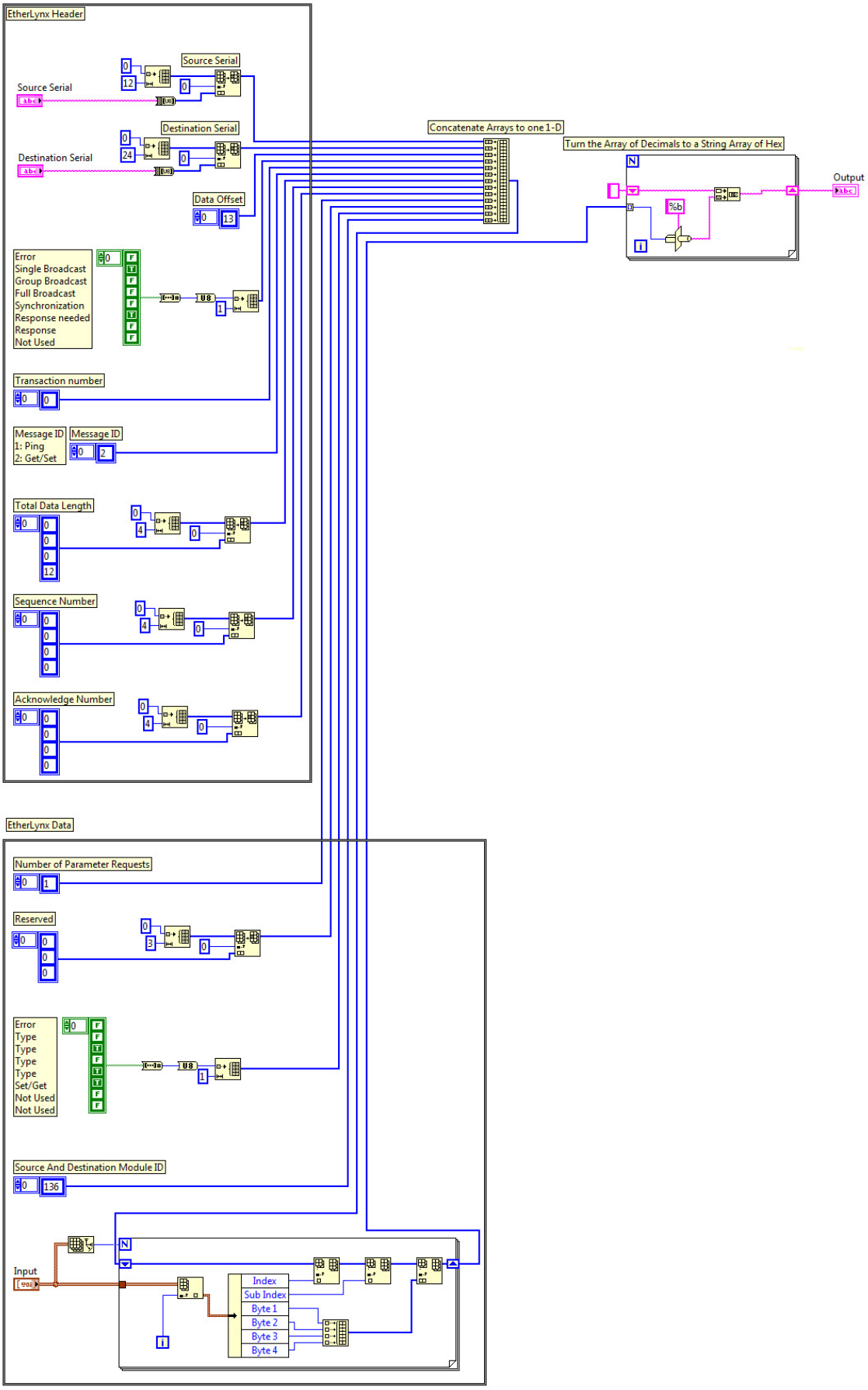

Figure 48. EtherLynx communication protocol LabVIEW send command block diagram.

5 TEST & RESULTS

5.1 Validation Tests

The simulation model developed requires a real LV network with several solar plants installed already to be tested. However, in the university there is just one PV plant of 5kW connected to a 10kW three-phase transformer less solar inverter available. Thereby, it was agreed to enlarge the inverter AC output using a 30 meters cable before the connection to the grid. By this procedure, the voltage raise at the point of injection as a consequence of the larger impedance. The main objective is to visualize the voltage behaviour with the optimized reactive power control parameters implemented and so, validate the theoretical curve parameters in practice.

Due to the length of the cable, it was situated in the floor of the laboratory making several rounds to avoid possible current inductions along it. It was believed to be long enough for the purpose of provoking enough voltage raise. The following section shows and compare the measurements collected using Elspec G4400 Blacbox and cRIO.

5.2 Real measurements

The measured variables are:

- Phase Voltages [V]
- Total Active Power [kW]
- Total Reactive Power [kVAr]
- Power Factor

Measurements were performed along several days in order to get sufficient data to show the proper response of the voltage. Nevertheless, Q(U) curve could not be tested as the new firmware version loaded was partially corrupted and the results obtained were not the expected ones. Data measured with the previous version is included to observe clearer the difference in voltage response when connecting the 30 meters cable to the inverter's output. During a day, diverse reactive power control modes were loaded for comparison purposes.

May 25th, 2012

Figure 49. Elspec measurements 2012. $\cos_{\varphi}$(P) curve.

According to the graph, the reactive power depends on the active power injection, reducing the Q production when the inverter approaches half of its generation capacity. The voltage remains within the limits, reaching a maximum of 1.045pu. The power factor stays close to the unity.

March 25th, 2013

Figure 50. Elspec measurements 2013. Q fixed and $\cos_{\varphi}$(P) curve.

On the other hand, with the cable connected the voltage level rises until 1.078pu (Figure 50) and it is clearly influenced by the power production as aimed. Both graphs show two Q response modes, fixed and power generation dependent. Diverse Q values are set with the purpose of comparing the voltage behaviour. It can be observed lower voltages at the PCC when the inverter absorbs reactive power instead of injecting. Sometimes, network external voltage variations may appear in the measurements.

April 5th, 2013

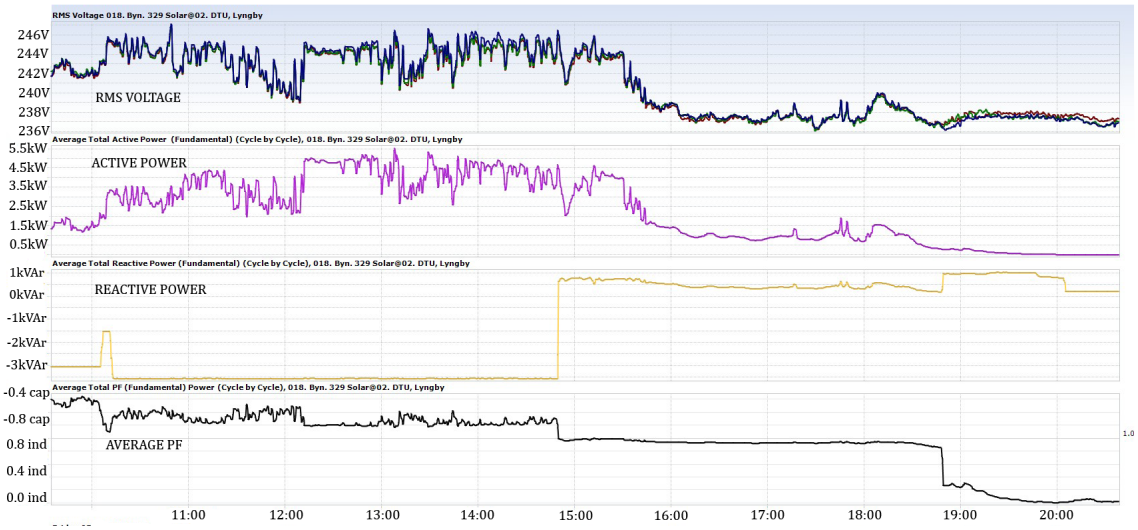

Figure 51. Elspec measurements 2013. Q fixed and $\cos_{\varphi}$(P) curve.

Although the P production is larger (5.5kW, limit) in Figure 51, the voltage remains lower (1.07pu) as a result of Q consumption. These results are consistent with the theory. Unfortunately, as stated before the inverter response for Q(U) curve was not able to be tested due to external conditions and thereby, the optimized parameters obtained in the project will have to be validated in the future.

April 7th, 2013

The last graph shows the electrical waveforms for a constant PF value. Comparing results, the voltage reaches 1.09pu at the maximum production when exporting Q instead of importing. Based on this data, the target of getting an over voltage increasing the impedance has been successfully achieved. The boundary of power generation of the PV power plant, restrict the maximum possible voltage. Under a certain level of active power generation, around 300W, the reactive power mode changes automatically to fixed Q which explains the behaviour at sunrise and sunset times.

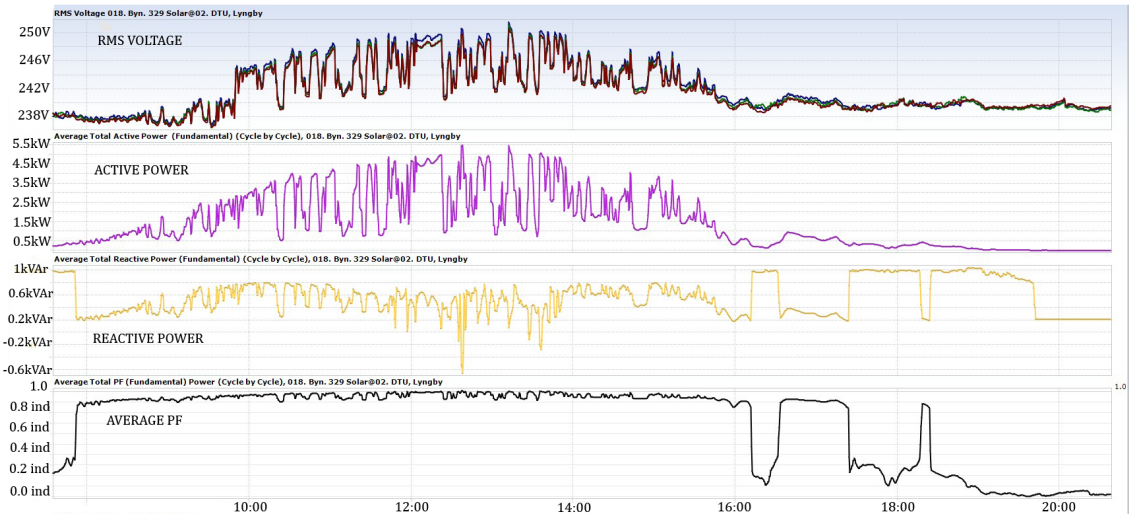

Figure 52. Elspec measurements 2013. $\cos_{\varphi}$ fixed.

5.3 Comparison

Now, Blackbox and cRIO measurements are compared. NI 9225 and 9927 modules were connected through wires to measure voltages and currents directly from the AC output of the solar inverter in the laboratory. An FPGA target was firstly deployed to the control board of the NI hardware using Ethernet communication. This target (VI file) runs embedded, gets time and magnitude values and store the data in FIFO registers (memory), continuously. The host computer calls the target from another VI file and proceeds with the electrical parameters calculation such as peak voltage and current waveforms, active and reactive power, power factor or energy.

The comparison has the objective of validating the self-sufficient data acquisition code which could be extended by programming a closed reactive control loop which could set curve parameters based on the voltage and power measurements. In other words, transform the model designed in Simulink into LabVIEW programming language. The LabVIEW code described in Chapter 4 will be inserted into the FPGA program to run simultaneously with the data measurement. This is considered the final stage of the testing platform that could be enhanced by adding new features required by the network operators and norms.

Aforementioned data, measured at a random time, is depicted below as an example. Voltage and current waveforms of Figure 54 correspond to the peak values of the framed data of Figure 53. RMS values are displayed below the waveforms. Red frames compare both values and they are practically equal.

V/I PU

	RMS	Min Value	Max Value	THD	Crest Factor	K Factor
V_A	239.42 V	0.0000 V	251.72 V	1.4264 %	1.4112	---
V_B	239.72 V	0.0000 V	251.95 V	1.1963 %	1.4115	---
V_C	239.46 V	0.0190 V	252.33 V	1.5334 %	1.4079	---
V_N	1.0794 V	0.0000 V	3.3569 V	- - - -	- - - -	---
V_{AB}	414.80 V	0.0000 V	436.07 V	1.1299 %	1.4160	---
V_{BC}	415.17 V	0.0000 V	436.91 V	1.1502 %	1.4276	---
V_{CA}	414.65 V	0.0000 V	436.36 V	1.3654 %	1.4251	---
I_A	3.5956 A	0.0000 A	10.554 A	8.3623 %	1.6863	1.8426
I_B	3.6704 A	0.0005 A	10.593 A	8.1723 %	1.6391	1.7611
I_C	3.6482 A	0.0005 A	10.570 A	8.5519 %	1.7049	1.8070
I_N	Inf	Inf	Inf	NaN	0.0000	NaN

Figure 53. Elspec voltage & current measurements.

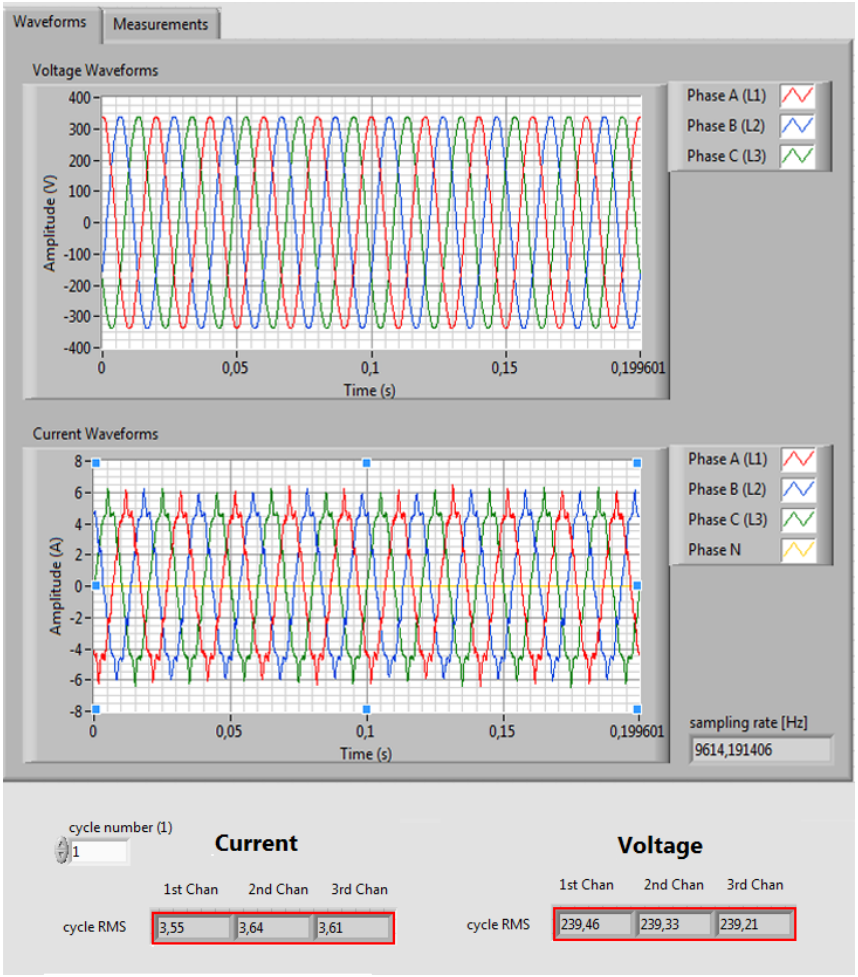

Figure 54. cRIO voltage & current measurements.

Power values of Figure 56 correspond to a single phase and use the opposite sign convention than Figure 55. Power factor is also presented as a negative value, related to inductive mode. Values are sufficiently similar to state that cRIO can properly work as a power analyser.

Power Summary

	Active Power	Reactive Power	Apparent Power	True PF	Displacement PF
Phase A	0.6849 kW	0.5394 kVAr	0.8718 kVA	0.7856 (Ind)	0.7907 (Ind)
Phase B	0.7103 kW	0.5392 kVAr	0.8918 kVA	0.7965 (Ind)	0.8026 (Ind)
Phase C	0.6982 kW	0.5398 kVAr	0.8825 kVA	0.7911 (Ind)	0.7949 (Ind)
Neutral	^^^^^ (o/fl)	NaN	Inf	0.0000 (Ind)	---
Total	**2.0934 kW**	**1.6184 kVAr**	**2.6461 kVA**	**0.7911 (Ind)**	**0.7961 (Ind)**

Figure 55. Elspec power measurements.

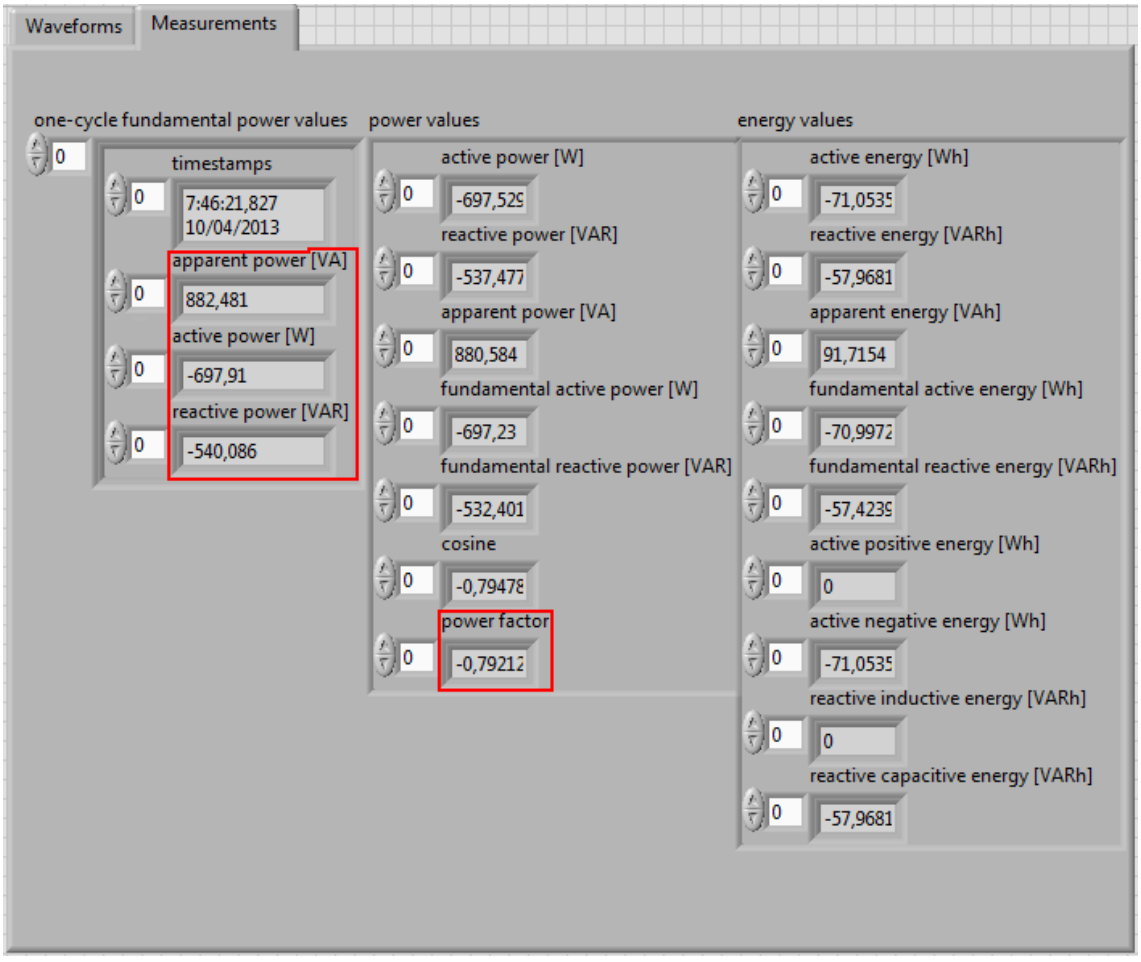

Figure 56. Elspec power & energy measurements.

6 CONCLUSIONS & DISCUSSION

6.1 Summary

This thesis provides the flexible testing platform capable of studying the possible hosting capacity for photovoltaic distributed generators of low-voltage networks. The principal objective of the current project is to validate the effectiveness of reactive power control strategies in voltage control with different PV power installed through the design and validation of a model. The maximum amount of PV power integration allowed is directly related to the characteristics of the network. In this specific case, constrains are: power losses, overloading of MV/LV transformer and cables, and over voltages at every PCC. The PV penetration level has been defined as in (Constantin et al., 2012), where 100% correspond to 5kW PV power install by all costumers in the grid.

A representative network of Bornholm system (71 consumers) has been modelled in Simulink software to perform the optimization of power losses and voltage. The solar inverter reactive control has been modelled implementing two types of control: $\cos_{\varphi}$(P) which depends on the active power output of the inverter and Q(U) based on the voltage value at the point of connection to the grid. The first, forces the reactive power to be independent of the distance to the transformer while the second works as an open loop trying to regulate the reactive power according to the voltage deviation from the reference. Theoretically, $\cos_{\varphi}$(P) shows better performance in the voltage control as all inverters actuate independently of the voltage level. However, the larger amount of losses reduces its efficiency. Nowadays, control operators require flexibility in terms of reactive power injection and consumption throughout the day, which lead the solar plants to be updated.

Furthermore, a network voltage control has been designed based on an On-Load Tap-Changer transformer capable of stepping up and down the voltage at the low-voltage side in order to keep the level in range. It works as a secondary control supporting the VAR control. This technology is still under research but soon will be implemented as a consequence of its advantages. In the model the voltage is calculated as a weighted average value based on the distance to the transformer.

The PV power production profiles utilized were measured during a summer week in an inverter located in the laboratory of the electrical department in DTU. On the other hand, the consumption profiles were obtained from typical Danish domestic consumers at different days of the year. According to this scheme, optimization simulations were perform

using both VAR control strategies with the purpose of observe the influence of each one upon network electrical parameters. A genetic algorithm was selected to obtain the PV power installation with the lowest power losses and voltage deviation, in each case.

Finally, a validation of the model has been realized by comparison of real measurements and optimization results. Communication via Ethernet implemented in LabVIEW software was developed and tested in the laboratory using the inverter connected to the PV panel of the roof. A long cable (large impedance) was connected between the inverter and the network for voltage variation purposes.

6.2 Achievements

The first relevant result obtained from the simulations is that depending on the consumption level the system optimal losses conditions differs, varying from 5% to 20%. This leads to a considerable amount of energy savings along the year, as calculated in (Constantin et al., 2012). However, in this study the advantage of using one reactive power control or another, and the effectiveness of the network voltage control are more interesting.

Based on the results, it can be conclude that Q(U) mode provides better results even at low PV power penetrations as a result of reducing the reactive power flow through the feeders. For small levels (5-10%), both controls achieve equal power losses but the feeders loading is lower when applying power factor mode. The raise of the current as a result of a voltage control via reactive power, increase the power flow and therefore, the losses a bit in these case. Nevertheless, as the PV power integration grows the efficiency of Q(U) control also does. The main drawback of $\cos_{\varphi}$(P) is the feed-forward of the active power which force all inverters to consume the same amount of reactive power independently of the distance to the transformer or the voltage level.

The implementation of MOGA brings a set of ideal reactive power curve parameters which leads to an optimal solution. The results indicate that a dead-band around the reference in Q(U) curve reduces the losses as well as modify the voltage sensitivity of the farthest inverters to the transformer. Meanwhile, the power factor improves its behaviour allowing injecting reactive power during overexcited conditions. The voltage level is considerably enhanced by applying reactive power control.

One more conclusion to be highlighted is that increasing the size of the transformer only improves the overloading condition but not the network voltage issue. On the contrary, PV penetration level can be increased even further by lowering the tap position in the MV/LV transformer having sufficient PV capacity to provide reactive power during the load peaks. This feature can be managed by installing an OLTC transformer similar to the ones typically used in transmission lines. The evolution of power electronics makes it feasible and profitable. The lifetime of the transformer can be increased if minimizing the amount of overloading hours.

In summary, when over voltages are observed at the end-customer site, both reactive power control strategies have beneficial effects. A tap changer may be used if necessary when the reactive control is not enough or even limiting the active power production at certain moments could be a solution. The communication bridge between the user and the inverter allows a continuous data transfer and hence, control of the electrical parameters. It has been validated the benefits of reactive power control in voltage regulation with high solar power installed. CRIO provides the flexibility of a stand-alone functioning plus the real-time power quality analyser. All the inverters in the network can be regulated and connected via Ethernet from a host computer through cRIO.

6.3 Future Work

The main idea is to provide a flexible computing tool capable of simulating different scenarios and provide optimal solutions. The conclusions obtained in this thesis may be used for further studies related to PV integration in LV networks. One good direction could be to analyse different types of solar power production and new and modern types of consumers in order to obtain the optimum reactive power technique recommended for each network or time schedule functioning. The expansion of the research to other types of grids would offer a wider view of the efficacy of reactive power control strategies in raising hosting capacity networks.

More study cases on Q(U) and $\cos_{\varphi}$(P) curves can be performed, with and without the tap changer transformer. Financial comparison of the profitability of updating the MV/LV transformer and the feeders to increase the hosting capacity of the network is suggested. An additional future analysis direction is the research of more advance VAR control techniques such as Q(U,P) or $\cos_{\varphi}$(U,P) which minimize the total power losses and voltage deviation with the optimum reactive power control.

Additionally, an extension of the simulation from daily to yearly losses could be arranged gathering solar production and load data for this period. Another possible study branch could be the implementation of embedded or stand-alone functioning of cRIO. FPGA programming provides a solution to set the proper parameters to the inverter at real-time according to the electrical data measured. Additionally, optimize the simulation model in terms of computational time to work embedded in the national instruments hardware.

REFERENCES

Anisa Shereen, M. (2012), Optimal allocation of dg units for radial distribution systems using genetic algorithm, *in* 'International Journal of Engineering and Advanced Technology'.

Aruna Jeyanthy, P. and Devaraj, D. (2010*a*), Multi-objective genetic algorithm for reactive power optimization inclusing voltage stability, *in* 'International Journal of Engineering Science and Technology'.

Aruna Jeyanthy, P. and Devaraj, D. (2010*b*), Optimal reactive power dispatch for voltage stability enhancement using real coded genetic algorithm, *in* 'International Journal of Computer and Electrical Engineering'.

Barker, P. P. and Mello, R. W. D. (2000), Determining the impact of distributed generation on power systems. i. radial distribution systems, *in* 'Power Engineering Society Summer Meeting, IEEE'.

Bauer, P. and De Haan, S. (1999), Solid state tap changers for utility transformers, *in* 'Africon, IEEE'.

Bauer, P. and Schoevaars, R. (2003), Bidirectional switch for a solid state tap changer, *in* 'Power Electronics Specialist Conference. IEEE 34th Annual'.

Braun, M., Stetz, T., Reimann, T., Valov, B. and Arnold, G. (2009), Optimal reactive power supply in distribution networks - technological and economic assessment for pv-systems, *in* '24th European Photovoltaic Solar Energy Conference'.

Brewin, B., Jupe, S., Bartlett, M., Jackson, K. and Hanmer, C. (2011), New technologies for low voltage distribution networks, *in* 'Innovative Smart Grid Technologies (ISGT Europe), 2nd IEEE PES International Conference and Exhibition on'.

Caldon, R., Turri, R., Prandoni, V. and Spelta, S. (2004), Control issues in mv distribution systems with large-scale integration of distributed generation, *in* 'Bulk Power System Dynamics and Control-VI'.

Caldon, R., Turri, R., Prandoni, V. and Spelta, S. (2005), Co-ordinated voltage regulation in distribution networks with embedded generation, *in* 'CIRED - 18th International Conference and Exhibition on Electricity Distribution'.

Chung, Y., Kwon, G., Park, T. and Lim, K. (2003), Dynamic voltage regulator with solid state switched tap changer, *in* 'Quality and Security of Electric Power Delivery Systems. CIGRE/PES International Symposium'.

Clark, K., Miller, N. W. and Walling, R. (2010), Modelling of ge solar photovoltaic plants for grid studies, Technical report, GE Energy.

Constantin, A., Lazar, R. D. and Kjær, D. S. B. (2012), Voltage control in low voltage networks by photovoltaic inverters - pvnet.dk, Technical report, Danfoss.

D'Adamo, C., Jupe, S. and Abbey, C. (2009), Global survey on planning and operation of active distribution networks, *in* '20th International Conference and Exhibition on Electricity Distribution, CIRED'.

Demirci, O., Torrey, D. A., Degeneff, R. C., Schaeffer, F. K. and Frazer, R. H. (1998), 'A new approach to solid-state on load tap changing transformers', *Power Delivery,IEEE* .

Demirok, E., Sera, D., Teodorescu, R. and Frederiksen, K. (2011), An optimized local reactive power control for high penetration of distributed solar inverters in low voltage networks, *in* '26th European Photovoltaic Solar Energy Conference and Exhibition'.

ENTSOE (2012), 'Network code for requirements for grid connection applicable to all generators'.
URL: *https://www.entsoe.eu/resources/network-codes/requirements-for-generators/*

Expósito, A. G. and Berjillos, D. M. (2007), 'Solid-state tap changers: New configurations and applications', *Power Delivery, IEEE Transactions on* .

Grid Converters for Photovoltaic and Wind Power Systems (2011), IEEE.

Hashim, T. J. T., Mohamed, A. and Shareef, H. (2012), 'A review on voltage control methods for active distribution networks', *PRZEGLAD ELEKTROTECHNICZNY* .

Hemdan, N. G. A. and Kurrat, M. (2012), Distributed generation location and capacity effect on voltage stability of distribution networks, *in* 'Transmission and Distribution Conference and Exposition (T D), IEEE PES'.

Hidalgo, R., Abbey, C. and Joós, G. (2010), 'A review of active distribution networks enabling technologies', *Power and Energy Society General Meeting, IEEE* .

Hiroyuki, H. and Kobayashi, H. (2007), A study of centralized voltage control method for distribution systems with distributed generation, *in* '19th International Conference on Electricity Distribution - CIRED'.

IEA, I. E. A. (2010), 'World energy outlook'.
URL: *http://www.iea.org/Textbase/npsum/weo2010sum.pdf*

Introduction to operations research (2006), McGraw-Hill.

Jorgensen, J., Sorensen, S., Behnke, K. and Eriksen, P. (2011), Ecogrid eu - a prototype for european smart grids, *in* 'Power and Energy Society General Meeting, IEEE'.

Kaestle, G. and Vrana, T. K. (2011), Improved requirements for the connection to the low voltage grid, *in* '21st International Conference on Electricity Distribution - CIRED'.

Kumm, D. T. (2011), Vde-ar-n 4105 generators connected to the low-voltage distribution network, Technical report, Forum Network Technology (FNN).

Lee, K., Park, Y. and Ortiz, J. (1985), A united approach to optimal real and reactive power dispatch, *in* 'IEEE Trans Pwr Appar Syst'.

Lund, T. (2007), Analysis of distribution systems with a high penetration do distributed generation, PhD thesis, Technical University of Denmark - DTU.

Man, E. A. (2012), Control of grid connected pv systems with grid support functions, Master's thesis, Aalborg University.

Markiewicz, H. and Klajn, A. (1999), En 50160 - voltage characteristics of electricity supplied by public distribution systems., Technical report, European Committee for Electrotechnical Standardization.

McDonald, M. D., Walling, R. A., D"Aquila, R. and Cleary, J. (2012), Effect of distributed generation on regional voltage stability, *in* 'Transmission and Distribution Conference and Exposition (T D), IEEE PES'.

McDonald, P. J. (2008), 'Adaptive intelligent power systems: Active distribution networks', *Energy Policy* .

Momoh, J. A., Guo, S., Ogbuobiri, E. and Adapa, R. (1994), The quadratic interior point method solving power system optimization problems, *in* 'IEEE Trans. Power Syst'.

Monroy, D., Gómez-Expósito, A. and Romero-Ramos, E. (2007), Improving the voltage regulation of secondary feeders by applying solid-state tap changers to mv/lv transformers, *in* '9th International Conference on Electrical Power, Quality and Utilization.'.

NI (2012), 'Labview and compactrio'.
URL: *http://www.ni.com/*

Omole, A. (2010), Voltage Stability Impact of Grid-Tied Photovoltaic Systems Utilizing Dynamic Reactive Power Control, PhD thesis, University of South Florida.

Popov, A. (2005), Genetic algorithms for optimization, Technical report, Florida Gulf-Coast University.

Power Electronics Handbook: Devices, Circuits and Applications (2011), Academic Press.

Santos, M., Salcedo, F., Tedeschi, E., Robles, E. and Villate, J. (2010), Centralized control of a wave energy farm, *in* '13th edition'.

Shuttleworth, R., Tian, X., Fan, C. and Power, A. (1996), 'New tap changing scheme', *Electric Power Applications, IEE Proceedings* - .

Østergaard, J. and Nielsen, J. E. (2012), The bornholm power system - an overview, *in* 'International Conference on Renewable Energies and Power Quality (ICREPQ)'.

Teng, J.-H., Luor, T.-S. and Liu, Y.-H. (2002), Strategic distributed generator placements for service reliability improvements, *in* 'Power Engineering Society Summer Meeting, IEEE'.

Theologitis, I. T., Troester, E. and Ackermann, T. (2011), Aspects of a generic photovoltaic model examined under the german grid code for medium voltage, *in* '1st International Workshop on Integration of Solar Power into Power Systems.'.

Timbus, A. (2007), Grid Monitoring and Advanced Control of Distributed Power Generation Systems, PhD thesis, Aalborg University.

Trebolle, D. T., Marín, P. F., Ortega, J. M. M. and Ramos, J. L. M. (2012), 'El control de tensión en redes de distribución con generación distribuida (i)', *Anales de Mecánica y Electricidad* .

Troester, E. (2009), New german grid codes for connecting pv systems to the medium voltage power grid, *in* '2nd International Workshop on Concentrating Photovoltaic Power Plants: Optical Design, Production, Grid Connection.'.

Unicrom, E. (2012), 'Transformadores de potencia: Pérdidas de potencia de un transformador eléctrico'.
URL: *http://www.unicrom.com/Tut_perdidas_transformador.asp*

Viawan, F. A. (2008), Voltage Control and Voltage Stability of Power Distribution Systems in the Presence of Distributed Generation, PhD thesis, Chalmers University of Technology.

Yang, G. Y., Østergaard, J., Kjær, S. B., Constantin, A., Ballegaard, H. P., Lazar, R. D., Borup, U., Stephansen, C., Mattesen, M. R. and Sørensen, J. B. (2011), Smart integration of photovoltaic power systems on the island of bornholm, *in* '1st International Workshop on Integration of Solar Power into Power Systems'.

Appendix 1. Data and Control Parameters

Table A1.1. Network cable parameters

Cable	Type	Length (km)	Resistance (Ohm/km)	Reactance (Ohm/km)
125LV_528	4X150 AL-M PEX	0.084	0.207	0.078
125LV_533	4X95 AL-M PVICS	0.03	0.321	0.082
528_529	4X50 AL-M PEX	0.105	0.641	0.081
528_1046	4X50 AL-M PEX	0.033	0.641	0.081
533_535	4X95 AL-M PVICS	0.047	0.321	0.082
533_534	4X50 AL-M PVICS	0.103	0.641	0.084
529_530	4X50 AL-M PEX	0.053	0.641	0.081
529_531	4X95 AL-M PVICS	0.076	0.321	0.082
529_10150	4X150 AL-M PEX	0.055	0.207	0.078
529_10157	4X50 AL-M PEX	0.003	0.207	0.078
10146_10147	4X50 AL-M PEX	0.068	0.641	0.081
535_536	4X95 AL-M PVICS	0.068	0.321	0.082
531_532	4X50 AL-M PEX	0.076	0.641	0.081
531_540	4X50 AL-M PEX	0.056	0.641	0.081
10150_10151	4X150 AL-M PEX	0.07	0.207	0.078
10147_10148	4X50 AL-M PEX	0.072	0.641	0.081
540_10149	4X150 AL-M PEX	0.032	0.207	0.078
10151_10152	4X150 AL-M PEX	0.026	0.207	0.078
10151_10156	4X50 AL-M PEX	0.062	0.641	0.081
536_537	4X95 AL-M PVICS	0.038	0.321	0.082
10152_10153	4X150 AL-M PEX	0.051	0.207	0.078
537_538	4X50 AL-M PVICS	0.065	0.641	0.084
537_9922	4X50 AL-M PVICS	0.038	0.641	0.084
10153_10154	4X150 AL-M PEX	0.041	0.207	0.078
9922_9923	4X50 AL-M PVICS	0.035	0.641	0.084
10154_389	4X150 AL-M PEX	0.063	0.207	0.078
389_359	4X150 AL-M PVICS	0.042	0.207	0.084
389_10155	4X150 AL-M PEX	0.026	0.207	0.078
10155_359	4X150 AL-M PEX	0.02	0.207	0.078
9923_9924	4X95 AL-M PEX	0.033	0.321	0.078
359_360	4X50 AL-M PVICS	0.035	0.641	0.084
9924_9925	4X95 AL-M PEX	0.052	0.321	0.078

Appendix 1.

Table A1.2. MV/LV transformer characteristics

MV\LV Transformer D\Y$_n$	
Parameter	Value
S_n	0.1 MVA
f_r	50 Hz
U_{HV}	10 kV
U_{LV}	0.4 kV
Phase Shift	150 deg
Taps	[-5,+5]
$\triangle V_{tap}$	2.5 %

MV\LV Transformer D\Y$_n$	
Parameter	Value
P_{fe}	0.257 kW
P_{cu}	0.4 kW
X/R	7.93
U_k	3.2 %
Z_e	32 Ω
R_e	12.015 Ω
X_e	29.66 Ω

$$Z_e = U_k \cdot \frac{U_{HV}^2}{S_n} \qquad R_e = \frac{P_{cu}}{I_n^2} \qquad X_e = \sqrt{Z_e^2 - R_e^2} \tag{14}$$

Table A1.3. Requirements for grid connection, (Theologitis et al., 2011).

Grid Codes	Voltage Band	Fault Ride Through	Reactive Power Supply			Frequency Band	Active Power Derating
	range	capability	capability	range	function	range	capability
Medium Voltage (<110 kV & >10 kV)	0,9 U_N ↔ 1,15 U_N	√	√	0,95$_{lagging}$ to 0,95$_{leading}$	cosφ(P) Q(U) cosφ$_{fix}$ Q$_{fix}$	47,5 Hz ↔ 51,5 Hz	capability √ function $\Delta(\frac{P}{P_M}) = 40\frac{\%}{Hz}(50,2Hz - f)$ $50,2Hz < f < 51,5Hz$
Low Voltage (<10 KV)	0,9 U_N ↔ 1,15 U_N	√**	√	0,90$_{lagging}$ to 0,90$_{leading}$***	cosφ(P) cosφ$_{fix}$	47,5 Hz ↔ 50,2 Hz	capability √ function $\Delta(\frac{P}{P_M}) = 40\frac{\%}{Hz}(50,2Hz - f)$ $50,2Hz < f < 51,5Hz$

Appendix 1.

Table A1.4. Simulink model control parameters

Parameter	Notation	Value
Solar Inverter model		
Proportional gain	K_v	0.05
Integral gain	K_{Vi}	15
Transfer function time	Tpwr	0.05
Nominal Active Power	P_{nom}	5e3 [W]
Nominal frequency	f_{nom}	50 [Hz]
Nominal Voltage	V_{nom}	400 [V]
Reactive current limit	I_{qhl}	1.25
Active current limit	I_{phl}	1.24
Maximum temperature dependent current	I_{maxTD}	1.7
Voltage Control model		
Transformer rated current	I_{set}	0.7
Low pass filter time	T_f	0.05
Proportional gain	K_v	0.05

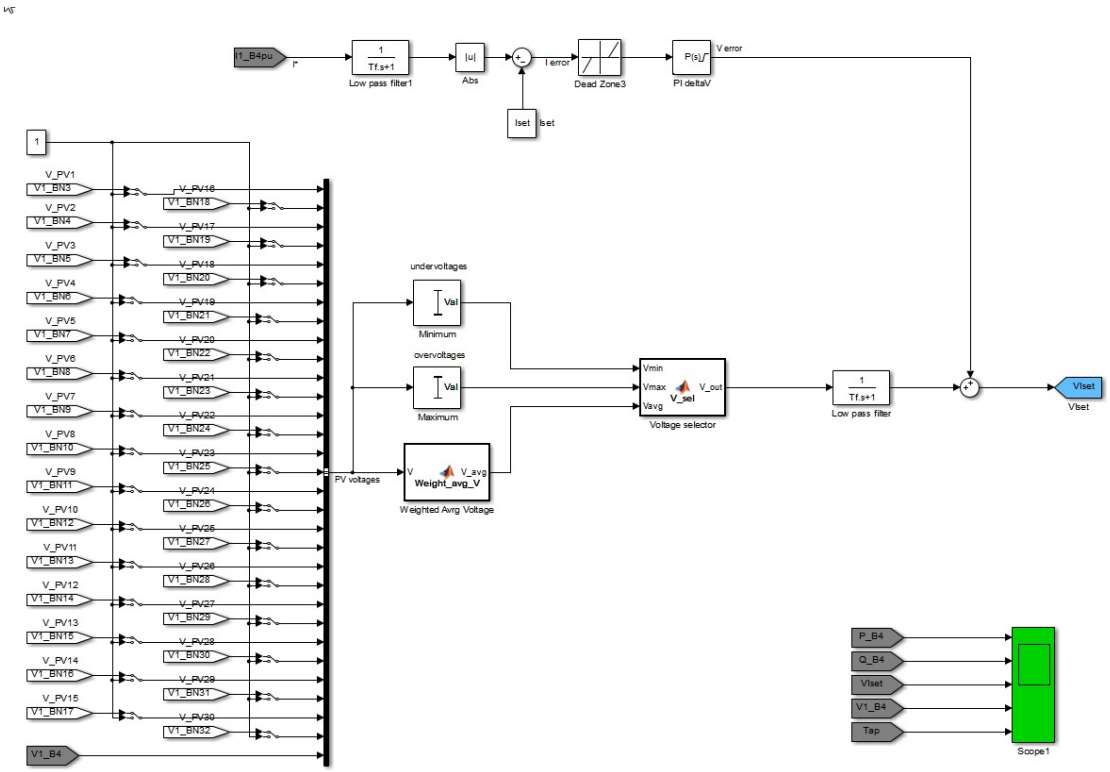

Figure A1.1. Network voltage weighted average control model.

Appendix 2. Matlab codes

Multi-Objective Genetic Algorithm (gamultiobj)

```
% Implementation of the MOGA for the optimization of the
    power losses and voltage stability in Bornholm.

clc; close all; clear all;
global x_hist y_hist mode count          % variables visible

% 'mode' parameter selects the reactive capability curve to
     apply. 'mode = 0' for cosphi(P) and 'mode = 1' for Q(U)
    .
count = 0;       % initialize number of function evaluations
mode = 0;        % define the reactive power control curve
if (mode == 0)                      % cosphi(P) curve
   y_hist = zeros(1e3,2);           % objective function values
   x_hist = zeros(1e3,7);           % parameters values
  % Parameters' limits must be given to the algorithm. Non-
     linear constraints are not present.
   A = [0 0 0 1 -1 0 0;             % Linear inequeality
        0 0 0 0 1 -1 0 ;            % constraints matrix
        0 0 0 0 0 1 -1];
   b = [0; 0; 0];                   % Linear inequality vector
   Aeq = [0 0 0 10 4 8 9];          % Linear equality matix
   beq = [1];                       % Linear equality vector
   lb = [0.02 0.9 -0.975...
         0.01 0.02 0.025 0.04];     % Lower bound on x
   ub = [0.35 1 -0.9 0.04...
         0.05 0.06 0.08];           % Higher bound on x
   X0 = [0.1 0.95 -0.95 0.02...
         0.03 0.035 0.04549];       % Intilial population of x

   options = gaoptimset('TolFun',1e-2,'StallGenLimit',5,'
      Display','iter','Generations',100,'InitialPopulation',
      X0,'PopulationSize',50,'PlotFcns',{@gaplotpareto;
      @gaplotparetodistance});

   [x,Fval,exitFlag,Output] = gamultiobj(@ff,7,A,b,Aeq,beq,
      lb,ub,options)
```

Appendix 2.

```
  % Stopping criteria is defined as the weighted average
     relative change in the best fitness function value
     over 'StallGenLimit' generations lower or equal to '
     TolFun' or the maximum number of gen. is reached.

else                                % Q(U) curve

  y_hist = zeros(1e3,2);            % objective function values
  x_hist = zeros(1e3,9);            % parameters values
  % Parameters' limits must be given to the algorithm. Non-
     linear constraints are not present.
  A = [0 0 0 0 1 -1 0 0 0;          % Linear inequeality
       0 0 0 0 0 1 -1 0 0;          % constraints matrix
       0 0 0 0 0 0 1 -1 0];
  b = [0; 0; 0];                    % Linear inequality vector
  Aeq = [0 0 0 0 10 4 8 9 0];       % Linear equality matix
  beq = [1];                        % Linear equality vector
  lb = [0.95 1.01 1.04 -0.4 0.01 0.02...
        0.025 0.04 0.02];           % Lower bound on x
  ub = [0.98 1.04 1.06 -0.15 0.04 0.05...
        0.06 0.08 0.35];            % Higher bound on x
  X0 = [0.96 1.02 1.045 -0.28 0.02 0.03...
        0.035 0.04549 0.1];         % Intilial population of x

  options = gaoptimset('TolFun',1e-2,'StallGenLimit',5,'
     Display','iter','Generations',100,'InitialPopulation',
     X0,'PopulationSize',60,'PlotFcns',{@gaplotpareto;
     @gaplotparetodistance});

  [x,Fval,exitFlag,Output] = gamultiobj(@ff,9,A,b,Aeq,beq,
     lb,ub,options)

  % Stopping criteria is defined as the weighted average
     relative change in the best fitness function value
     over 'StallGenLimit' generations lower or equal to '
     TolFun' or the maximum number of gen. is reached.
end
```

Appendix 2.

FITNESS FUNCTION (ff.m)

```
% Fitness function optimized by MOGA. The function calls
    the Simulink model after setting the parameters.

function y = ff(x)

global x_hist y_hist mode count          % variables visible
% Setting the parameters. Select the type of reactive power
    control to simulate in order to use the correct number
   of parameters in each case. 'mode = 0' for cosphi(P) and
    'mode = 1' for Q(U).
if (mode == 0)                          % cosphi(P) curve
   apsel = x(1);                        % Active power injection
   cosphi1 = x(2);                      % cosphi overexcited
   cosphi2 = x(3);                      % cosphi uderexcited
   w1 = x(4);                           % weighted Voltage 1
   w2 = x(5);                           % weighted Voltage 2
   w3 = x(6);                           % weighted Voltage 3
   w4 = x(7);                           % weighted Voltage 4
  % The rest of parameters will maintain constant values.
  U1 = 0.9; U2 = 0.8; U3 = 1.1; Q = 0.3;
else                                    % Q(U) curve
   U1 = x(1);                           % Undervoltage param.
   U2 = x(2);                           % Overvoltage param.1
   U3 = x(3);                           % Overvoltage param.2
  Q = x(4);                             % Reactive power of U3
   w1 = x(5);                           % weighted Voltage 1
   w2 = x(6);                           % weighted Voltage 2
   w3 = x(7);                           % weighted Voltage 3
   w4 = x(8);                           % weighted Voltage 2
   apsel = x(9);
  % The rest of parameters will maintain constant values.
   cosphi1 = 0.95; cosphi2 = -0.95;
end
```

Appendix 2.

```
parameters                          % Load model parameters

% Run the model
opt = simset('DstWorkspace','current','SrcWorkspace','
    current');          % Move data to function workspace
tic;                    % Meaure the simulation time
simOut = sim('LV_network',[],opt);
toc;

%%%%%% Calculation of power losses (Ploss) %%%%%%
% Cable Losses (P_L)
R = [12.015,0.00963,0.066023,0.015087,0.021828,...
0.012198,0.041665,0.024358,0.022435,0.010593,0.016692,...
0.017388,0.021153,0.043588,0.046152,0.067305,0.033973,...
0.024396,0.048716,0.035896,0.006624,0.000621,0.011385,...
0.01449,0.039742,0.005382,0.010557,0.008487,0.013041,...
0.005382,0.00414,0.008694,0.022435];
% [Re,R(i)]. Re = equivalent resistance of trafo.
%            R(i) = three-phases resistance value.

P_L = 0;                    % Initialized cable losses
[m_i,n_i]=size(I);
for i=1:m_i                 % m_i total number of lines.
  for j=3:n_i               % n_i total number of columns.
  P_L = P_L + ((I(i,j))^2*R(j-1))/1e3; % Day Losses [kWh]
  end
end

% Transformer losses (Iron losses(P_fe)+Copper losses(P_cu)
    )
P_fe = 257*24/1e3;          % Constant losses [kWh].
P_cu = 0;                   % Initialize copper losses
for i=1:m_i
  P_cu = P_cu + ((I(i,1))^2*R(1))/1e3; % Day Losses kWh]
end

P_T = P_fe + P_cu;          % Total transformer losses day[kWh]
```

Appendix 2.

```
%%%%%%%%%%Deviations%%%%%%%%%%
Vmax = 1.05; Vmin = 0.95;  % PV bus voltages limits [pu]
Qmax = 2.18; Qmin = -Qmax; % PV reactive power limits[kVAr]

% Voltage over boundaries
[m_v,n_v] = size(V);
DeltaV = 0;
for i=1:m_v                % m_v total number of time steps
  for j=1:n_v              % n_v total number of buses.
    if (V(i,j) < Vmin)
      DeltaV = DeltaV + (Vmin-V(i,j))^2;
    elseif (V(i,j) > Vmax)
      DeltaV = DeltaV + (V(i,j)-Vmax)^2;
    else
      DeltaV = DeltaV;
    end
  end
end
% Reactive power over boundaries
[m_q,n_q] = size(Q);
DeltaQ = 0;
for i=1:m_q                % m_q total number of time steps
  for j=1:n_q              % n_q total number of inverters
    if (Q(i,j) < Qmin)
      DeltaQ = DeltaQ + (Qmin-Q(i,j))^2;
    elseif (Q(i,j) > Qmax)
      DeltaQ = DeltaQ + (Q(i,j)-Qmax)^2;
    else
      DeltaQ = DeltaQ;
    end
  end
end

% Over flow in lines
Vr = 400*sqrt(3);          % Rated voltage
Smax = zeros(1,n_i);
Usc = 3.2;                 % Short circuit impedance voltage
```

Appendix 2.

```
In1 = 1e5/(1e4*sqrt(3));
In2 = 1e5/(400*sqrt(3));
Isc1 = In1*100/Usc;      % Short-circuit current
Isc2 = In2*100/Usc;      % Short-circuit current
Ir = [Isc1 Isc2 139 92 139 139 139 92 92 92 188 188 248 124
    124 124 124 124 139 124 124 248 248 248 248 124 248 248
    248 248 248 248 183 92]; % cables rated currents [A]

for i=1:m_i
  for j=1:n_i
    Smax(i,j) = Vr*Ir(1,j)/1e3; % Line flow limit
  end
end

DeltaS = 0;              % Initialize flow deviation
for i=1:m_i
  for j=1:n_i
    if (Vr*V1(i,j)*I(i,j)/1e3 > Smax(i,j))
        DeltaS = DeltaS+(Vr*V1(i,j)*I(i,j)/1e3-Smax(i,j))^2
    else
        DeltaS = DeltaS;
    end
  end
end

%%%%%%%%% Voltage Deviation (Vdev) %%%%%%%%

Vref = 1;                % reference voltage [1pu]
Vdev_t = 0;
for i=1:m_v              % m_v total number of time steps
  for j=1:n_v            % n_v total number of inverters.
    Vdev_t = Vdev_t + abs(V(i,j) - Vref);
  end
end
Vdev = Vdev_t/n_v;  % sum of voltage deviations.

% Minimize the number of tap changes
tap = 0;
```

Appendix 2.

```
m_T = size(T);
for i=1:m_T
    tap = tap + T(i);
end

%%%%%%%% First Objective Function, F1 %%%%%%%

energy = P_L + P_T;      % Total energy losses [kWh]
F1 = energy;

%%%%%%%  Second Objective Function, F2 %%%%%%%

F2 = Vdev;

%%%%%%%  Objective Function, y %%%%%%%

Wv = 0.6;          % penalty factor overvoltages
Wq = 0.15;         % penalty factor over reactive power
Ws = 0.25;         % penalty factor overflow
y = zeros(1,2); % Initialize objective function
y(1) = F1+Wv*DeltaV+Wq*DeltaQ+Ws*DeltaS;
y(2) = F2+tap;

objF = y           % To visualise the value at each iteration

% Historic record of parameters and fitness values
count = count + 1;       % Number of function evaluation
x_hist(count,:) = x;     % Parameters
y_hist(count,:) = y;     % Objective values
```

Appendix 3. Optimization results

The rest of electrical data obtained from the simulations in other cases is shown below. Additionally, active and reactive power values of each solar inverter are aggregated as well as the optimization graphs summarized in Table 2.

Load 1 (winter)

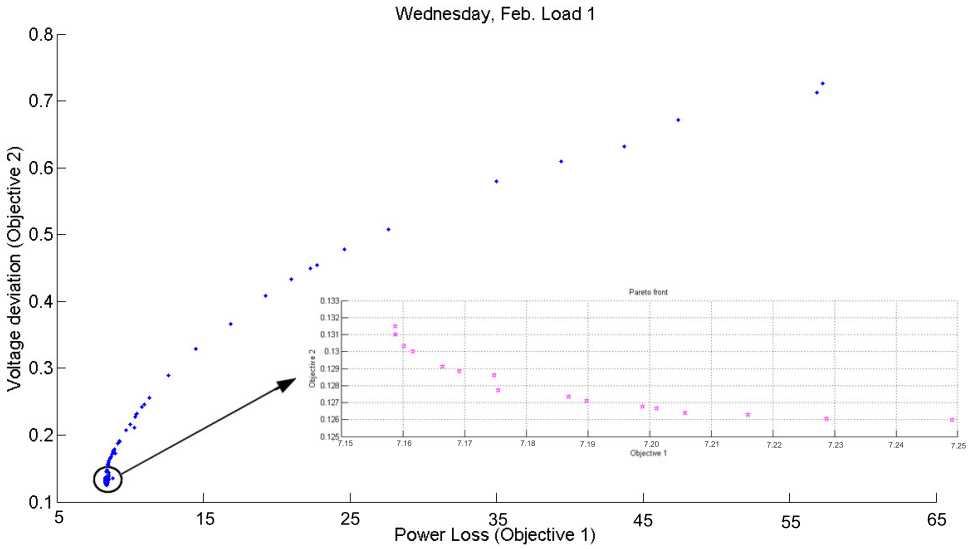

Figure A3.1. cosφ(P) optimization pareto results

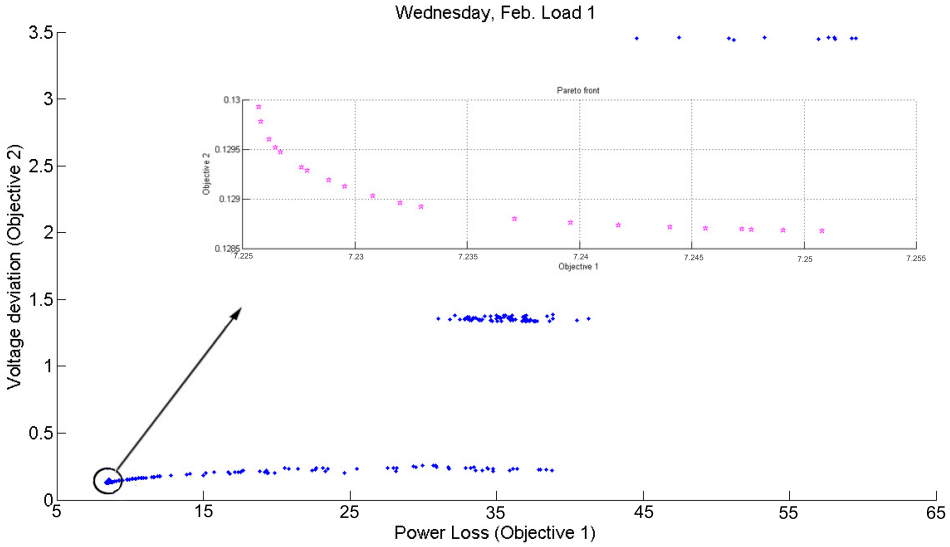

Figure A3.2. Q(U) optimization pareto results

Appendix 3.

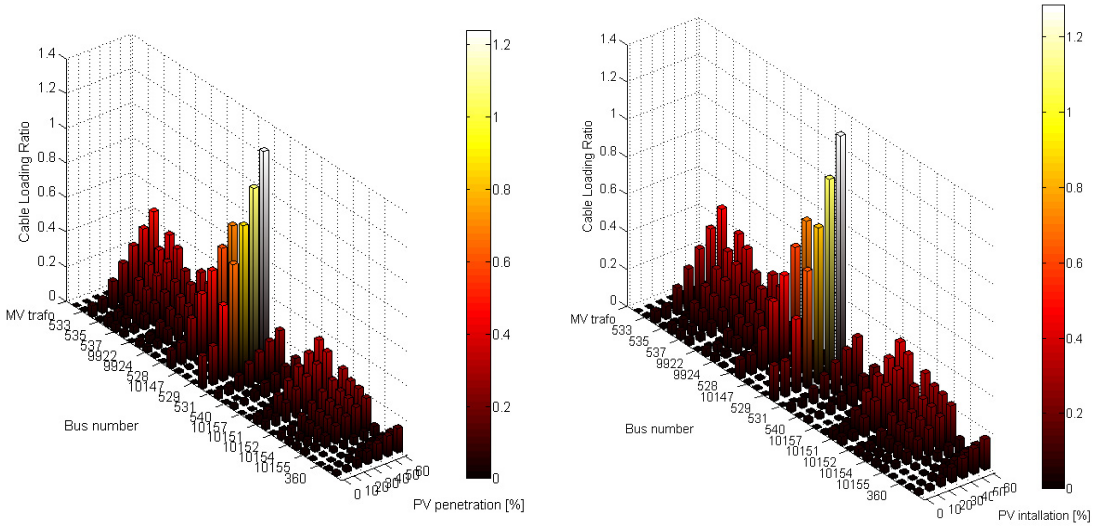

Figure A3.3. cosφ(P) vs Q(U) load flow ratio with network voltage control enabled.

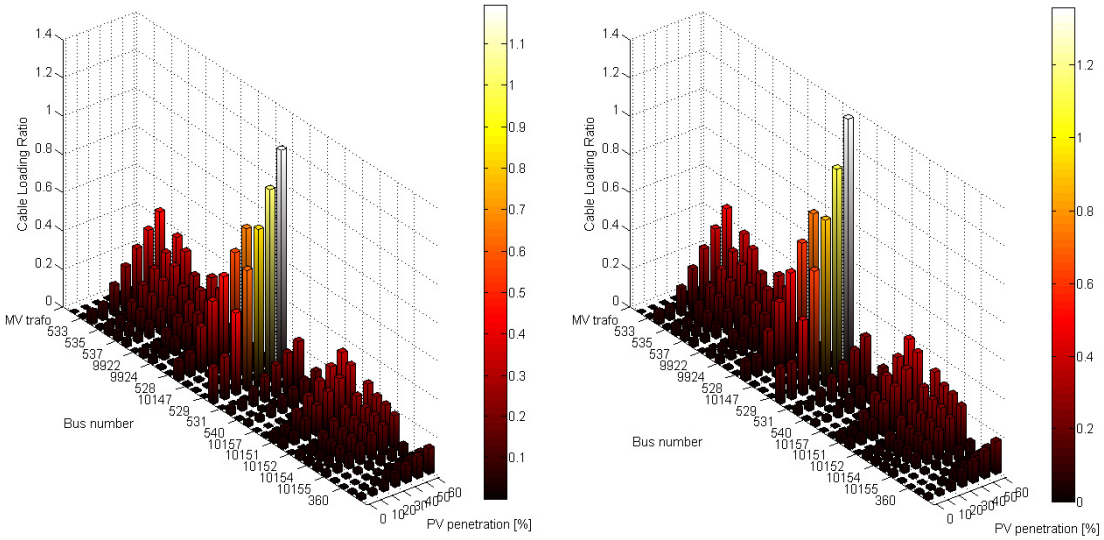

Figure A3.4. cosφ(P) vs Q(U) load flow ratio with network voltage control disabled.

Appendix 3.

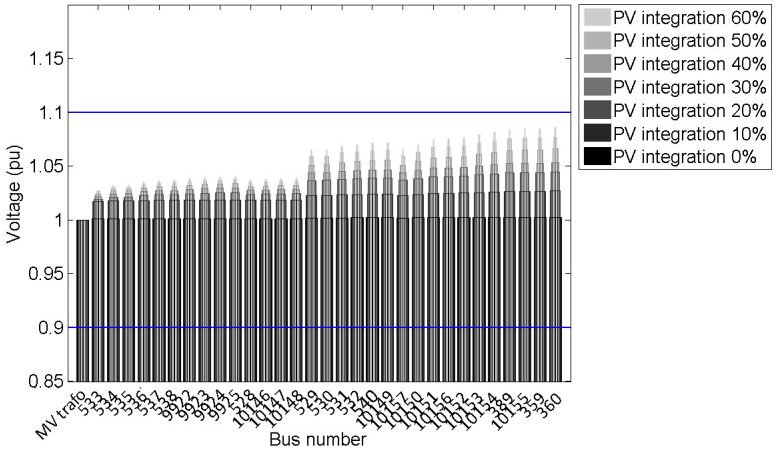

Figure A3.5. cosφ(P) voltage values at PCC. Network voltage control enabled.

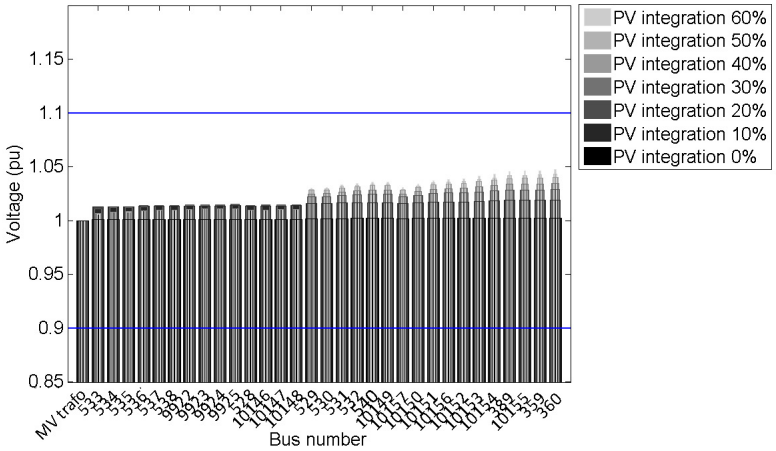

Figure A3.6. Q(U) voltage values at PCC. Network voltage control enabled.

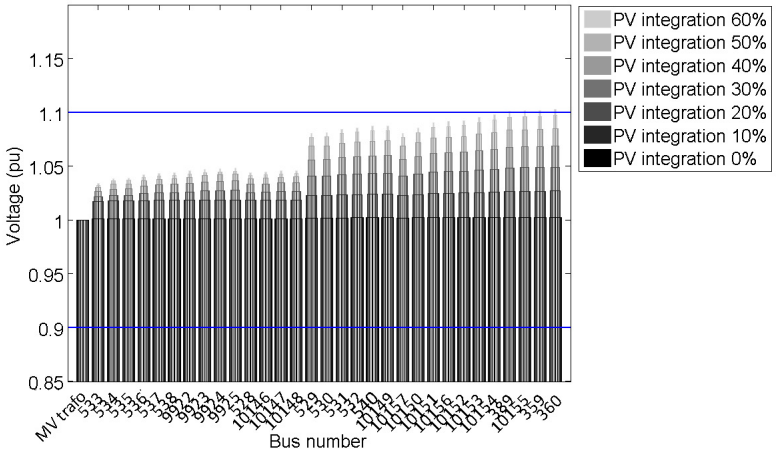

Figure A3.7. cosφ(P) voltage values at PCC. Network voltage control disabled.

Appendix 3.

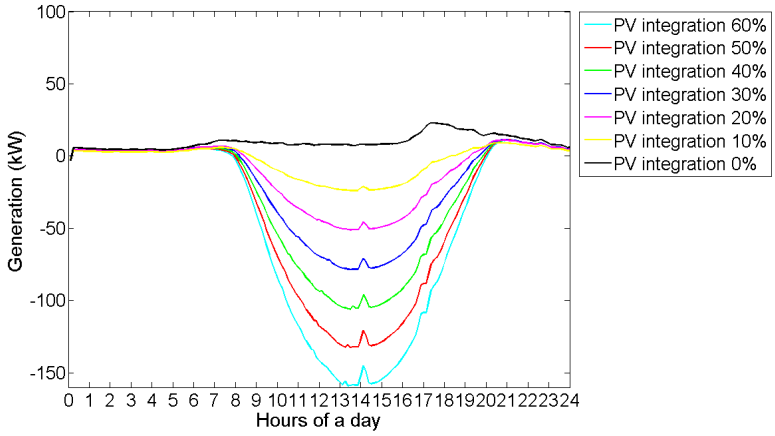

Figure A3.8. Active power at transformer LV side. Network voltage control enabled.

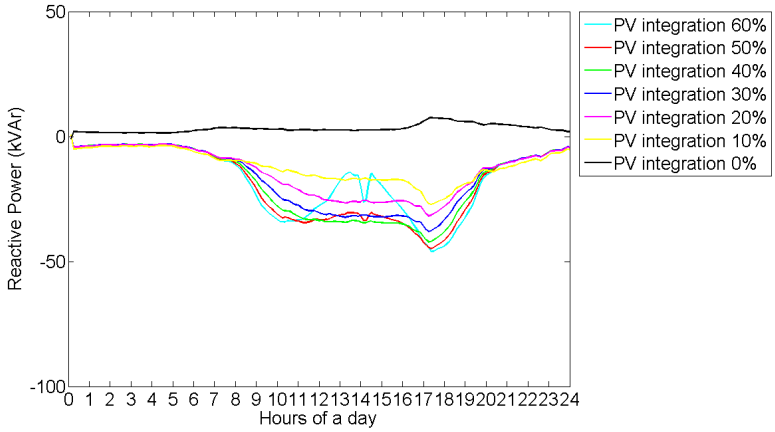

Figure A3.9. cosφ(P) reactive power at transformer LV side. Network voltage control enabled.

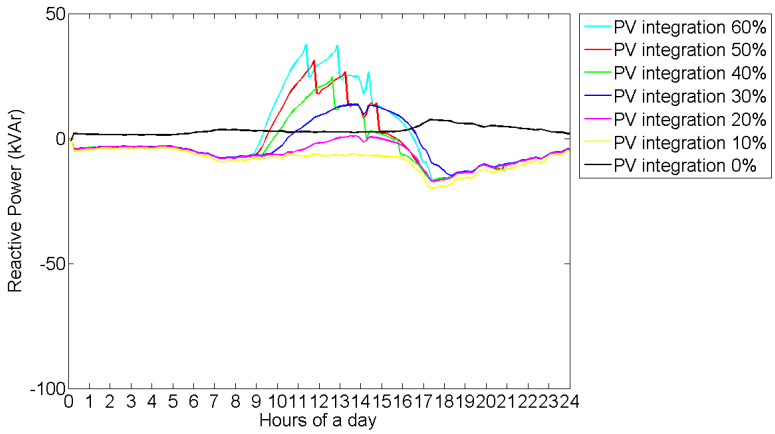

Figure A3.10. Q(U) reactive power at transformer LV side. Network voltage control enabled.

Appendix 3.

Load 3 (winter)

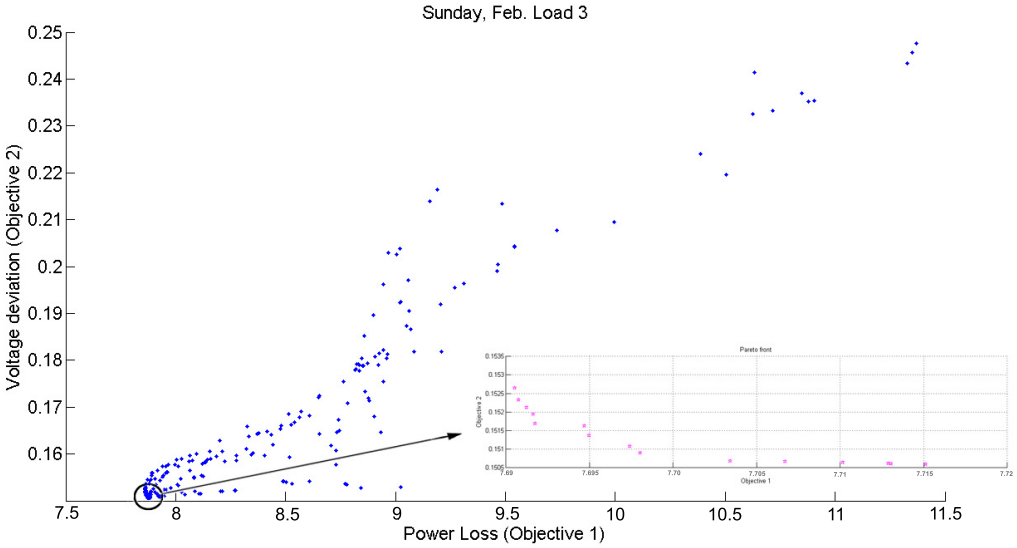

Figure A3.11. cosφ(P) optimization pareto results

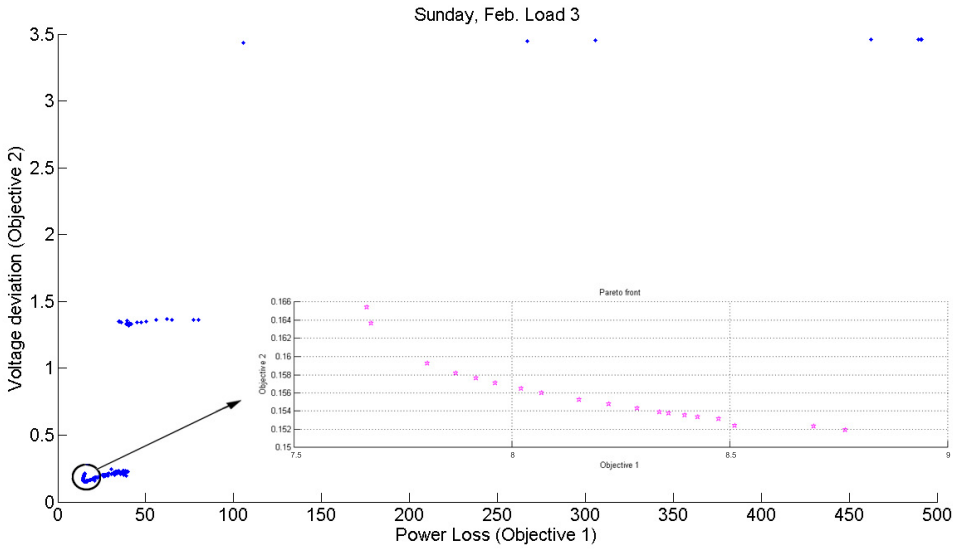

Figure A3.12. Q(U) optimization pareto results

Appendix 3.

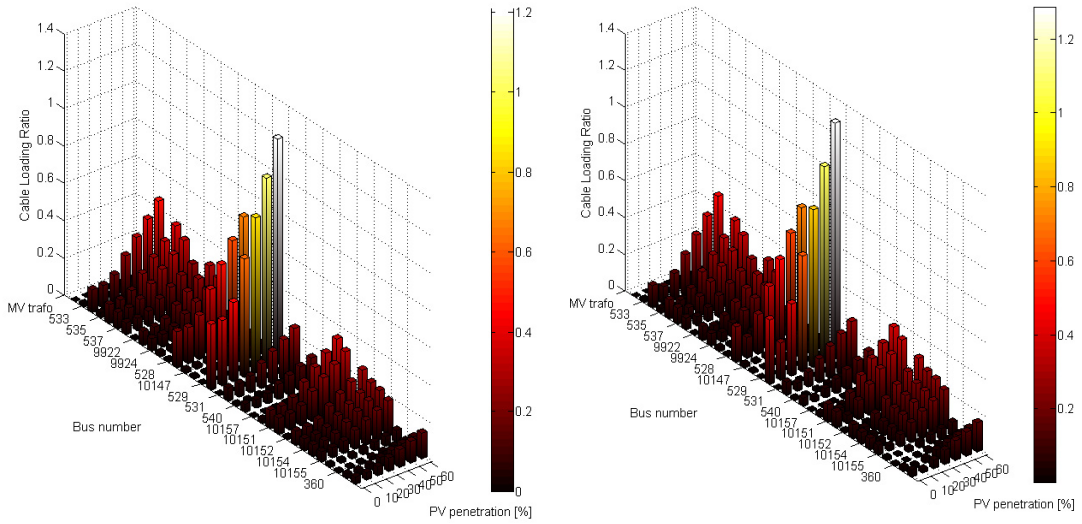

Figure A3.13. cosφ(P) vs Q(U) load flow ratio with network voltage control enabled.

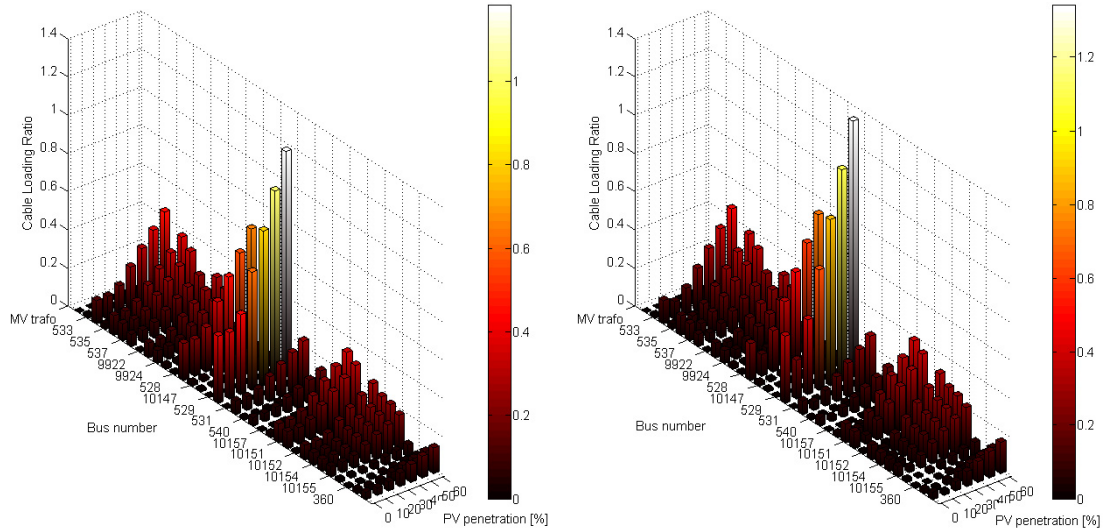

Figure A3.14. cosφ(P) vs Q(U) load flow ratio with network voltage control disabled.

Appendix 3.

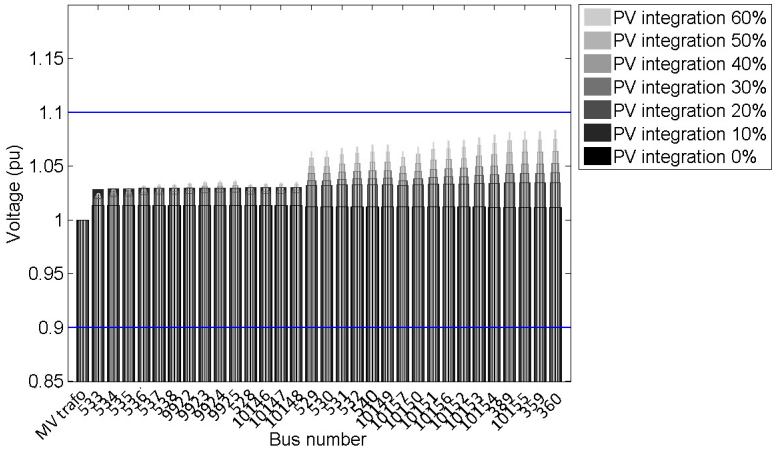

Figure A3.15. cosφ(P) voltage values at PCC. Network voltage control enabled.

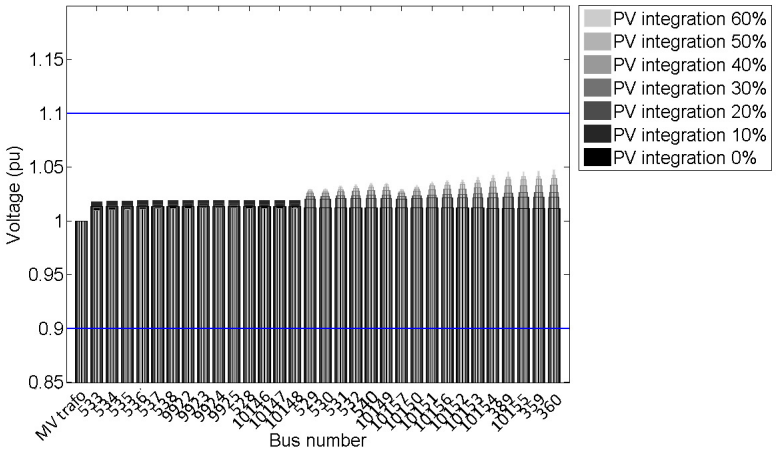

Figure A3.16. Q(U) voltage values at PCC. Network voltage control enabled.

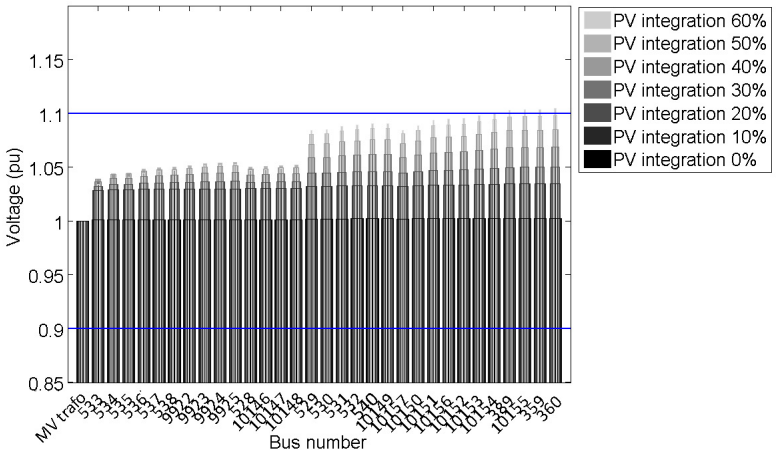

Figure A3.17. cosφ(P) voltage values at PCC. Network voltage control disabled.

Appendix 3.

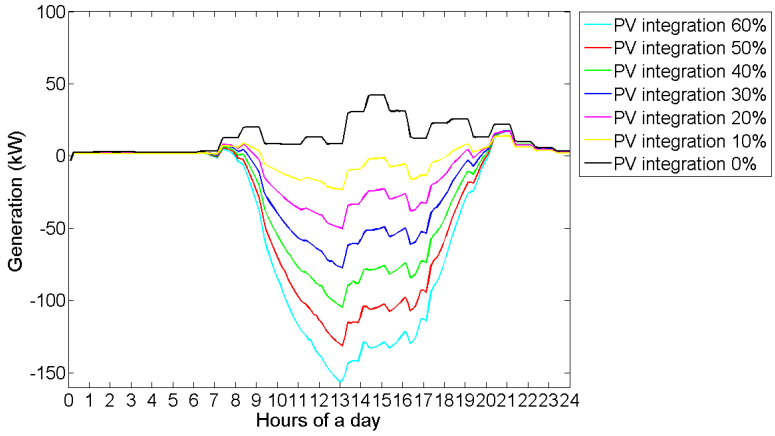

Figure A3.18. Active power at PCC. Network voltage control enabled.

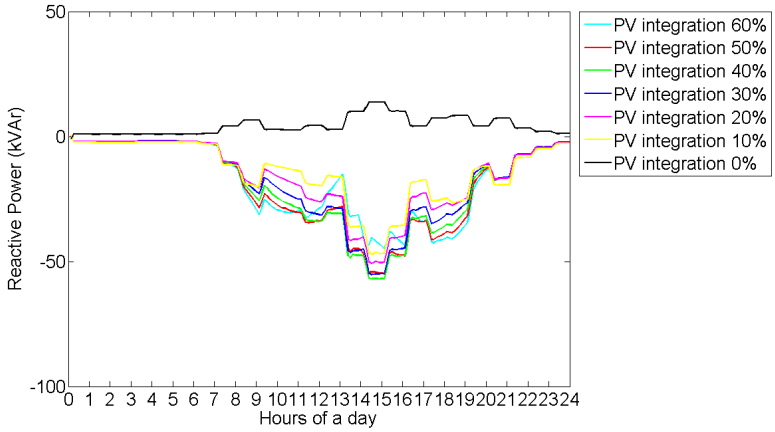

Figure A3.19. cosφ(P) reactive power at transformer LV side. Network voltage control enabled.

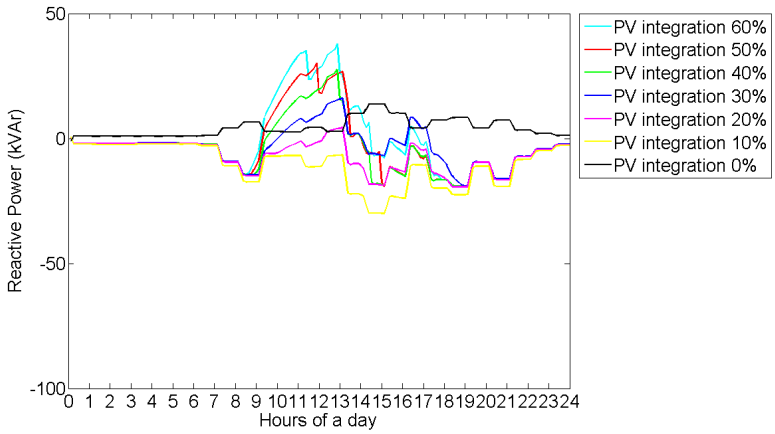

Figure A3.20. Q(U) reactive power at transformer LV side. Network voltage control enabled.

Appendix 3.

Load 3 (summer)

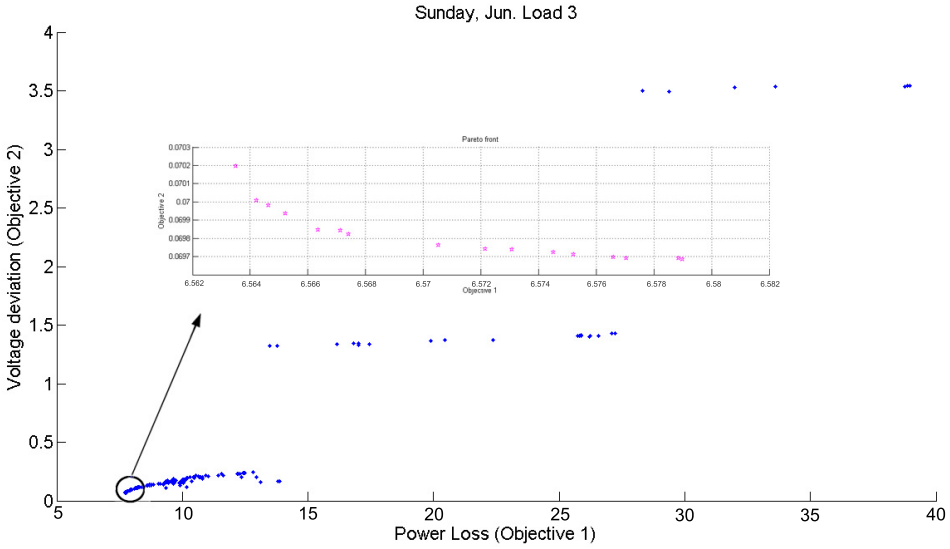

Figure A3.21. cosφ(P) optimization pareto results

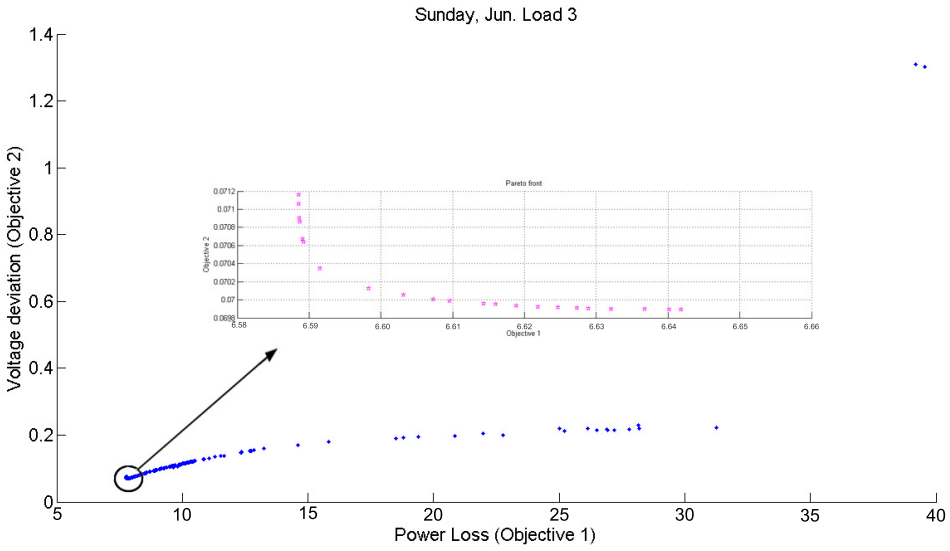

Figure A3.22. Q(U) optimization pareto results

Appendix 3.

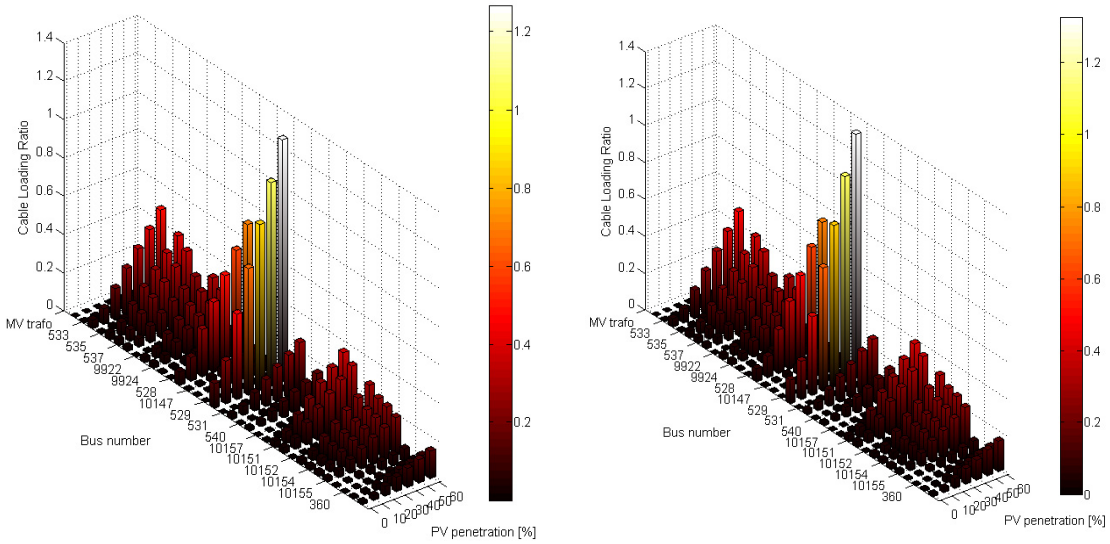

Figure A3.23. cosφ(P) vs Q(U) load flow ratio with network voltage control enabled.

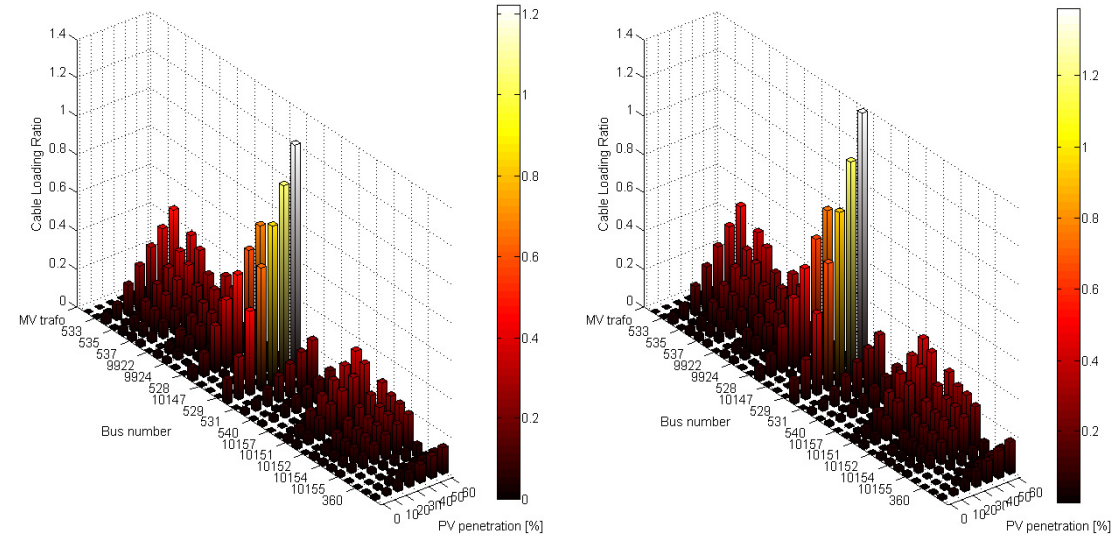

Figure A3.24. cosφ(P) vs Q(U) load flow ratio with network voltage control disabled.

Appendix 3.

Load 5 (winter)

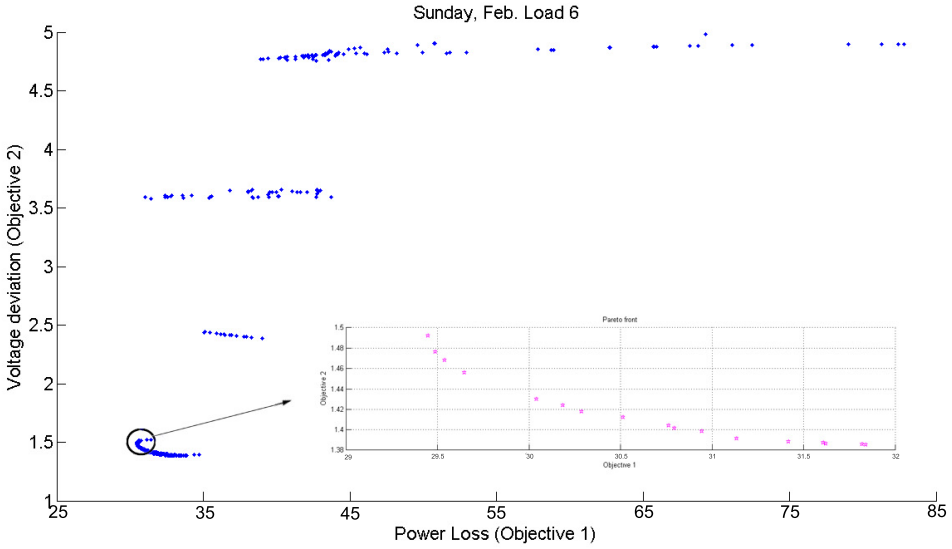

Figure A3.25. cosφ(P) optimization pareto results

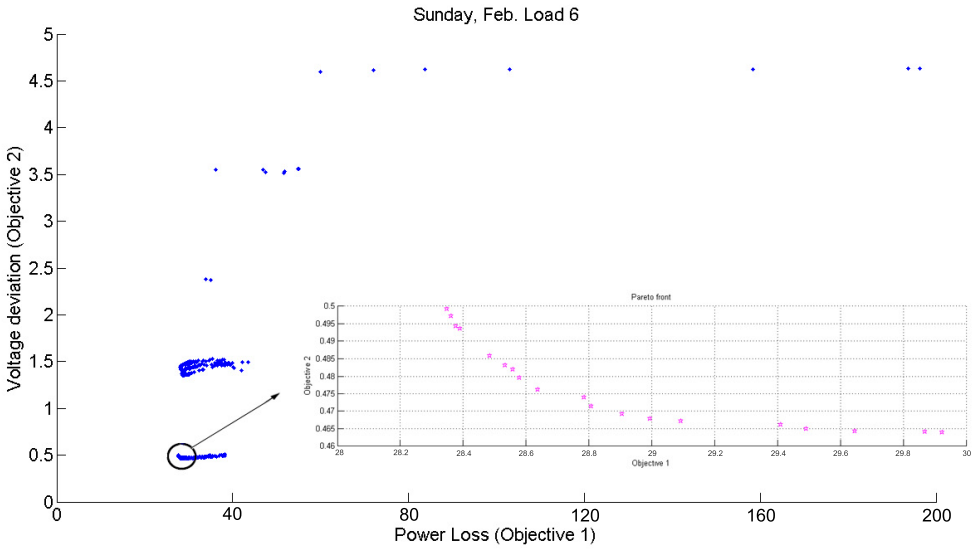

Figure A3.26. Q(U) optimization pareto results

Appendix 3.

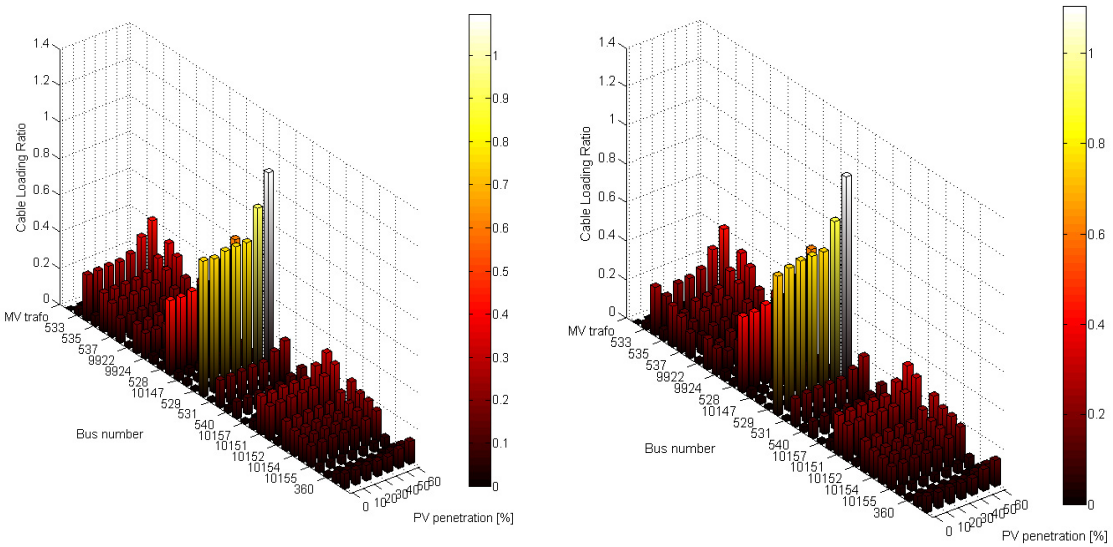

Figure A3.27. cosφ(P) vs Q(U) load flow ratio with network voltage control enabled.

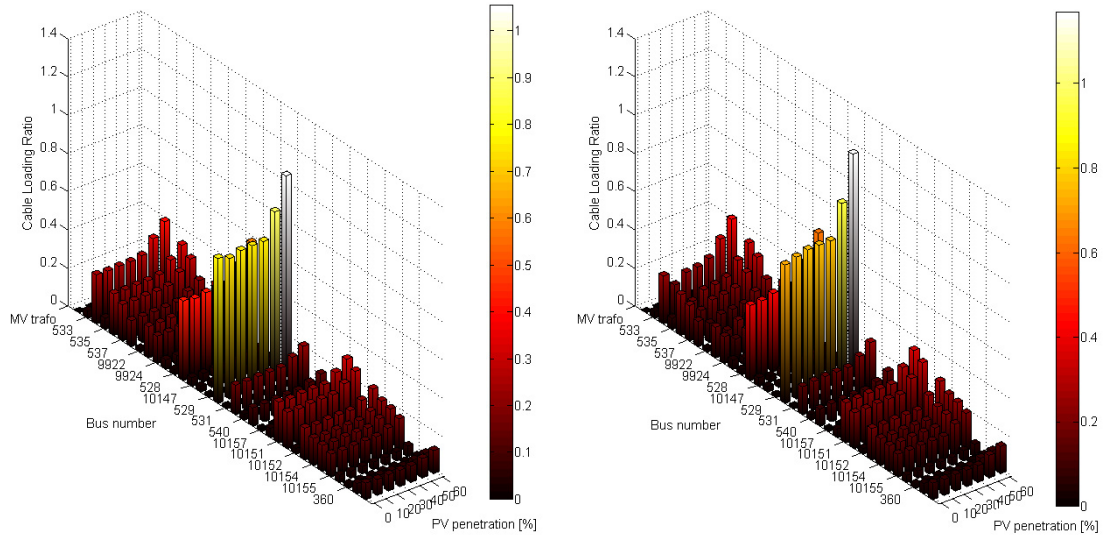

Figure A3.28. cosφ(P) vs Q(U) load flow ratio with network voltage control disabled.

Appendix 3.

Load 5 (summer)

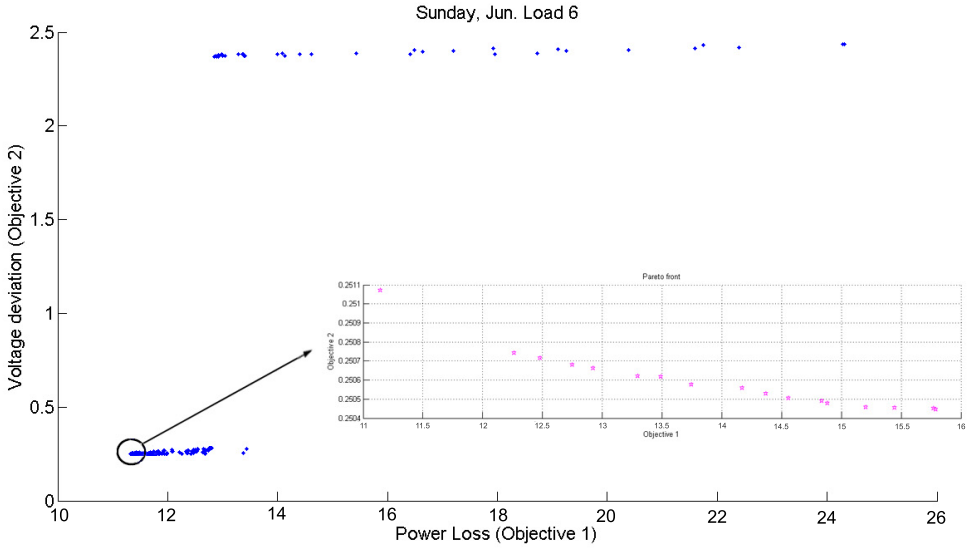

Figure A3.29. cosφ(P) optimization pareto results

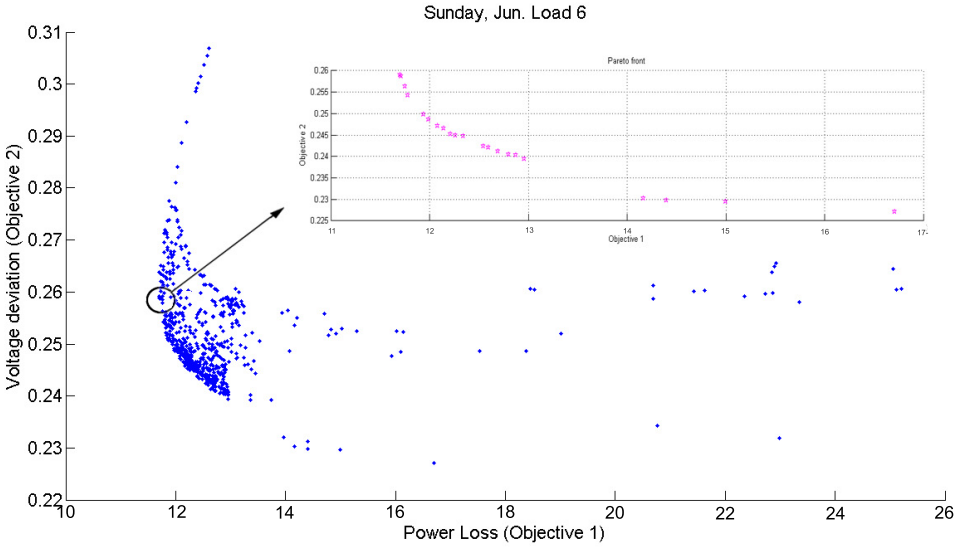

Figure A3.30. Q(U) optimization pareto results

Appendix 3.

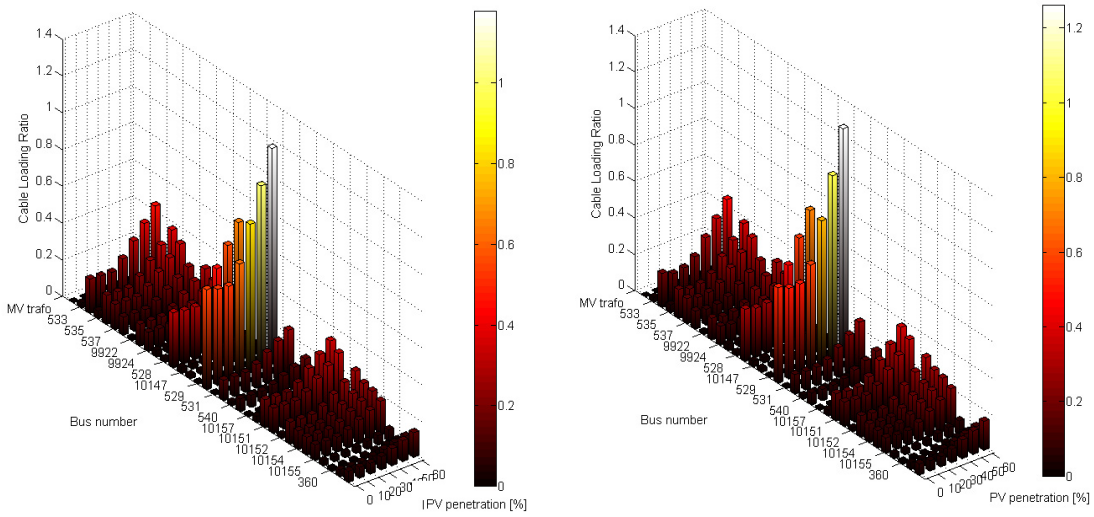

Figure A3.31. cosφ(P) vs Q(U) load flow ratio with network voltage control enabled.

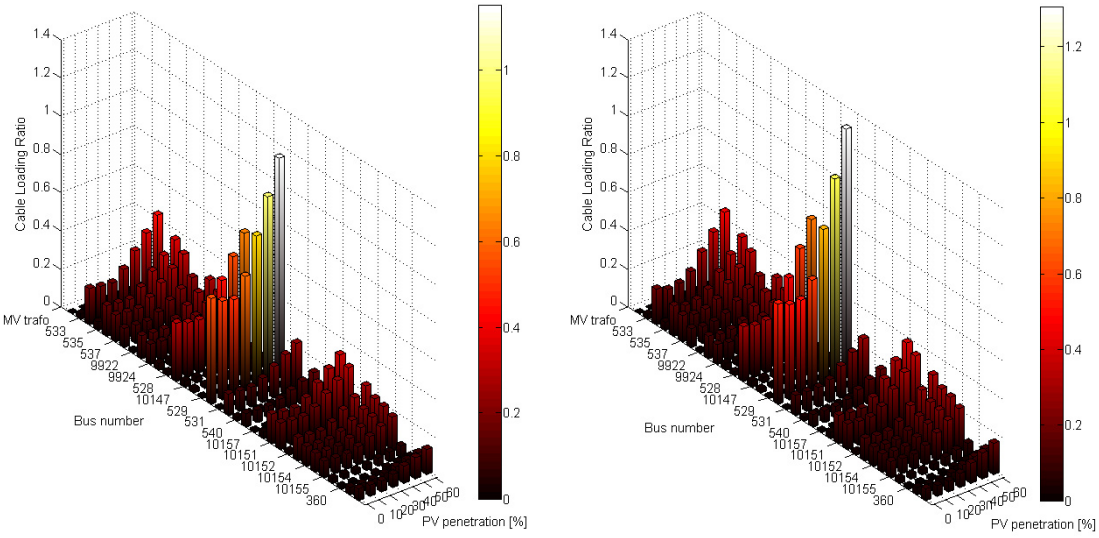

Figure A3.32. cosφ(P) vs Q(U) load flow ratio with network voltage control disabled.

Appendix 3.

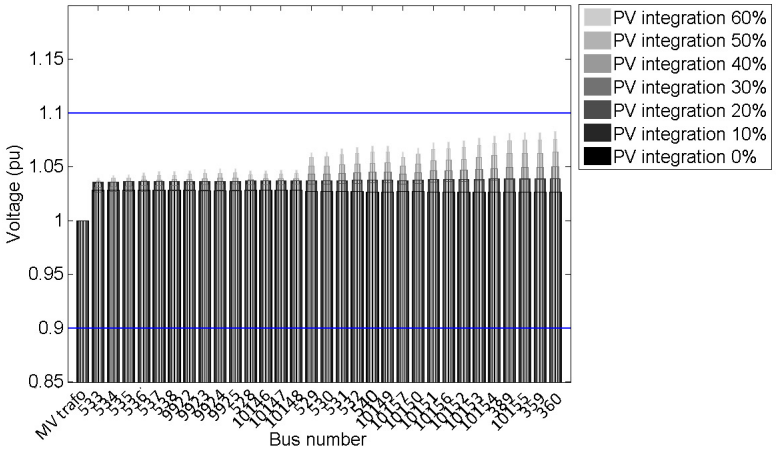

Figure A3.33. cosφ(P) voltage values at PCC. Network voltage control enabled.

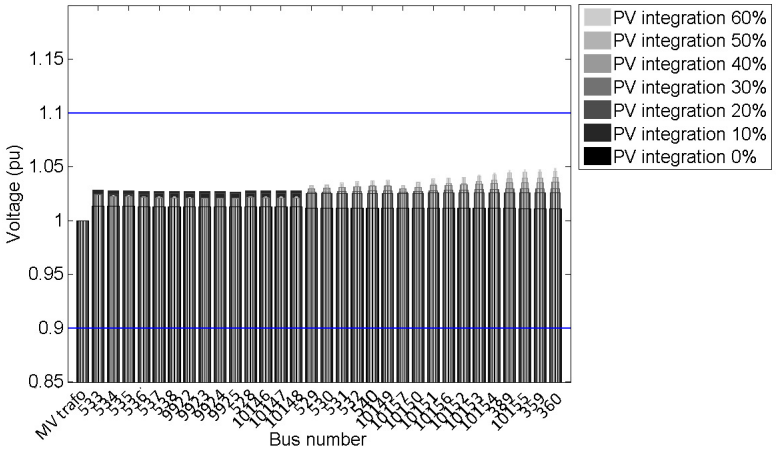

Figure A3.34. Q(U) voltage values at PCC. Network voltage control enabled.

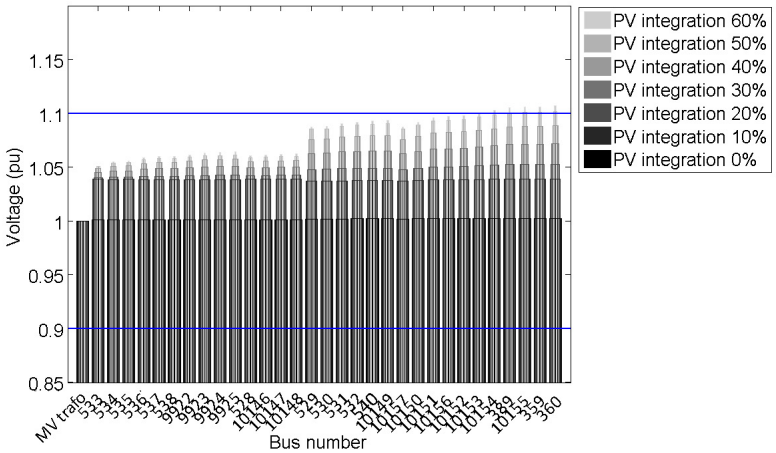

Figure A3.35. cosφ(P) voltage values at PCC. Network voltage control disabled.

Appendix 3.

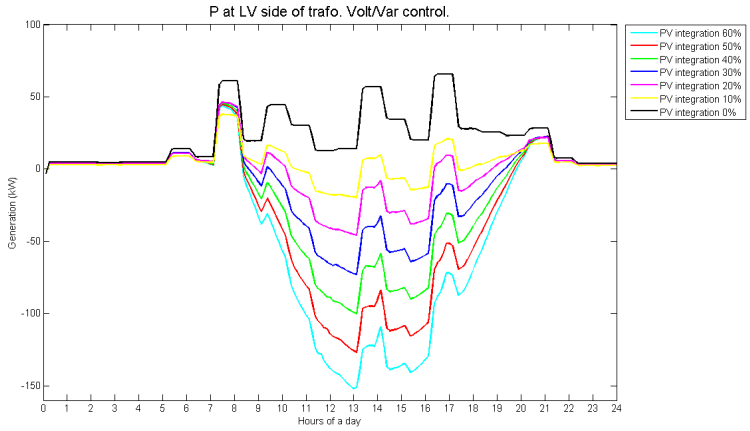

Figure A3.36. Active power at transformer LV side. Network voltage control enabled.

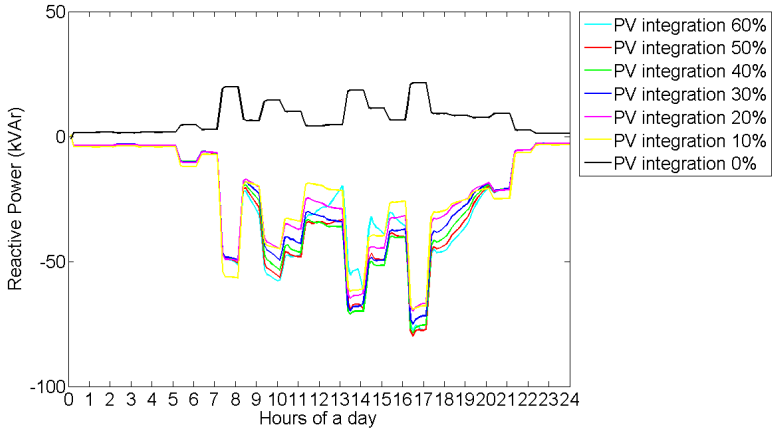

Figure A3.37. cosφ(P) reactive power at transformer LV side. Network voltage control enabled.

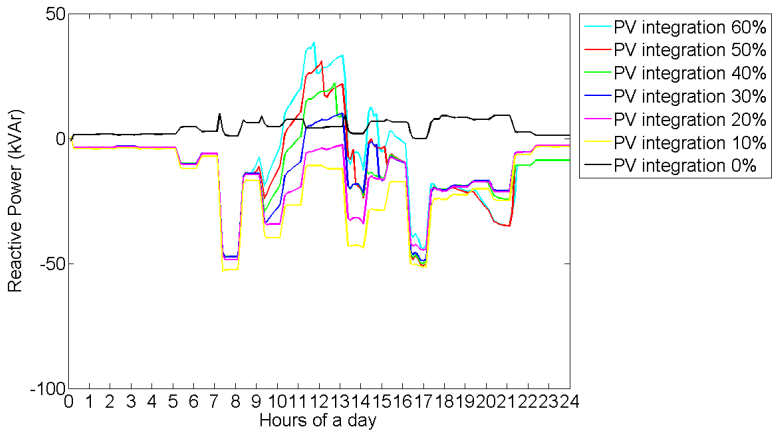

Figure A3.38. Q(U) reactive power at transformer LV side. Network voltage control enabled.

Appendix 4. Inverter Data Sheet

MAKING MODERN LIVING POSSIBLE

TLX Inverter Series

Three phase transformerless inverter series from 6-15 kW

The TLX series includes TLX, TLX+, TLX Pro and TLX Pro+

35 kg

The weight of 6-15 kW

Ensuring easy and troublefree installation of high performance inverters

The high performance transformerless three-phase TLX inverter series, with efficiency of 98 % deliver maximum energy in all conditions.

Flexibility
Integrating 1000 V_{DC} input range, 250-800 V MPP range and multiple DC inputs with each their own individually regulated MPP tracker, allows for more modules in a series and longer strings, while providing greater flexibility in the PV setup.

Simplicity
The TLX Pro series includes master inverter technology capable of controlling up to 100 inverters from a single inverter. Likewise, the integrated webserver, allows you to control, monitor and adjust your PV system from any online device.

1.6 Billion hours of Experience
The TLX series has been installed all over the world in both residential 6 kW systems to over 100 MW utility plants.

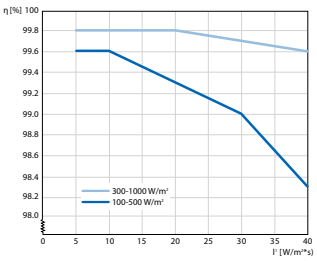

MPP efficiency

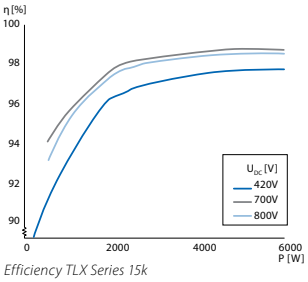

Efficiency TLX Series 15k

- η98 %
- 1000 V_{DC}
- 250-800 V_{MPP}
- 3×230 V_{AC}
- 6-15 kW
- PV Sweep
- Compact dimensions
- 12 pcs per pallet place
- 35 days integrated data storage
- 35 kg
- Full built-in monitoring
- 2-3 independant MPP trackers
- SMS via GSM option
- Replication of setting to 100 inverters
- Multiple languages and grid-codes
- ConnectSmart™ compliant

www.danfoss.com/solar

Figure A4.1. TLX inverter series specifications

Appendix 4.

For additional technical data and functional descriptions please refer to the reference manual found on www.danfoss.com/solar

Unit	Parameter	TLX series				
	AC					
|S|	Rated apparent power	6.0 kVA	8.0 kVA	10 kVA	12.5 kVA	15 kVA
$P_{ac,r}$	Rated active power[1]	6.0 kW	8.0 kW	10 kW	12.5 kW	15 kW
	Reactive power range	0-3.6 kVAr	0-4.8 kVAr	0-6.0 kVAr	0-7.5 kVAr	0-9.0 kVAr
$V_{ac,r}$	Rated grid voltage (range)	3P + N + PE – 230 V / 400 V (± 20 %)				
	Nominal current AC	3 × 8.7 A	3 × 11.6 A	3 × 14.5 A	3 × 18.1 A	3 × 21.7 A
I_{acmax}	Max. current AC	3 × 9.0 A	3 × 11.9 A	3 × 14.9 A	3 × 18.7 A	3 × 22.4 A
	AC current distortion (THD %)	< 4 %		< 5 %		
$cosphi_{ac,r}$	Power factor – unregulated	> 0.99 at 100 % load and 0.95 at 20 % load				
	Power factor – regulated	0.8 over-excited – 0.8 under-excited (TLX+ and TLX Pro+)				
	"Connecting" power loss	10 W				
	Night-time power loss (off grid)	< 5 W				
f_r	Rated grid frequency (range)	50 Hz ± 5 Hz				
	DC					
$P_{mpptmax}$	Maximum PV input power per MPPT	8.0 kW				
$\Sigma_{P\ mpptmax}$	Max./nom. converted PV input power, total	6.2 kW	8.25 kW	10.3 kW	12.9 kW	15.5 kW
$V_{dc,r}$	Nominal voltage DC	700 V				
V_{mppmin} V_{mppmax}	MPP voltage-nominal power[2]	260 - 800 V	345-800 V	430-800 V	358-800 V	430-800 V
	MPP tracker	2 (2 × MC4)			3 (3 × MC4)	
V_{dcmax}	Max. DC voltage	1000 V				
$V_{dcstart}$	Turn on voltage	250 V				
V_{dcmin}	Turn off voltage	250 V				
I_{dcmax}	Max. current DC	2 × 12 A			3 × 12 A	
	Max. short circuit current DC at STC	2 × 12 A			3 × 12 A	
	Min. on grid power	20 W				
	Efficiency					
	Max. efficiency	97.8 %	97.9 %	98 %		
	Euro efficiency at $V_{dc,r}$	96.5 %	97.0 %	97.0 %	97.3 %	97.4 %
	MPP efficiency, static	99.9 %				
	Enclosure					
	Dimensions (H, W, D)	700 × 525 × 250 mm				
	Weight	35 kg				
	Acoustic noise level	max. 56 db(A)				
	Operation temperature range	-25..60 °C (45..60 °C – degrading at high loads)				
	Storage temperature	-25..60 °C				
	Relative humidity	95 % (non-condensing)				
	Ancilliary Services					
	Active power	Fixed, set point curves, remotely controlled, Fault Ride Through				
	Reactive power	Constant, set point curves, remotely controlled, Fault Ride Through (TLX+ and TLX Pro+)				
	Safety					
	Approvals and certificates	CE, VDE0126-1-1, RD1565/2010, TOR/D4, TOR/D2, G59/2-1 (8-15 kW), G83/1-1 (8-10k), PPC, AS4777, SI4777, EN 50438, C10/11, PPDS, IEC 61727, UTE NF C15-712-1, NF C 15-100, VDE-AR-N 4105 (only '+' variants), RD 1699, CEI 0-21, BDEW/2008-2011				
	Electrical Safety	IEC 62109-1/IEC 62109-2 (Class I, grounded – communication part Class II, PELV)				
	Functional safety	Voltage and frequency monitoring, islanding detection, residual current monitoring				

[1] At rated grid voltage (Vac,r), Cos(phi) = 1
[2] At symmetric input configuration. At asymmetrical input configuration. V_{mppmin} can be as low as 250 V.

Danfoss Solar Inverters A/S
Ulsnaes 1
DK-6300 Graasten
Denmark
Tel: +45 7488 1300
Fax: +45 7488 1301
E-mail: solar-inverters@danfoss.com
www.danfoss.com/solar

DKSI.PFP.204.A3.02 February 2013© Produced by Danfoss A/S ©

Figure A4.2. TLX inverter series specifications